AN ABSTRACT OF THE THESIS OF

Matthew Ryan Dawson for the degree of Master of Science in Civil Engineering presented on May 9, 2008.

Title: Scale Effects on Reinforced Concrete Beams Strengthened for Shear with Discrete Externally Bonded Carbon Fiber-Reinforced Polymer U-Wraps.

Abstract approved:

Christopher C. Higgins

Current ACI design provisions for shear in reinforced concrete (RC) beams strengthened with externally bonded carbon fiber-reinforced polymer (CFRP) U-wraps may not adequately account for the effect of scale. This paper describes tests of 6 geometrically scaled beams to identify possible scale effects of such beams. Results indicated that effective depth (d), shear span-to-depth ratio (a/d), flexural-tension steel reinforcement ratio (ρ_s), transverse steel reinforcement ratio (ρ_v), FRP reinforcement ratio (ρ_f), FRP strip width (w_f) and U-wrap orientation may affect the shear capacity of scaled specimens. In addition, local strain variations in surface bonded CFRP are investigated and recommendations on how to quantify CFRP strain are provided.

Scale Effects on Reinforced Concrete Beams Strengthened For Shear with Discrete

Externally Bonded Carbon Fiber-Reinforced Polymer U-Wraps

by

Matthew Ryan Dawson

A THESIS

submitted to

Oregon State University

in partial fulfillment of

the requirements for the

degree of

Master of Science

Presented May 9, 2008

Commencement June 2008

<u>Master of Science</u> thesis of <u>Matthew Ryan Dawson</u>

presented on <u>May 9, 2008.</u>

APPROVED:

_____

Major Professor, representing Civil Engineering

_____

Head of the School of Civil and Construction Engineering

_____

Dean of the Graduate School

I understand that my thesis will become part of the permanent collection of Oregon State

University libraries. My signature below authorizes release of my thesis to any reader

upon request.

_____

Matthew Ryan Dawson, Author

ACKNOWLEDGEMENTS

The author expresses sincere appreciation to Dr. Christopher C. Higgins for his guidance

and encouragement in the planning, implementation and analysis of this research. The

author also wishes to thank the following graduate students for their assistance with

laboratory experimentation and in critically discussing the findings of this research: O.

Murat Hamutcuoglu, Daniel A. Howell, Carl C. Koester, Mikal M. Mitchell, Thomas

Schumacher, A. Ekin Senturk, Matthew Smith, Gautam J. Sopal and O. Tugrul Turan.

TABLE OF CONTENTS

TABLE OF CONTENTS (Continued)

LIST OF FIGURES

LIST OF FIGURES (Continued)

LIST OF FIGURES (Continued)

LIST OF TABLES

LIST OF TABLES (Continued)

SCALE EFFECTS ON REINFORCED CONCRETE BEAMS STRENGTHENED FOR SHEAR WITH DISCRETE EXTERNALLY BONDED CARBON FIBER-REINFORCED POLYMER U-WRAPS

INTRODUCTION

Many 1950s-vintage conventionally reinforced concrete (RC) deck girder bridges remain in the national inventory and are nearing the end of their originally intended design life. Field inspections in Oregon revealed large numbers of these bridges exhibit significant diagonal cracks in the girders and bent caps [ODOT 2002]. Over-estimation of the concrete contribution to shear resistance during design, reduced anchorage requirements for flexural steel, increasing service load magnitudes and volumes, as well as shrinkage and temperature effects, may contribute to diagonal cracking of bridge members. With the large population of cracked bridges and limited resources available for replacement, effective repair methods are needed. Many strengthening techniques for RC elements have been studied, including externally bonded steel plates, post-tensioning, internal and external stirrups as well as many others. Externally bonded carbon fiber-reinforced polymers (CFRP) are becoming more widely accepted for the repair and strengthening of RC members. CFRP materials possess many unique properties: they offer high strength for low weight, are relatively simple to apply, can be installed quickly and tend to have lower labor costs [Bakis *et al*. 2002].

BACKGROUND

Research on the use of externally bonded CFRP for RC beam strengthening began at the Swiss Federal Laboratories for Materials Testing and Research (EMPA) in 1984 [Meier *et al*. 1993]. This research focused mainly on the flexural strengthening of RC beams,

although several findings pertinent to shear strengthening were made. CFRP debonding

from concrete was first observed and U-wraps were developed for shear. This research

was conducted on moderately scaled laboratory beams and in-service structures.

In North America, externally bonded CFRP U-wraps are commonly designed with the ACI

440.2R-02 [2002] design code. A survey of transportation officials from 27 US states and

Canadian provinces found that 10 states and 2 provinces had used FRP for shear

strengthening [Higgins *et al*. 2006]. Of those 12 states and provinces, 4 had used ACI

440.2R-02 for design.

ACI 440.2R-02 Design Provisions

The ACI design code for externally bonded CFRP for shear applications is based largely

upon the results of small-scale tests. ACI 440.2R-02 references several researchers that

have demonstrated RC beams partially-wrapped with CFRP possessed increased shear

strengths [Malvar *et al*. 1995, Chajes *et al*. 1995, Sato *et al*. 1996, Norris *et al*. 1997,

Kachlakev and McCurry 2000].

Malvar *et al*. [1995] tested a total of 6 rectangular beams without transverse steel

reinforcement. Two of those beams were reinforced for shear by FRP jackets. These

beams had effective depths, d, of 133 mm (5.25 in.), flexural-tension steel reinforcement

ratios, ρ_s, of 0.00838 and overall lengths, L, of 1676 mm (66 in.). Chajes *et al*. [1995]

developed an equation for FRP shear contribution based on tests of 12 T-beams without

transverse steel reinforcement. Eight of those beams were reinforced for shear with

continuous FRP U-jackets. These beams had d = 152 mm (6 in.), ρ_s = 0.0207 and L = 1219

mm (48 in.). Sato *et al*. [1996] tested 6 rectangular beams without transverse steel

reinforcement. Five of those beams were reinforced for shear with discrete or continuous

side-bonded and U-jacketed FRP. These beams had d = 260 mm (10.2 in.), ρ_s = 0.0328

and L = 2200 mm (86 in.). Norris *et al*. [1997] tested 6 rectangular beams with transverse

steel reinforcement that were precracked before 5 were strengthened for shear with FRP U-

jackets. These beams had d = 163 mm (6.4 in.), ρ_s = 0.0193 and L = 1219 mm (48 in.).

Kachlakev and McCurry [2000] tested 4 rectangular beams without transverse steel

reinforcement. Two of these beams were reinforced for shear by FRP U-jackets. These

beams were designed to have the same capacity as a specific bridge that had been repaired

with FRP in the field. These beams had d = 704 mm (27.7 in.), ρ_s = 0.00542 and 0.00806

(tension steel was transitioned into the compression zone) and L = 6096 mm (240 in.).

Many different approaches were developed to predict FRP shear contribution during the

late 1990s [Triantafillou 1998, Khalifa *et al*. 1998], and were calibrated with some of the

ACI referenced research. These methods treated external FRP reinforcement analogously

to internal steel reinforcement and assumed that the FRP contribution could be added to

existing ACI concrete and steel contributions. Design equations were based upon strain in

the FRP, which were limited to account for premature debonding failures. The total shear

capacity was limited by the failure of a concrete strut in compression. The design methods

presented by Triantafillou [1998] and Khalifa *et al*. [1998] were calibrated using test

specimens with effective depths no greater than 0.36 m (14 in).

Khalifa *et al*. [1998] applied bond strength models based upon material tests [Horiguchi

and Saeki 1997, Maeda *et al*. 1997] to limit the strain in the FRP at failure. Horiguchi and

Saeki [1997] determined that different FRP-to-concrete bond tests provided different estimates of bond strength. Relationships between concrete compressive strength and bond strength were developed for each test. Maeda *et al*. [1997] determined through material tests that FRP bond strength was dependent on an effective bond length. The ultimate strength of FRP strips of varying bond lengths were the same as long as the actual bond length was longer than the effective bond length.

The ACI 440.2R-02 design code for externally bonded FRP adopted the approach of Triantafillou [1998], Khalifa *et al*. [1998] and others. The code acknowledges the strain limitations used to account for debonding, the use of moderate-scale specimens, the need for realistically scaled tests and an improved design approach. A brief summary of the ACI 440.2R-02 design method for U-wraps follows.

ACI 440.2R-02 limits the ultimate strain of the FRP, ε_{fu}, to an effective strain, ε_{fe}, using a bond-reduction coefficient, κ_v, which is based on the development length, L_e (mm) [in.], and other FRP properties:

$$L_e = \frac{416}{(n\, t_f E_f)^{0.58}} \qquad \text{(10-7) SI} \quad [1]$$

$$L_e = \frac{2500}{(n\, t_f E_f)^{0.58}} \qquad \text{(10-7) US} \quad [2]$$

$$k_1 = \left(\frac{f_c{'}}{254}\right)^{2/3} \qquad \text{(10-8) SI} \quad [3]$$

$$k_1 = \left(\frac{f_c{'}}{4000}\right)^{2/3} \qquad \text{(10-8) US} \quad [4]$$

$$k_2 = \left(\frac{d_f - L_e}{d_f} \right) \qquad \text{(10-9)} \quad [5]$$

$$\kappa_v = \frac{k_1 k_2 L_e}{468 \varepsilon_{fu}} \leq 0.75 \qquad \text{(10-10)} \quad [6]$$

$$\varepsilon_{fe} = \kappa_v \varepsilon_{fu} \leq 0.004 \qquad \text{(10-6b)} \quad [7]$$

where n = number of FRP layers, t_f = FRP thickness (mm) [in.], E_f = FRP elastic modulus

(GPa) [ksi], f_c' = concrete compression strength (MPa) [psi] and d_f = depth of FRP

reinforcement (mm) [in.].

ACI 440.2R-02 treats the FRP analogously to internal steel reinforcement to calculate its

shear contribution, V_f, with the exception of the limited effective strain for debonding

failure:

$$A_{fv} = 2n t_f w_f \qquad \text{(10-4)} \quad [8]$$

$$f_{fe} = \varepsilon_{fe} E_f \qquad \text{(10-5)} \quad [9]$$

$$V_f = \frac{A_{fv} f_{fe} (\sin \alpha + \cos \alpha) d_f}{s_f} \qquad \text{(10-3)} \quad [10]$$

where w_f = FRP strip width (mm) [in.], f_{fe} = effective FRP strength (MPa) [ksi], A_{fv} = area

of FRP shear reinforcement (mm^2) [in.^{2}], α = FRP strip orientation from horizontal axis (˚)

and s_f = FRP strip spacing (mm) [in.].

ACI 440.2R-02 takes a reduced FRP shear contribution, $\psi_f V_f$ (N) [lb], and combines it with

the concrete, V_c (N) [lb], and steel, V_s (N) [lb], shear contributions from ACI 318-05 with

reinforcement limits:

$$\phi V_n = \phi\left(V_c + V_s + \psi_f V_f\right) \qquad\qquad (10\text{-}2) \quad [11]$$

$$V_s + V_f \leq 0.66\sqrt{f_c{}'}b_w d \qquad\qquad (10\text{-}11)\text{SI} \quad [12]$$

$$V_s + V_f \leq 8\sqrt{f_c{}'}b_w d \qquad\qquad (10\text{-}11)\text{US} \quad [13]$$

where $f_c{}'$ = concrete compression strength (MPa) [psi], b_w = beam width (mm) [in.] and d =

effective depth (mm) [in.]. The reduction factor for shear, ϕ, is equal to 0.85, as stated in

ACI 318-05. The additional reduction factor for FRP, ψ_f, is equal to 0.85 for U-wrapping.

The ACI 318-05 concrete shear contribution for members subjected to shear and flexure is

expressed in Eqn. (11-3) US:

$$V_c = 2\sqrt{f_c{}'}b_w d \qquad\qquad [14]$$

The ACI 318-05 transverse steel shear contribution is expressed in Eqn. (11-15) US:

$$V_s = \frac{A_v f_{yt} d}{s} \qquad\qquad [15]$$

where A_v = area of transverse steel reinforcement (mm^2) [in.^{2}], f_{yt} = transverse steel yield

strength (MPa) [ksi] and s = spacing (mm) [in.].

Testing of five full-scale beams repaired with CFRP indicated that the ACI approach

provided conservative shear capacity predictions for T-beams and less conservative shear

capacity predictions for inverted T-beams [Higgins *et al*. 2006]. For a consistent level of

reliability, Higgins *et al*. [2006] recommended a reduction factor of 2 when CFRP strips

are anchored in flexural-tension zones. T-beams had d = 1115 mm (43.9 in.), ρ_s = 0.0152

and L = 7925 mm (312 in.). Inverted T-beams had d = 1151 mm (45.3 in.), ρ_s = 0.0148 and

$L = 7925$ mm (312 in.). Higgins *et al*. [2006] cautioned that the effect of scale on RC

beams was not well understood.

Scale Effect in RC Beams

Kani [1967] noted that then-current ACI shear design provisions were based upon beam

tests with depths less than 380 mm (15 in.) and did not consider strength reduction at larger

scales. Kani [1967] believed that increasing the effective depth would reduce beam

capacity and he developed a series of tests using RC beams with no transverse steel

reinforcement, regularly varying depths and consistent flexural reinforcement ratios to

demonstrate this concept. Kani [1967] also observed that beam behavior depended heavily

on the shear span-to-depth ratio, *a/d*, when all other properties remained constant, and that

beam width had no significant effect on relative beam strength.

Kuchma *et al*. [1997] determined through RC beam tests found in the literature, mostly

without transverse steel reinforcement, that the scale effect on shear capacity was related to

the distance between layers of longitudinal reinforcement. Kuchma *et al*. [1997] stated that

members of any height with equally spaced layers of longitudinal reinforcement failed at

about the same shear stress. Increasing the longitudinal reinforcement ratio, ρ_s, was found

to reduce crack widths and increase shear capacity.

Angelakos *et al.* [2001] described the results from 21 tests of large-scale, lightly reinforced

concrete members. The tests indicated that concrete cylinder strength had little effect on

shear capacity while increased longitudinal reinforcement ratios and the presence of

transverse steel reinforcement increased capacity. Angelakos *et al.* [2001] stated that the

ACI method overestimated the shear capacity of large beams when minimum stirrups were provided and recommended the use of AASHTO LRFD shear design provisions, which were developed using modified compression field theory (MCFT) and provided more consistent results.

Tompos and Frosch [2002] tested six full- and half-scale beams with effective depth, length and width scaled geometrically, having constant longitudinal steel reinforcement ratios and d/s, and constructed from a single batch of concrete and consistent heats of reinforcing steel. Tompos and Frosch [2002] used the results from these tests with additional results from the literature to draw conclusions about the effect of scale on RC beam shear capacity. It was concluded that ACI overestimated the concrete shear contribution, which is not influenced by shear reinforcement but longitudinal reinforcement. Tompos and Frosch [2002] stated that for values of $\rho_s \leq 1$ %, which are common in design, the actual concrete contribution was less than that predicted by ACI Eqn. (11-3). They also concluded that stirrup shear contribution was determined by its location relative to the failure diagonal crack, the number of stirrups crossing the failure diagonal crack and the stirrup development length.

The literature on scale effects in RC beams emphasizes that the ACI shear contribution predictions are not consistent for beams with effective depths larger than those on which the code was based. Shear capacity in RC beams has been correlated to effective depth, a/d ratio and the amount of longitudinal reinforcement. Scaled beam tests from the literature were used to guide the design of CFRP strengthened specimens in this project.

RESEARCH SIGNIFICANCE

The current provisions of ACI 440.2R-02 for shear strengthening were developed using experimental results from small-sized specimens. Small-scale reinforced concrete (RC) beams repaired with externally bonded carbon fiber-reinforced polymers (CFRP) would be preferable for experimental studies since more tests could be conducted than with full-scale beams given the same level of resources. Each small-scale beam would require less construction time, fewer materials and smaller load frames with lower capacities, which would facilitate testing at more laboratories. Conditioning time for environmental durability studies would be greatly reduced since more specimens could fit into a climatic chamber and it would take less time to cycle the temperature regime of the concrete.

Unfortunately, the effect of scale is not well understood for CFRP applications to RC beams. The results from small-scale testing may not be directly extrapolated to full-scale beams. This paper describes an experimental program for six RC beams strengthened for shear with externally bonded CFRP at three geometric scales and offers recommendations for further research.

EXPERIMENTAL PROGRAM

Test Specimens[1]

Six specimens at three scales (F = full, H = half, and Q = quarter scale) were used in a

series of eight tests to characterize the behavior of CFRP shear strengthened RC beams.

Overall height, width and length of the specimens were scaled geometrically, as shown in

Table 1. Schematics of specimen elevations and sections may be found in Figs. 1 and 2.

Table 1: Specimen dimensions, effective depths and steel reinforcement ratios.

Scale	L (mm) [in.]	b_w (mm) [in.]	h (mm) [in.]	d (mm) [in.]	ρ_s	ρ_v
F	7920 [312]	356 [14]	1070 [42]	937 [36.9]	0.0134	0.00238
H	3960 [156]	178 [7]	533 [21]	464 [18.3]	0.0138	0.00238
Q	1980 [78]	88.9 [3.5]	267 [10.5]	238 [9.38]	0.0136	0.00238

The relatively small flexural reinforcing steel ratios were similar to RC bridge beams seen

in practice and were approximately the same at each scale. Longitudinal flexural-tension

steel reinforcement for all specimens consisted of #19 ASTM A615 Grade 420 (#6 Grade

60) bars. Longitudinal compression steel reinforcement for all specimens consisted of #13

ASTM A615 Grade 420 (#6 Grade 60) bars. Longitudinal bars in the full-scale specimens

were bundled in four-bar groups. Transverse steel consisted of #13 ASTM A615 Grade

280 (#4 Grade 40) open stirrups for the full-scale specimens, undeformed 6 mm (#2)

ASTM A36 open stirrups for the half-scale and undeformed 6 mm (#2) ASTM A36

alternating single leg stirrups for the quarter-scale. Reinforcing steel was fabricated by a

local rebar fabricator and the materials were from the same heats for all the different scales.

---

[1] A more in-depth discussion of scaling for test specimens may be found in Appendix A.

d = 937 mm [36.9 in]

610 mm [24 in]

Shear span, *a*

L = 7920 mm [312 in]
Specimen FT10

d = 238 mm [9.38 in]

152 mm [6 in]

L = 1980 mm [78 in]
Specimen QT

d = 464 mm [18.3 in]

305 mm [12 in]

L = 3960 mm [156 in]
Specimen HT2.5
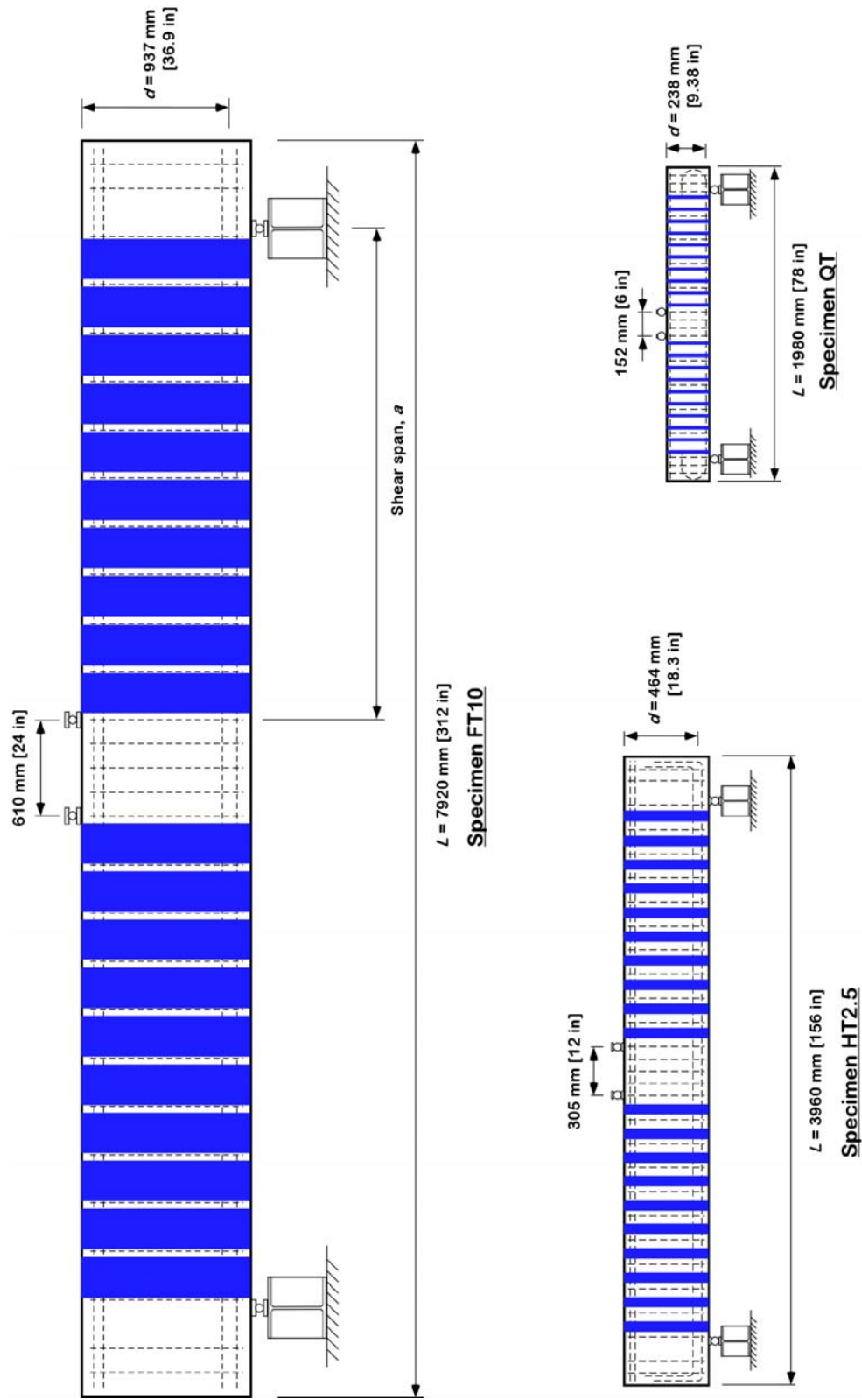
Fig. 1 – Elevation views of specimens FT10, HT2.5 and QT.

(16) #13 A615 Gr. 420
[(16) #4 Gr. 60]

Closed Stirrup
#13 A615 Gr. 280 @ 305 mm (typ.)
[#4 Gr. 40 @ 12 in]

Wabo® MBrace CF130
(1) ply
w_f = 254 mm [10 in]
s_f = 305 mm [12 in]

(16) #19 Gr. 420
[(16) #6 Gr. 60]

Specimen FT10

(4) #13 Gr. 420
[(4) #4 Gr. 60]

Wabo® MBrace CF130
(1) ply
w_f = 64 mm [2.5 in]
s_f = 152 mm [6 in]

Closed Stirrup
#6 A36 @ 152 mm (typ.)
[#2 A36 @ 6 in]

(4) #19 Gr. 420
[(4) #6 Gr. 60]

Specimen HT2.5

(1) #13 Gr. 420
[(1) #4 Gr. 60]

Wabo® MBrace CF130
(1) ply
w_f = 16 mm [0.625 in]
s_f = 76 mm [3 in]

Alternating Single Leg
#6 A36 @ 152 mm (typ.)
[#2 A36 @ 6 in]

(1) #19 Gr. 420
[(4) #6 Gr. 60]

Specimen QT

Fig. 2 – Cross-sectional views of specimens FT10, HT2.5 and QT.

Actual steel reinforcing properties were determined from tensile tests per ASTM A 370

and ASTM E 8. Three 406 mm (16 in.) long samples were cut from each material and

tested with a 489 kN (110 kip) universal testing machine. Tensile specimens were tested

with constant head speeds of 0.0169 mm/sec (0.000667 in./sec) for #13 (#4) and #19 (#6)

bars and 0.0141 mm/sec (0.000556 in./sec) for #6 (#2) bars. Strain was measured using a

class B1 extensometer with 50 mm (2 in.) gage length. Data were recorded at a frequency

of 10 Hz using commercially available data acquisition software. Measured steel

properties are given in Table 2.

Table 2: Reinforcing steel properties.

Material	Bar Size (mm) [in.]	Grade (MPa) [ksi]	f_y (MPa) [ksi]	f_{ult} (MPa) [ksi]
F Stirrups	#13 [#4]	A615 Gr. 280 [Gr. 40]	326 [47.3]	529 [76.7]
H and Q Stirrups	#6 [#2]	A36	308 [44.6]	443 [64.3]
Compr. Steel	#13 [#4]	A615 Gr. 420 [Gr. 60]	453 [65.7]	752 [109]
Flexural Steel	#19 [#6]	A615 Gr. 420 [Gr. 60]	402 [58.3]	680 [98.6]

Concrete was delivered to the laboratory by a local ready-mix supplier. A single concrete

mix design was used for all test specimens, which were cast simultaneously. The concrete

mix was designed to have properties similar to 1950s vintage concrete, specifically a lower

compression strength and lack of admixtures. Target 28-day compression strength was

20.7 MPa (3000 psi) and the maximum aggregate size was 13 mm (0.5 in.). Actual 28-day

cylinder compression strength was 27.8 MPa (4030 psi). Results from cylinder

compression and split tensile tests taken at the day of test for each specimen are shown in

Table 3.

Table 3: Concrete cylinder properties at time of specimen tests.

Specimen	f'_c (MPa) [psi]	f_t (MPa) [psi]
FC	32.1 [4660]	2.65 [385]
FT	33.4 [4850]	2.86 [415]
HC	32.8 [4760]	2.79 [405]
HT	33.7 [4890]	2.79 [405]
QC	34.6 [5020]	2.93 [425]
QT	34.6 [5020]	2.93 [425]

All specimens were strengthened with externally bonded CFRP strips in a U-wrap

configuration. This configuration was chosen as it represents the most likely bridge retrofit

condition, *i.e.* where full wrapping is prohibited by the deck. Specimens with labels

ending in "T" had CFRP strips with the free edge in the tension zone (T = tension zone),

while labels ending in "C" had CFRP strips with the free edge in the compression zone (C

= compression zone). The free edge terminating in the tension zone simulated an

application in a negative moment region for a continuous bridge girder (*i.e.* span near

continuous support). The free edge in the compression zone simulated an application in a

positive moment region for a bridge girder (*i.e.* near an abutment or joint).

A number following the two-letter designation indicates the width of fabric in inches for

specimens tested twice (*i.e.* FT10, FT5, HT5, HT2.5). CFRP strip widths were reduced by

manually removing portions. CFRP strip widths and reinforcement ratios for each

specimen are provided in Table 4.

Table 4: CFRP reinforcement ratios.

Specimen	w_f (mm) [in.]	ρ_f
FC	254 [10]	0.00238
FT10	254 [10]	0.00476
FT5	127 [5]	0.00238
HC	127 [5]	0.00952
HT5	127 [5]	0.00952
HT2.5	64 [2.5]	0.00476
QC	16 [0.625]	0.00476
QT	16 [0.625]	0.00476

The RC beams were cured for three months before CFRP was applied. Application involved several steps, illustrated by Fig. 3(a) – (f), in accordance with the manufacturer's product specifications [Watson Bowman Acme 2002]. All of the CFRP materials were provided by the Watson Bowman Acme Corporation (BASF) and consisted of the Wabo® MBrace CF130 unidirectional high strength carbon fiber fabric, low viscosity epoxy primer, high viscosity epoxy paste ("putty") and epoxy encapsulation resin ("saturant").

The RC beams were first ground to remove the surface layer of material (Fig. 3(a)). Heated tents were constructed around the specimens to raise their temperature before application. The CFRP primer coat was applied with 9.5 mm (3/8 in.) nap rollers to the clean, prepared surface (Fig. 3(b)). Before the primer cured, the putty was applied using drywall taping knives and trowels (Fig. 3(c)). The putty filled surface voids in the concrete. The first coat of saturant was then applied to the surface of the beam using fresh 9.5 mm (3/8 in.) nap rollers once the putty became viscous enough to remain in the concrete voids (Fig. 3(d)). Pre-cut fabric was then placed on the saturant and plastic putty knives were used to thoroughly work the saturant into the fibers (Fig. 3(e)). A final layer of saturant was applied, which helped to further saturate the fibers (Fig. 3(f)).

Fig. 3 – CFRP application process.

After CFRP application, specimens FC and FT were cured for 7 days between 5-15˚C (41-59˚F) with an average temperature of 12˚C (53˚F). Specimens HC, HT, QC and QT were

cured for 7 days between 5-11˚C (41-52˚F) with an average temperature of 8˚C (47˚F).
Curing temperatures were monitored with thermocouples to ensure that the application met
installation specifications. The minimum specified curing temperature was 4˚C (40˚F).
Specimens continued to cure for more than 30 days under ambient laboratory temperatures.

The manufacturer's product information reported an ultimate tensile strength, f_{fu}, of 3800
MPa (550 ksi), a tensile modulus, E_{fu}, of 227 GPa (33,000 ksi) and an ultimate rupture
strain, ε_{fu}, of 1.67% per ASTM D 3039 [Watson Bowman Acme 2003]. Actual CFRP
properties were determined from 30 tensile coupon tests in accordance with ASTM D
3039. Two 457 x 508 mm (18 x 20 in.) CFRP panels were made on the day of CFRP
application. These panels were cured under the same conditions as the half and quarter
scale beams.

Three months after the CFRP application, the panels were cut into thirty 25 x 357 mm (1 x
14 in) tensile coupons with a wet tile saw and 25 x 57 mm (1 x 2.25 in.) tabs cut from
perforated programming board were attached with cyanoacrylate adhesive to make 30
tensile coupons. Coupons were tested with an 89 kN (20 kip) universal testing machine at
constant head speed of 2 mm/min (0.05 in./min). Strain was measured via a class B1
extensometer with 25 mm (1 in.) gage length. Data were recorded at a frequency of 2 Hz
using commercially available data acquisition software. Coupon test results are compared
with the manufacturer's design values in Table 5.

Table 5: Specified and actual CFRP 0˚ tensile properties.

Property	Wabo® Design	Test Mean	Test St. Dev.
Coupon Thickness, t_f **(mm) [in.]**	0.6 – 1.0 [0.02 – 0.04]	1.16 [0.0458]	0.314 [0.0124]
Tensile Strength, f_{fu} (MPa) [ksi]	625 – 1042[a] [89 – 179]	725 [105]	218 [31.6]
Unit Stress, $f_{fu}t_f$ (kN/mm/ply) [kip/in./ply]	0.625 [3.57]	0.777 [4.44]	0.0422 [0.241]
Elastic Modulus, E_f (GPa) [ksi]	37.4 – 62.4[a] [5300 – 10700]	36.6 [5300]	9.34 [1350]
Rupture Strain, ε_{fu} (%)	1.67	1.97	0.161
Nom. Fabric Thickness, t_f* **(mm) [in.]**	0.165 [0.0065]	n/a	n/a
Tensile Strength, f_{fu}* (MPa) [ksi]	3800 [550]	4720 [684]	253 [36.7]
Elastic Modulus, E_f* (GPa) [ksi]	227 [33000]	241 [35000]	16.5 [2390]

a: values not provided; calculated with other given values
*: values based on nominal fabric thickness

After structural testing of the specimens was completed, direct tension pull-off tests per

ASTM D 4541 were performed on intact CFRP strips. A 16 kN (3600 lb) capacity

portable adhesive strength tester with digital manometer was employed. Square steel

dollies with a surface area of 2580 mm^2 (4 in.^{2}) were bonded to the clean, prepared CFRP

surfaces and allowed to cure for 24 hours. The CFRP to be tested was cut flush to the

edges of the dolly using a high-speed abrasive cutting wheel. The dolly was pulled with

the portable tester and maximum load was recorded. Dimensions of the dolly were

measured using calipers. Bond strengths were found by dividing the maximum load by the

cross-sectional area of the dolly.

Bond strengths for each specimen were averaged from at least three tests that resulted in

cohesive failures in the surface layer of the concrete. Two cohesive failures in concrete

bonded to CFRP are shown in Fig. 4. Pull-off test results are shown in Table 6. Product

specifications required a minimum bond strength of 1.4 MPa (200 psi) [Watson Bowman

Acme 2002].

Fig. 4 – Cohesive failure of concrete surface bonded to CFRP caused by direct-tension

pull-off tests.

Table 6 – Bond strengths of CFRP.

Specimen	Mean f_{bond} (MPa) [psi]	St. Dev.
FC	3.46 [503]	0.593 [86.1]
FT	4.37 [634]	0.646 [93.7]
HC	2.26 [328]	1.01 [147]
HT	3.91 [567]	0.397 [57.5]
QC	3.27 [474]	0.0383 [5.55]
QT	3.04 [441]	0.657 [95.2]

Instrumentation

Typical instrumentation applied to the test specimens is shown schematically in Fig. 5.

Reinforcing steel bars and CFRP strips were instrumented with general purpose strain

gages. CEA-06-125UN-120 gages were affixed to the #13 (#4) and #19 (#6) bars. EA-06-

015DJ-120/LE gages were affixed to #6 (#2) stirrups. CFRP strips were instrumented with

either N2A-06-20CBW-120 or EA-06-20CBW-120 gages. Gages on the CFRP strips had

a 50 mm (2 in) length, which allowed for strain averaging.
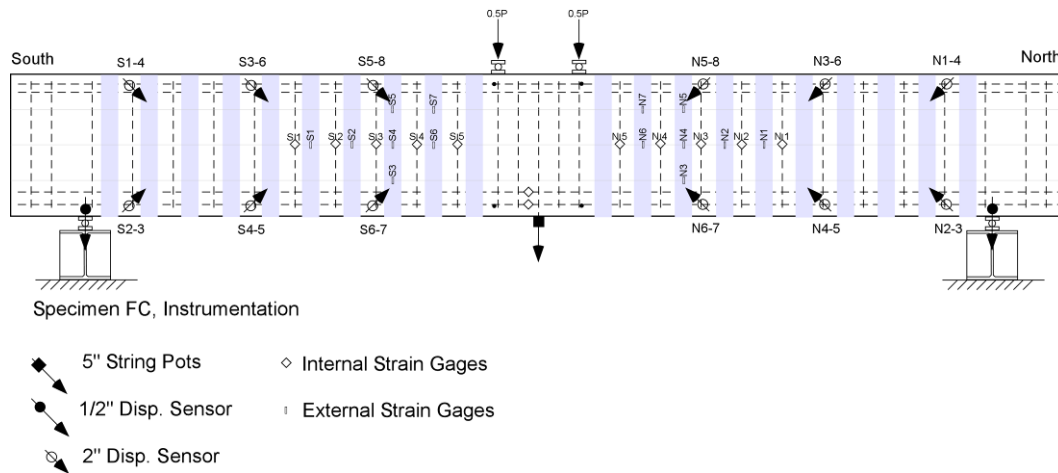
Fig. 5 – Specimen FC instrumentation (typical).

Mid-span displacements were measured with 127 mm (5 in.) range string potentiometers,

diagonal displacements were measured with 51 mm (2 in.) range string potentiometers and

support settlements were measured with 13 mm (0.5 in.) range displacement sensors.

Support settlements, which represent rigid body motion of the specimen at the supports,

were averaged and subtracted from the mid-span displacement to reveal the specimen

deformation.

Actuators were equipped with load cells rated for 2450 kN (550 kips) and 1110 kN (250 kips) at the full and smaller scales, respectively.

The actuator load cells, strain gages, string potentiometers and displacement sensors were connected to a high-speed, multi-channel, 16-bit data acquisition system. The system recorded sensor readings and converted signals into corresponding forces, strains and displacements. Data from sensors were archived for retrieval and post-processing.

The widths of diagonal cracks for specimens FC, QT and QC were measured visually with a crack comparator.

Test Protocol

Specimens were tested in a four-point bending setup using multiple load steps, which involved moving the supports inward at regular intervals of *a/d*, as described in Table 7. Moving the supports allowed for greater shear-to-moment ratios, *V/M*, precluding flexural failure until the eventual failure in a shear dominant mode. Load points remained in the same position for all load steps, creating a small constant moment region with no shear. Shear and moment diagrams for this test setup are shown in Fig. 6. Load points were centered on the reinforcing steel at 610 mm (24 in.), 305 mm (12 in.) and 153 mm (6 in.) apart, respectively, for the full, half and quarter scale specimens.

Table 7: Shear-span-to-depth ratios (*a/d*) for load steps.

Load Step	0	1	2	3	4	5
a/d	3.3	3.0	2.5	2.0	1.5	1.0
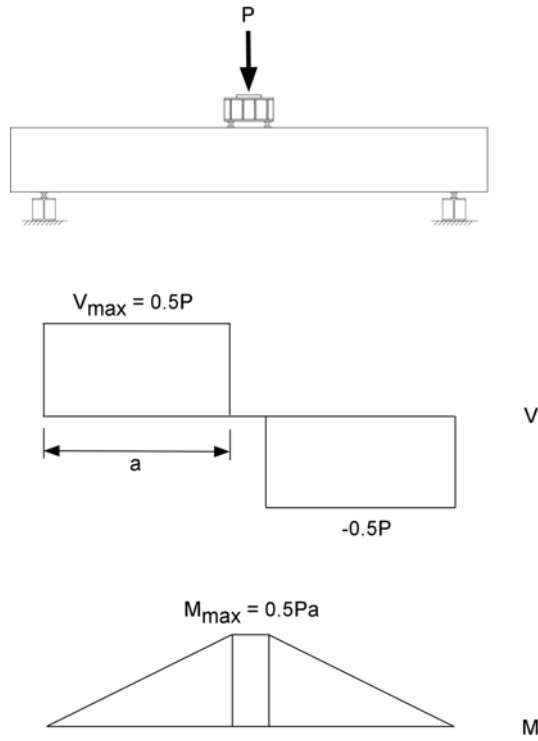
Fig. 6 – Shear and moment diagrams for test setup at all scales.

For each load step, the specimen was loaded to approximately 95% of the expected flexural capacity. Expected flexural capacities were found by increasing the calculated ACI nominal moment capacity by 20%, as described by Eqns. 16 and 17. A test of specimen HC well past flexural yielding and prior to concrete crushing indicated that the member capacity was approximately 20% greater than nominal capacity.

$$M_{max} = 1.2M_n \tag{16}$$

$$P_{max} = \frac{2M_{max}}{a} \tag{17}$$

Due to the large differences in the sizes of test specimens, three loading frames were used for this research. The loading frames are shown schematically in Fig. 7. Full scale specimens were tested with a 2224 kN (500 kip) capacity hydraulic actuator. Half and quarter scale specimens were tested with a 890 kN (200 kip) capacity hydraulic actuator. The 2224 kN (500 kip) actuator was operated under closed loop servo-hydraulic force control. The 890 kN (200 kip) actuator was operated manually with a hand pump. Lateral bracing was provided at the support locations for the full and half scale specimens, but was not practical for the quarter scale because of the small specimen size.
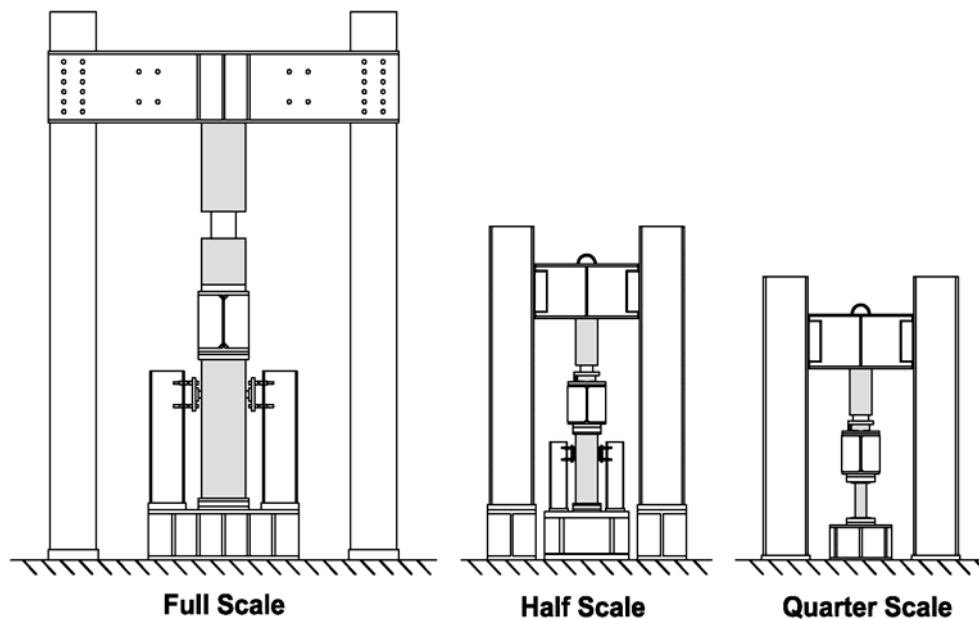
Fig. 7 – Loading frames for full, half and quarter scale beams.

Detailed descriptions of the test protocol for each specimen, including values of applied

shear, mid-span displacement as well as crack propagation and debonding observations,

follow.

Specimen FC

Specimen FC underwent a total of 8 load steps, as shown in Fig. 8 and Table 8, with CFRP

strip widths of 127 mm (5 in.) in the U-wrap configuration.
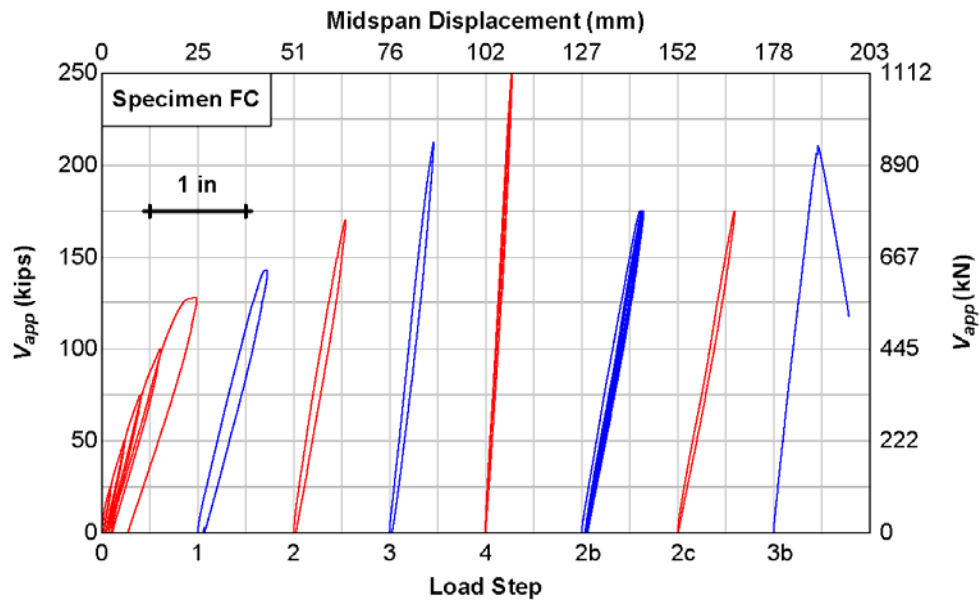
Fig. 8 – Shear versus displacement for Specimen FC.

During load step 0 (a/d = 3.3), the specimen was loaded cyclically to 222, 445, 667, 890

and 1139 kN (50, 100, 150, 200 and 256 kips). The largest measured diagonal crack width

during load step 0 was 0.51 mm (0.020 in.). The maximum applied force of 1139 kN (256

kip) approached the flexural capacity of the specimen at this support configuration. Thus,

the specimen was unloaded and the supports were moved inward to allow continued testing

for shear. Instruments were zeroed for the new specimen configuration. Support locations

and mapped crack observations for all Specimen FC load steps are shown in Fig. 9.

During load step 1 (a/d = 3.0), the specimen was loaded monotonically to 1272 kN (286

kips). The largest measured diagonal crack width was 0.76 mm (0.030 in.). The maximum

applied force approached the flexural capacity of the specimen at this support

configuration. Thus, the specimen was unloaded and the supports were moved inward to

allow continued testing for shear. Instruments were zeroed for the new specimen

configuration.

During load step 2 (a/d = 2.5), the specimen was loaded monotonically to 1512 kN (340

kips). Load step 2 saw no wider diagonal cracks than previously recorded. The maximum

applied force approached the flexural capacity of the specimen at this support

configuration. Thus, the specimen was unloaded and the supports were moved inward to

allow continued testing for shear. Instruments were zeroed for the new specimen

configuration.

During load step 3 (a/d = 2.0), the specimen was loaded monotonically to 1886 kN (424

kips). The largest measured diagonal crack width was 1.02 mm (0.040 in.). The maximum

applied force approached the flexural capacity of the specimen at this support

configuration. Thus, the specimen was unloaded and the supports were moved inward to

allow continued testing for shear. Instruments were zeroed for the new specimen
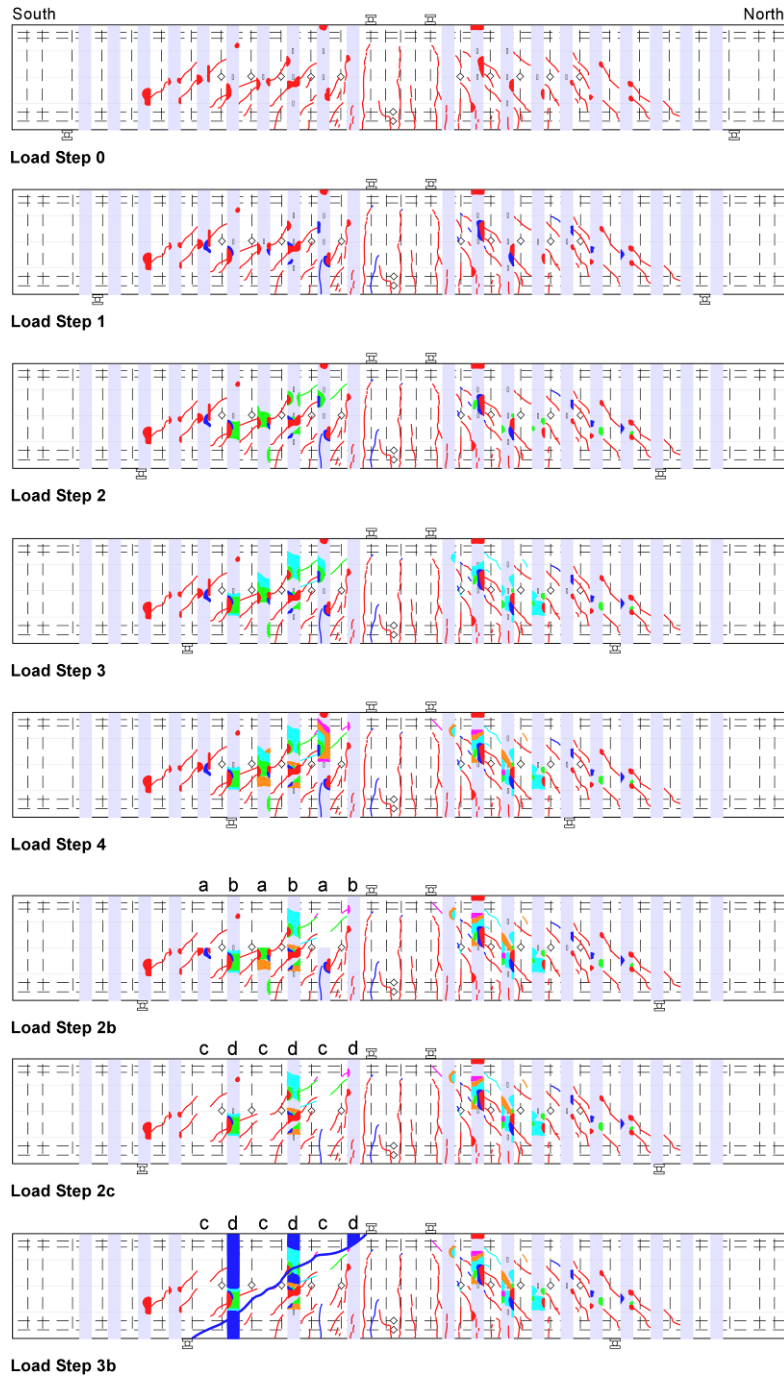
configuration.

a: strip removed to mid-height on east face.
b: strip removed to mid-height on west face.
c: strip removed on east face.
d: strip removed on west face

Fig. 9 – Specimen FC crack observations, support configurations and strain gage locations.

During load step 4 ($a/d = 1.5$), the specimen was loaded to the maximum actuator force of 2224 kN (500 kips) twice, in an effort to produce failure. The largest measured diagonal crack width during load step 4 was 1.27 mm (0.050 in.).

As the limit of the actuator was met during load step 4, the supports were moved back to an $a/d = 2.5$ and alternating strips in the south shear span were manually removed from the top of the beam down to mid-height. This test configuration is called load step 2b, which indicates the second loading at the load step 2 support location ($a/d = 2.5$).

Before load step 2b, the fifth, seventh and ninth strips from the south end of the specimen were debonded to mid-height on the east face. The sixth, eighth and tenth strips were debonded to mid-height on the west face. During load step 2b ($a/d = 2.5$), the specimen was loaded to 1557 kN (350 kips) four times, in an effort to produce shear failure. This repeated loading did not succeed in producing failure.

For load step 2c ($a/d = 2.5$), strips that had been manually debonded to mid-height were then debonded over the full height of the beam and the specimen was loaded to 1557 kN (350 kips). Failure did not occur during this load step.

Specimen FC was finally failed in shear during load step 3b ($a/d = 2.0$) with an applied force of 1868 kN (420 kips). After failure, CFRP strips in the south span were observed to be debonded, a large diagonal crack extended through the compression zone and some stirrups were fractured.

Table 8: Specimen FC loading summary.

Load Step	a/d	Loading Type	V_{app} (kN) [kips]	C.L. Disp. @ V_{app} (mm) [in.]	Max. Measured Diagonal Crack Width (mm) [in.]
0	3.3	5 cycles	569 [128]	25 [0.98]	0.51 [0.020]
1	3.0	monotonic	636 [143]	18 [0.72]	0.76 [0.030]
2	2.5	monotonic	756 [170]	14 [0.54]	0.76 [0.030]
3	2.0	monotonic	943 [212]	11 [0.45]	1.02 [0.040]
4	1.5	2 cycles	1112 [250]	6.9 [0.27]	1.27 [0.050]
2b	2.5	4 cycles	778 [175]	16 [0.64]	-
2c	2.5	monotonic	778 [175]	15 [0.59]	-
3b	2.0	monotonic	934 [210]	12 [0.46]	-

Specimen FT10

Specimen FT underwent 5 load steps, as shown in Figs. 10 and 11 and Table 9, with CFRP strip widths of 254 mm (10 in) in the inverted U-wrap configuration.
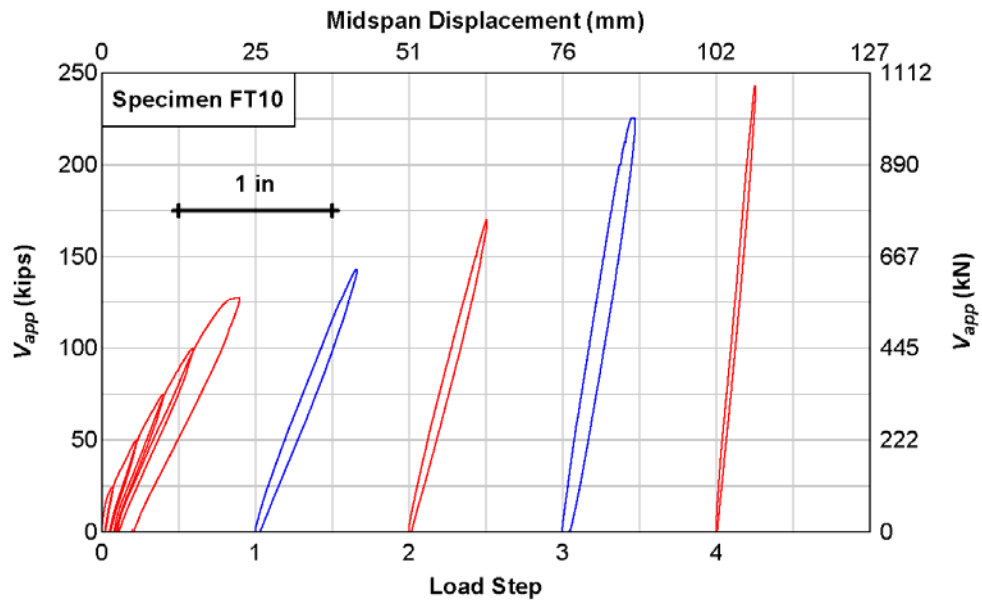
Fig. 10 – Shear versus displacement for Specimen FT10.

South   North

Load Step 0

Load Step 1

Load Step 2

Load Step 3
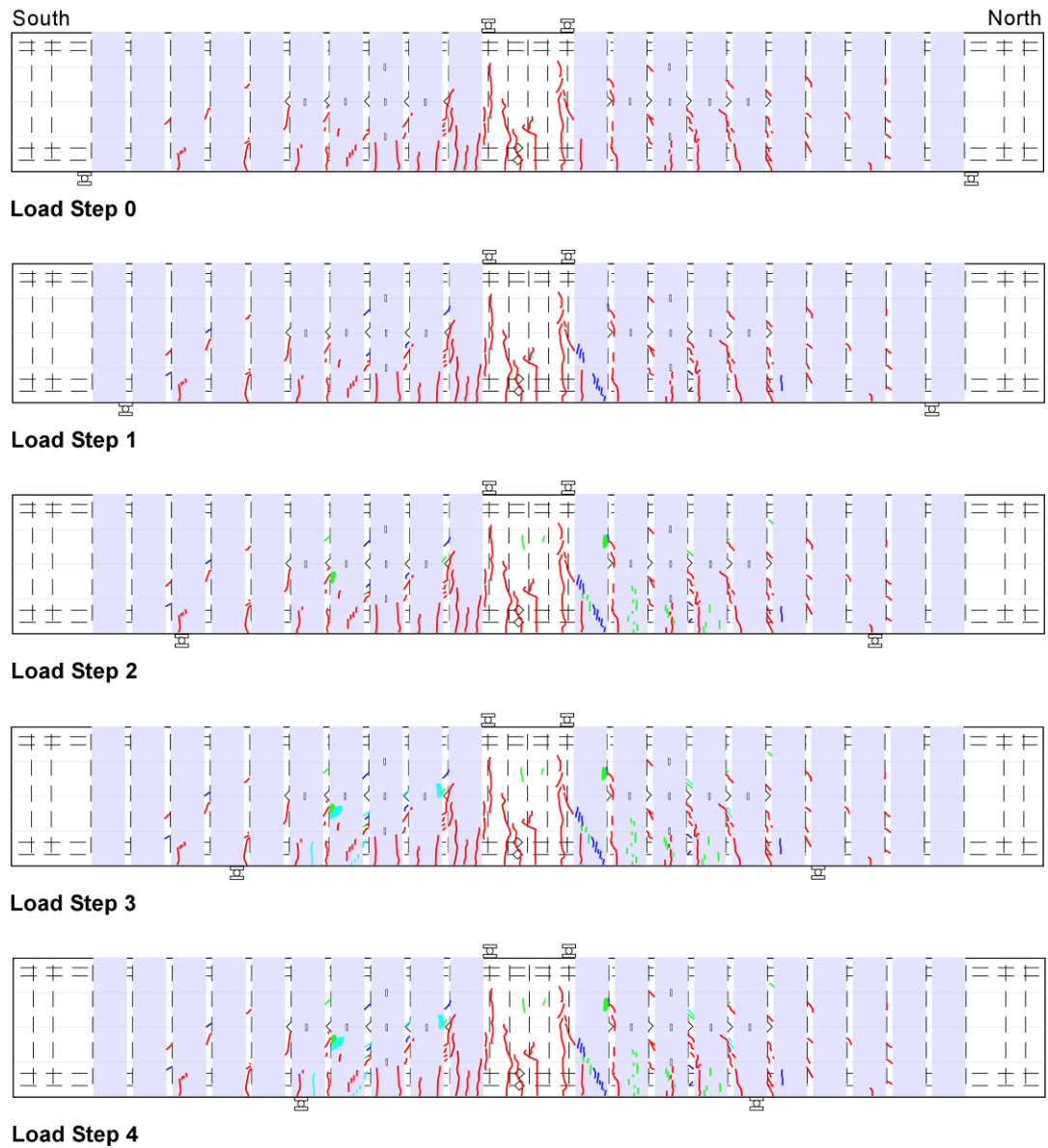
Load Step 4

Fig. 11 – Specimen FT10 crack maps and strain gages.

During load step 0 (*a/d* = 3.3), the specimen was loaded cyclically to 222, 445, 667, 890 and 1139 kN (50, 100, 150, 200 and 256 kips). The maximum applied force of 1139 kN (256 kip) approached the flexural capacity of the specimen at this support configuration.

Thus, the specimen was unloaded and the supports were moved inward to allow continued testing for shear. Instruments were zeroed for the new specimen configuration.

After each load step that did not produce a shear failure, the supports were moved inward and instruments were zeroed.

During load step 1 ($a/d = 3.0$), the specimen was loaded monotonically to 1272 kN (286 kips). During load step 2 ($a/d = 2.5$), the specimen was loaded monotonically to 1512 kN (340 kips). During load step 3 ($a/d = 2.0$), the specimen was loaded monotonically to 2002 kN (450 kips). During load step 4 ($a/d = 1.5$), the specimen was loaded to 2162 kN (486 kips). This was believed to be the maximum actuator force until the hydraulic line pressure was increased during a later test.

As the limit of the actuator was approached during load step 4, the supports were moved back to an $a/d = 2.5$ and the CFRP strip widths were reduced to 127 mm (5 in). The specimen was retested as Specimen FT5.

Table 9: Specimen FT10 load summary.

Load Step	a/d	Loading Type	V_{app} (kN) [kips]	C.L. Disp. @ V_{app} (mm) [in.]
0	3.3	5 cycles	569 [128]	23 [0.90]
1	3.0	monotonic	636 [143]	17 [0.66]
2	2.5	monotonic	756 [170]	13 [0.51]
3	2.0	monotonic	1001 [225]	12 [0.46]
4	1.5	monotonic	1081 [243]	6.4 [0.25]

Specimen FT5

Specimen FT5 underwent 10 load steps, as shown in Figs. 12 and 13 and Table 10.
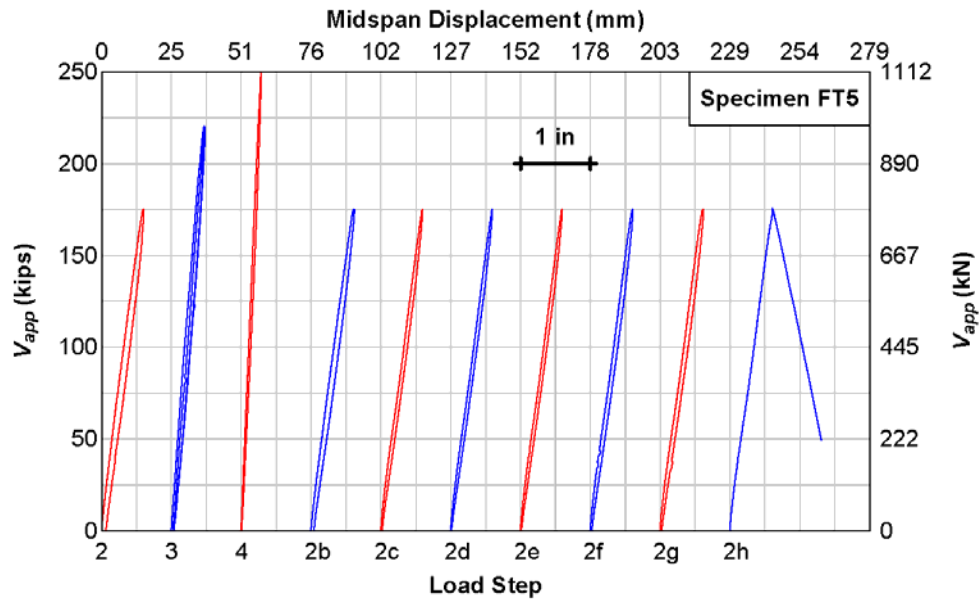
Fig. 12 –Shear versus displacement for Specimen FT5.

During load step 2 (*a/d* = 2.5), the specimen was loaded monotonically to 1557 kN (350 kips). The maximum applied force of 1557 kN (350 kips) approached the flexural capacity of the specimen at this support configuration. Thus, the specimen was unloaded and the supports were moved inward to allow continued testing for shear. Instruments were zeroed for the new specimen configuration.

After each load step that did not produce a shear failure, the supports were moved inward and instruments were zeroed.
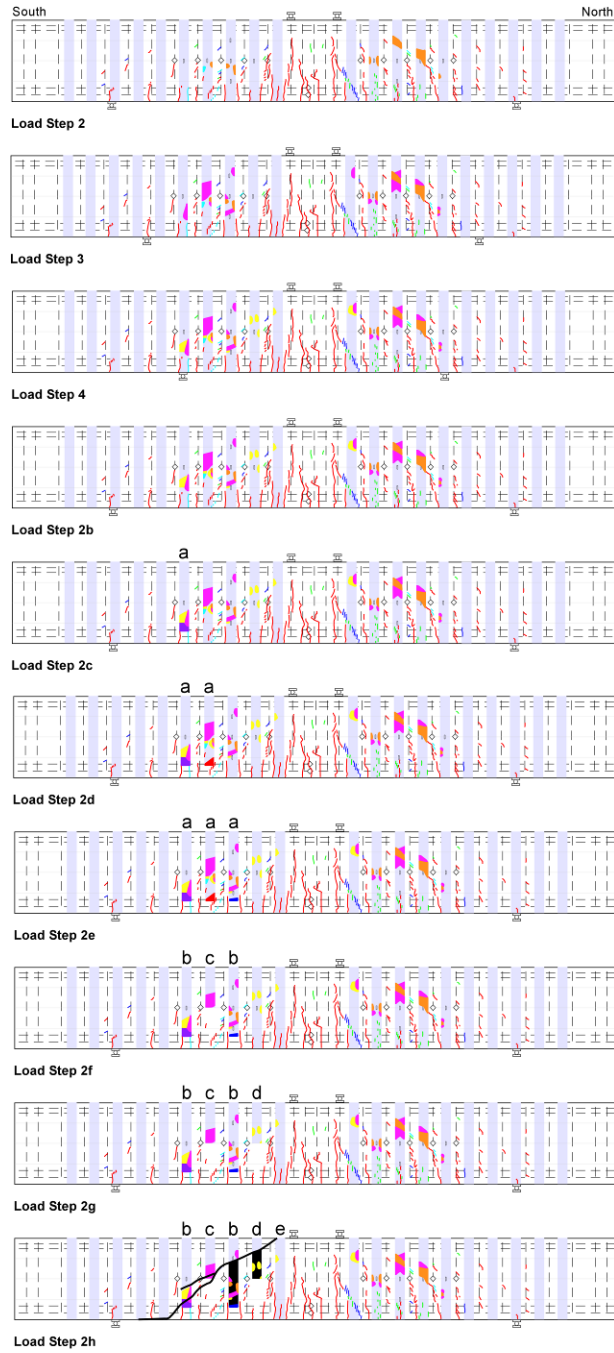
a: 152 mm (6 in) of strip removed from bottom on both faces.
b: strip removed to mid-height on west face, no further removal on east face.
c: strip removed to mid-height on east face, no further removal on west face.
d: strip removed to mid-height on east face, full strip intact on west face.
e: strip removed to mid-height on west face, full strip intact on east face.

Fig. 13 – Specimen FT5 crack maps and strain gages.

During load step 3 (*a/d* = 2.0), the specimen was loaded to 1957 kN (440 kips) twice in an

attempt to cause failure. This was unsuccessful and testing continued at load step 4.

During load step 4 (*a/d* = 1.5), the specimen was loaded to the maximum actuator force of

2224 kN (500 kips).

As the limit of the actuator was met during load step 4, the supports were moved back to an

a/d = 2.5 with the intent to remove CFRP strips gradually over the course of multiple load

steps.

No CFRP strips were removed for load step 2b. This test configuration is called load step

2b because it indicates the second loading at the load step 2 support location (*a/d* = 2.5).

During this load step, the specimen was loaded to 1557 kN (350 kips).

For load step 2c (*a/d* = 2.5), 152 mm (6 in.) were removed from the bottom of the sixth

strip from the south end and the specimen was loaded to 1557 kN (350 kips). For load step

2d (*a/d* = 2.5), 152 mm (6 in.) were removed from the bottom of the seventh strip from the

south end and the specimen was loaded to 1557 kN (350 kips). For load step 2e (*a/d* =

2.5), 152 mm (6 in.) were removed from the bottom of the eighth strip from the south end

and the specimen was loaded to 1557 kN (350 kips).

For load step 2f (*a/d* = 2.5), the CFRP strip was removed to mid-height on the west face for

the sixth and eighth strips from the south end of the specimen and on the east face for the

seventh strip. During this load step the specimen was loaded to 1557 kN (350 kips).

For load step 2g (*a/d* = 2.5), the CFRP strip was removed to mid-height on the east face for the ninth strip from the south end of the specimen. During this load step the specimen was loaded to 1557 kN (350 kips).

For load step 2h (*a/d* = 2.5), the CFRP strip was removed to mid-height on the west face for the tenth strip from the south end of the specimen. During this load step the specimen was loaded to 1557 kN (350 kips). Specimen FT5 was finally failed in shear during this load step. After failure, CFRP strips in the south span were observed to be debonded, a large diagonal crack extended through the compression zone and some stirrups were fractured.

Table 10: Specimen FT5 loading summary.

Load Step	*a/d*	Loading Type	V_{app} (kN) [kips]	C.L. Disp. @ V_{app} (mm) [in.]
2	2.5	monotonic	778 [175]	15 [0.60]
3	2.0	2 cycles	979 [220]	12 [0.47]
4	1.5	monotonic	1112 [250]	7.1 [0.28]
2b	2.5	monotonic	778 [175]	16 [0.62]
2c	2.5	monotonic	778 [175]	15 [0.59]
2d	2.5	monotonic	778 [175]	15 [0.59]
2e	2.5	monotonic	778 [175]	15 [0.59]
2f	2.5	monotonic	778 [175]	15 [0.61]
2g	2.5	monotonic	778 [175]	15 [0.61]
2h	2.5	monotonic	783 [176]	15 [0.61]

Specimen HC

Specimen HC underwent 8 load steps, as shown in Figs. 14 and 15 and Table 11, with

CFRP strip widths of 127 mm (5 in.) in the U-wrap configuration.

Fig. 14 – Force versus displacement for Specimen HC.

During load step 0, the specimen was taken to its flexural capacity, which was indicated by

yielding of the flexural reinforcing steel and excessive mid-span displacement. From this

step, it was determined that the actual moment capacities of these rectangular specimens

were about 20% greater than the calculated ACI nominal moment capacities.

Fig. 15 – Specimen HC crack propagation maps and strain gages.

During load step 0 (*a/d* = 3.3), the specimen was loaded cyclically to 89, 178, 267 and 294

kN (20, 40, 60 and 66 kips). The maximum applied force of 294 kN (66 kips) reached the

flexural capacity of the specimen at this support configuration. Thus, the specimen was

unloaded and the supports were moved inward to allow continued testing for shear.

Instruments were zeroed for the new specimen configuration.

After each subsequent load step that did not produce a shear failure, the supports were

moved inward and instruments were zeroed.

During load step 1 (*a/d* = 3.0), the specimen was loaded monotonically to 267 kN (60

kips). During load step 2 (*a/d* = 2.5), the specimen was loaded monotonically to 294 kN

(66 kips). During load step 3 (*a/d* = 2.0), the specimen was loaded monotonically to 342

kN (77 kips).

The applied forces in load steps 1 – 3 were based upon the nominal moment capacity.

Steps 2 and 3 were repeated as 2b and 3b with higher applied forces, which were based

upon the 20% increase in moment capacity. During load step 2b (*a/d* = 2.5), the specimen

was loaded monotonically to 365 kN (82 kips). During load step 3b (*a/d* = 2.0), the

specimen was loaded monotonically to 467 kN (105 kips).

During load step 4 (*a/d* = 1.5), the specimen was loaded to 618 kN (139 kips). During load

step 5 (*a/d* = 1.0), the specimen was loaded to 845 kN (190 kips). Failure occurred during

load step 5. After failure, CFRP strips in the west span were observed to be debonded, a

large diagonal crack extended through the compression zone and some stirrups were

fractured. At this value of *a/d*, the diagonal crack formed nearly a straight path from support to load point.

Table 11: Specimen HC loading summary.

Load Step	*a/d*	Loading Type	V_{app} (kN) [kips]	C.L. Disp. @ V_{app} (mm) [in]
0	3.3	4 cycles	147 [33]	24 [0.93]
1	3.0	monotonic	133 [30]	8.6 [0.34]
2	2.5	monotonic	147 [33]	5.8 [0.23]
3	2.0	monotonic	173 [39]	4.6 [0.18]
2b	2.5	monotonic	187 [42]	8.1 [0.32]
3b	2.0	monotonic	236 [53]	6.6 [0.26]
4	1.5	monotonic	311 [70]	5.1 [0.20]
5	1.0	monotonic	423 [95]	3.3 [0.13]

Specimen HT5

Specimen HT5 underwent six load steps, as shown in Fig. 16 and 17 and Table 12, with CFRP strips widths of 127 mm (5 in) in the inverted U-wrap configuration.
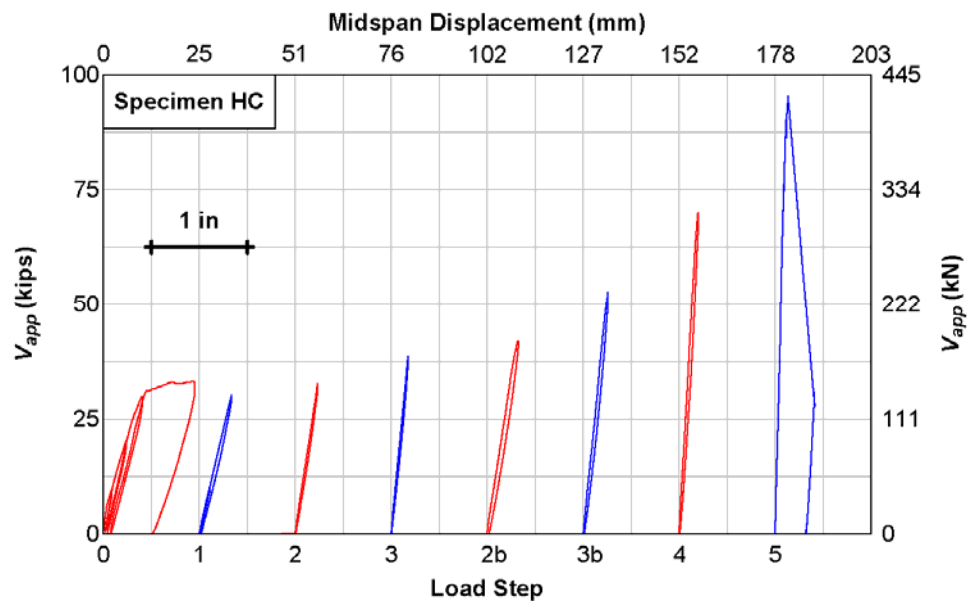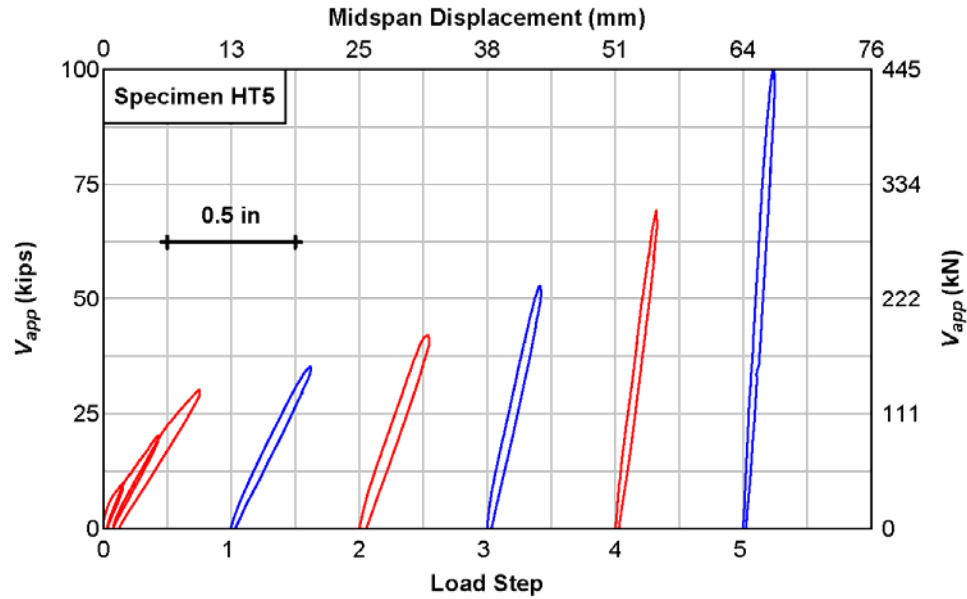

Fig. 16 – Shear versus displacement for Specimen HT5.

East   West

Load Step 0

Load Step 1

Load Step 2
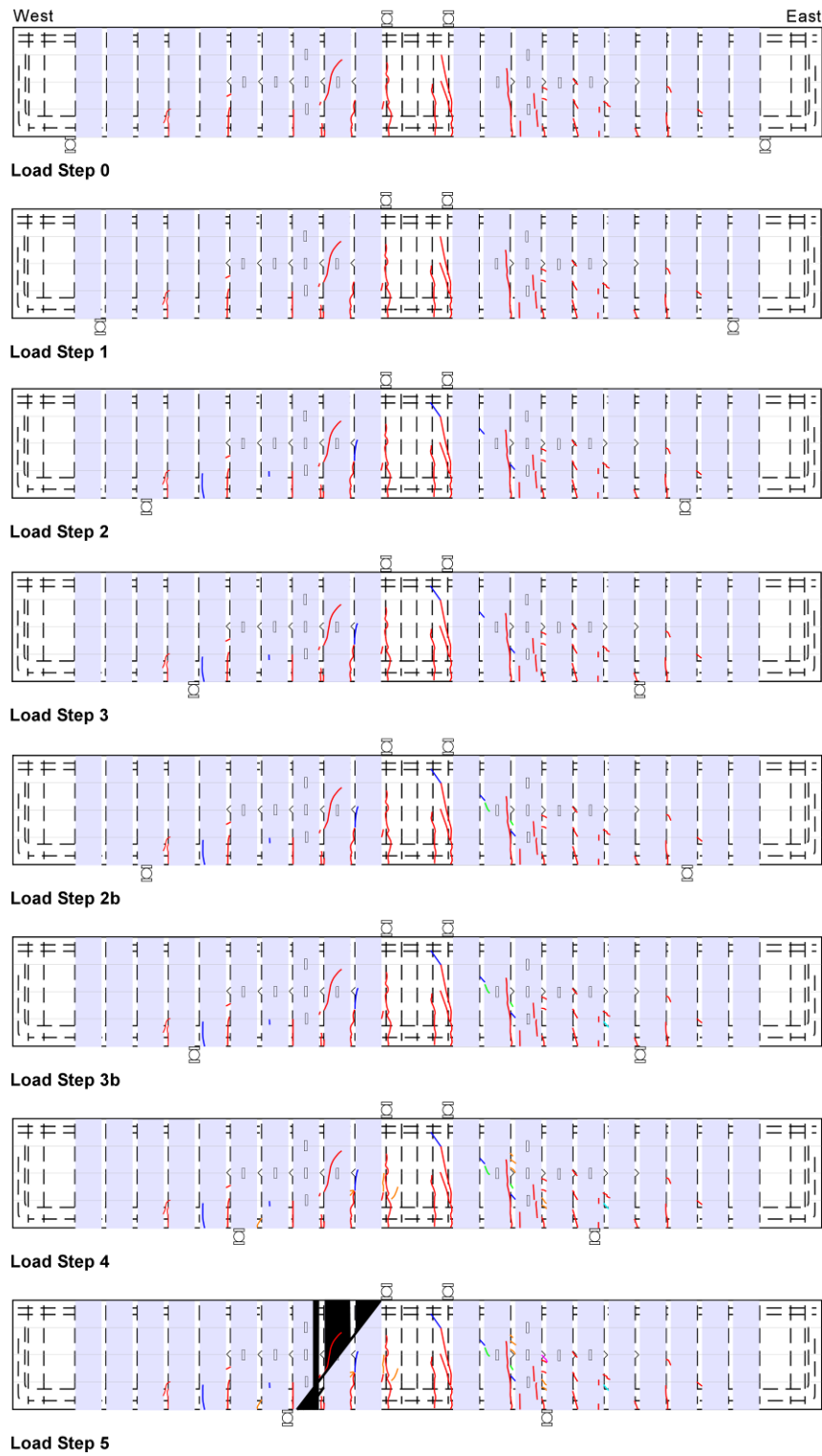
Load Step 3

Load Step 4
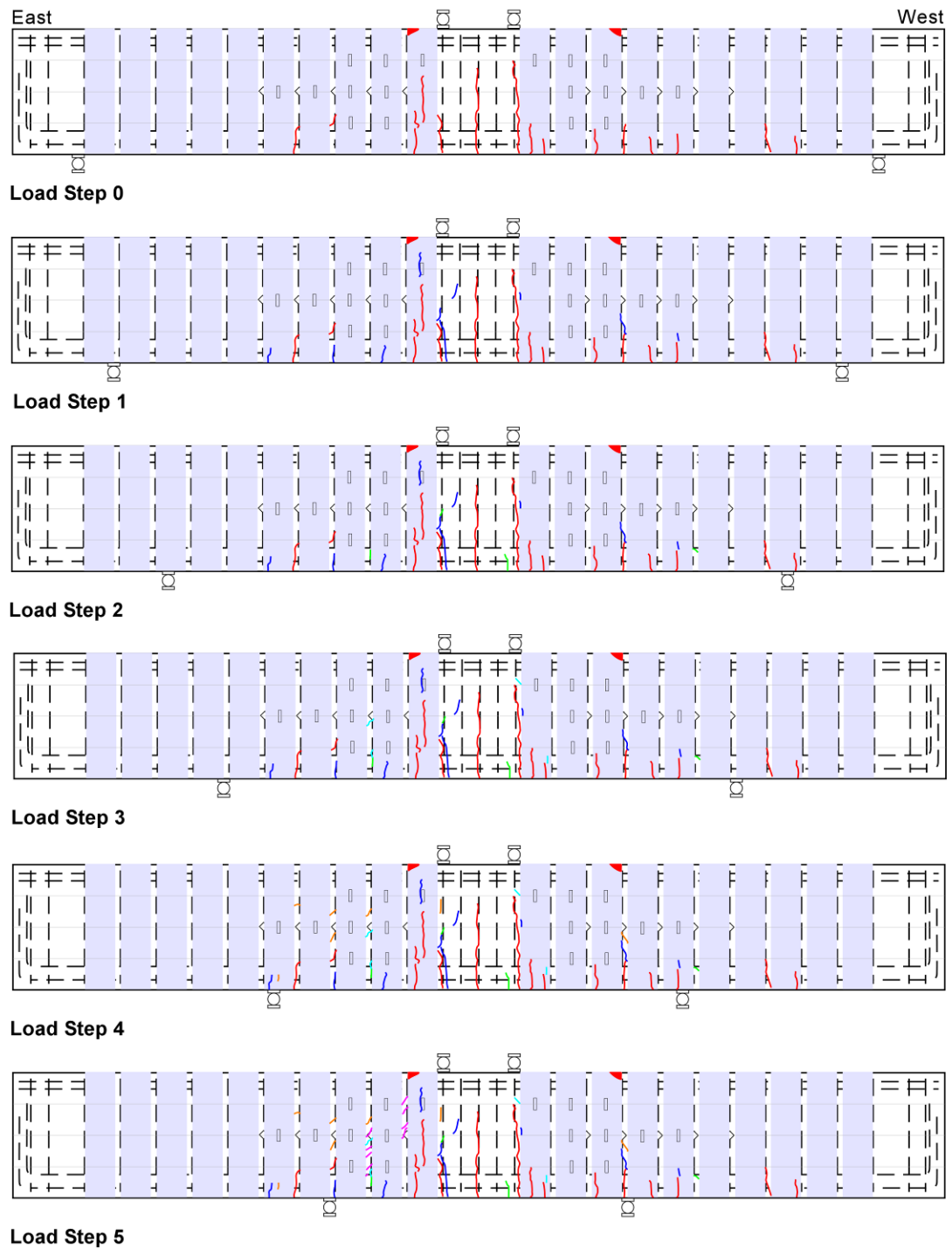
Load Step 5

Fig. 17 – Specimen HT5 crack propagation maps and strain gage locations.

During load step 0 (*a/d* = 3.3), the specimen was loaded cyclically to 89, 178 and 267 kN

(20, 40 and 60 kips). The maximum applied force of 1139 kN (256 kip) approached the

flexural capacity of the specimen at this support configuration. Thus, the specimen was

unloaded and the supports were moved inward to allow continued testing for shear.

Instruments were zeroed for the new specimen configuration.

After each load step that did not produce a shear failure, the supports were moved inward

and instruments were zeroed.

During load step 1 (*a/d* = 3.0), the specimen was loaded monotonically to 311 kN (70

kips). During load step 2 (*a/d* = 2.5), the specimen was loaded monotonically to 374 kN

(84 kips). During load step 3 (*a/d* = 2.0), the specimen was loaded monotonically to 471

kN (106 kips). During load step 4 (*a/d* = 1.5), the specimen was loaded to 614 kN (138

kips). During load step 5 (*a/d* = 1.0), the specimen was loaded to 890 kN (200 kips).

As the limit of the actuator was reached during load step 5, the supports were moved back

to an *a/d* = 2.5 and the CFRP strip widths were reduced to 64 mm (2.5 in). The specimen

was retested as Specimen HT2.5.

Table 12: Specimen HT5 loading summary.

Load Step	*a/d*	Loading Type	V_{max} (kN) [kips]	C.L. Disp. @ V_{max} (mm) [in.]
0	3.3	3 cycles	133 [30]	9.7 [0.38]
1	3.0	monotonic	156 [35]	7.9 [0.31]
2	2.5	monotonic	187 [42]	6.9 [0.27]
3	2.0	monotonic	236 [53]	5.3 [0.21]
4	1.5	monotonic	307 [69]	4.1 [0.16]
5	1.0	monotonic	445 [100]	3.0 [0.12]

Specimen HT2.5

Specimen HT2.5 underwent six load steps, as shown in Figs. 18 and 19 and Table 13, with

strip widths of 64 mm (2.5 in.) in the inverted U-wrap configuration.
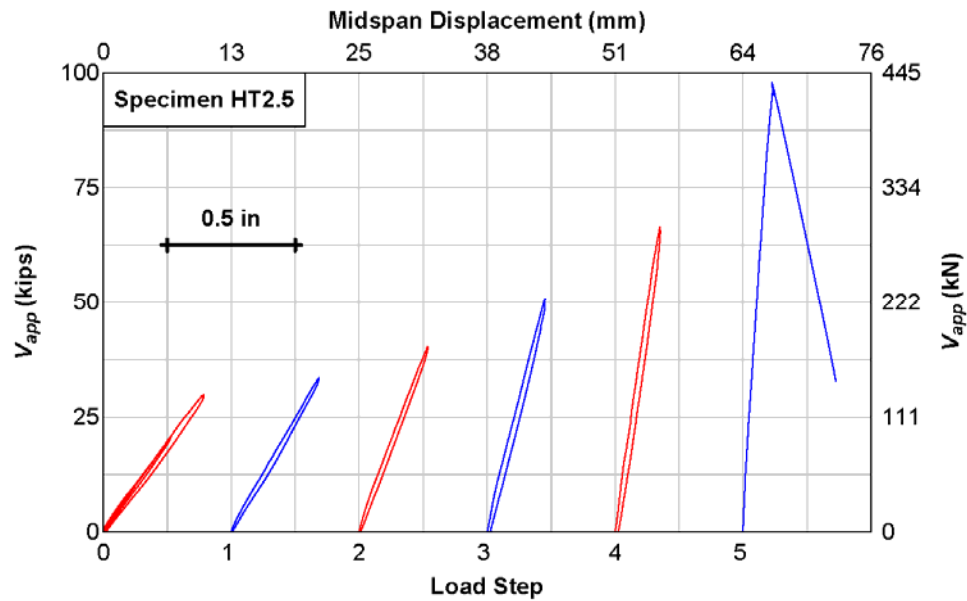
Fig. 18 – Shear versus displacement for Specimen HT2.5.

During load step 0 ($a/d = 3.3$), the specimen was loaded cyclically to 89, 178 and 267 kN

(20, 40 and 60 kips). The maximum applied force of 178 kN (60 kips) approached the

flexural capacity of the specimen at this support configuration. Thus, the specimen was

unloaded and the supports were moved inward to allow continued testing for shear.

Instruments were zeroed for the new specimen configuration.

After each load step that did not produce a shear failure, the supports were moved inward

and instruments were zeroed.

East
West

Load Step 0

Load Step 1

Load Step 2

Load Step 3

Load Step 4
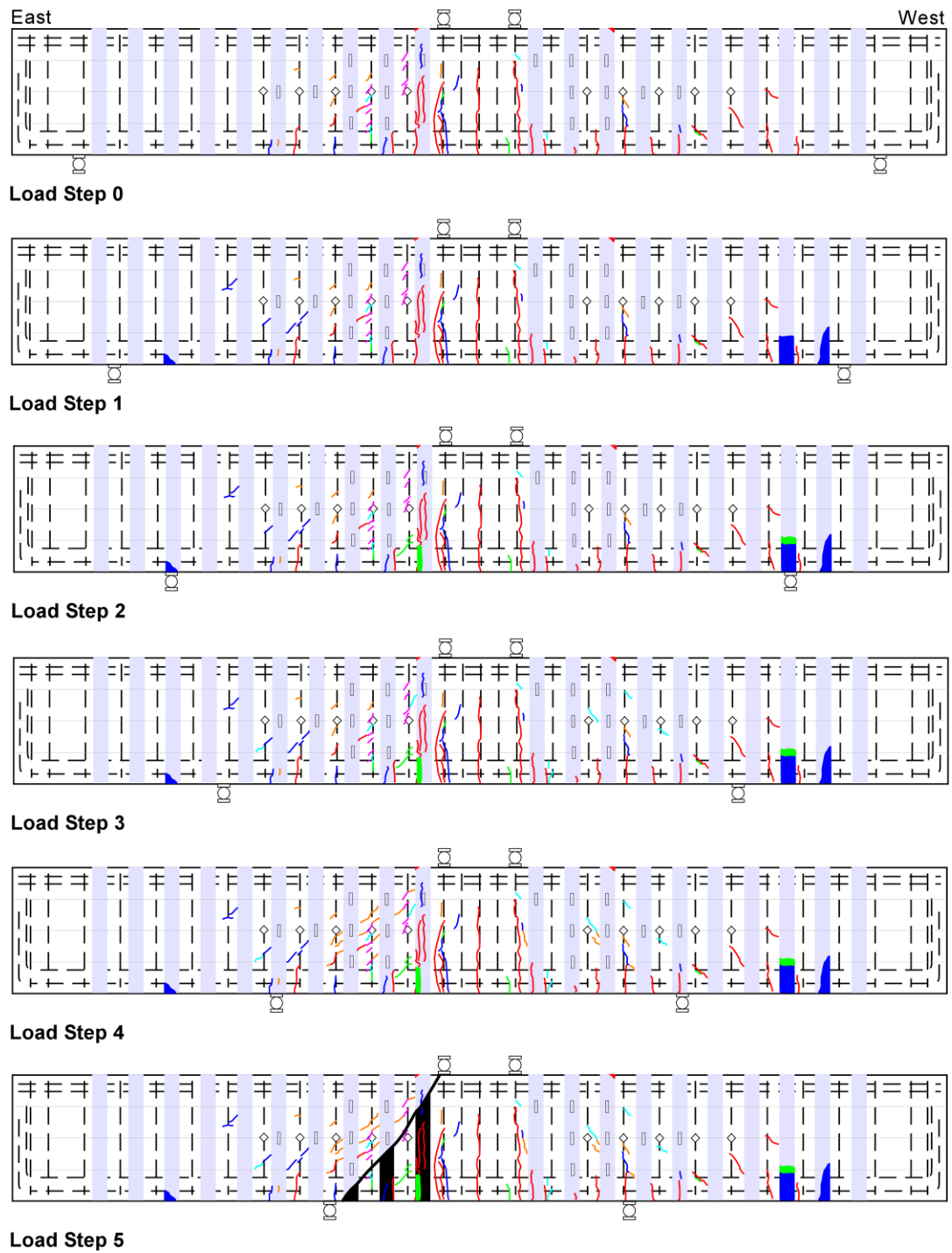
Load Step 5

Fig. 19 – Specimen HT2.5 crack propagation maps and strain gage locations.

During load step 1 ($a/d = 3.0$), the specimen was loaded monotonically to 294 kN (66 kips). During load step 2 ($a/d = 2.5$), the specimen was loaded monotonically to 356 kN (80 kips). During load step 3 ($a/d = 2.0$), the specimen was loaded monotonically to 454 kN (102 kips). During load step 4 ($a/d = 1.5$), the specimen was loaded to 587 kN (132 kips). During load step 5 ($a/d = 1.0$), the specimen was loaded to 867 kN (195 kips).

Failure occurred during load step 5. At failure, CFRP strips in the east span were observed to be debonded, a large diagonal crack extended through the compression zone and some stirrups fractured.

Table 13: Specimen HT2.5 loading summary.

Load Step	a/d	Loading Type	V_{app} (kN) [kips]	C.L. Disp. @ V_{app} (mm) [in.]
0	3.3	3 cycles	133 [30]	9.7 [0.39]
1	3.0	monotonic	147 [33]	7.9 [0.34]
2	2.5	monotonic	178 [40]	6.9 [0.27]
3	2.0	monotonic	227 [51]	5.3 [0.23]
4	1.5	monotonic	298 [67]	4.1 [0.18]
5	1.0	monotonic	436 [98]	3.0 [0.11]

Specimen QC

Specimen QC underwent seven load steps, as shown by Fig. 20 and 21 and Table 14, with

strip widths of 16 mm (0.625 in.) in the U-wrap configuration.
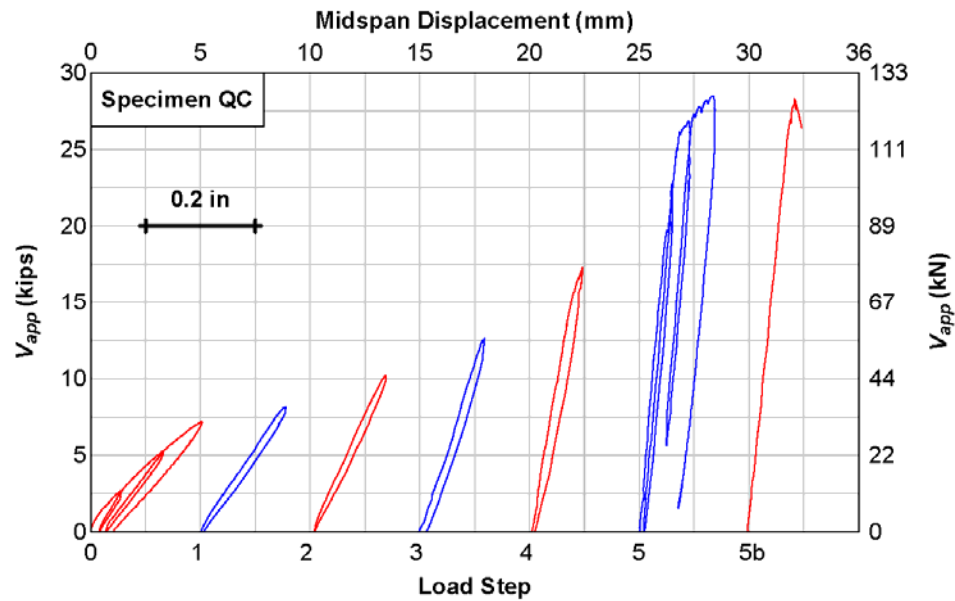
Fig. 20 – Shear versus displacement for Specimen QC.

During load step 0 (a/d = 3.3), the specimen was loaded cyclically to 24, 49 and 62 kN

(5.4, 11 and 14 kips). The largest measured diagonal crack width during load step 0 was

0.25 mm (0.010 in.). The maximum applied force of 62 kN (14 kips) approached the

flexural capacity of the specimen at this support configuration. Thus, the specimen was

unloaded and the supports were moved inward to allow continued testing for shear.

Instruments were zeroed for the new specimen configuration.

After each load step that did not produce a shear failure, the supports were moved inward

and instruments were zeroed.

East West

Load Step 0

Load Step 1

Load Step 2

Load Step 3

Load Step 4

Load Step 5
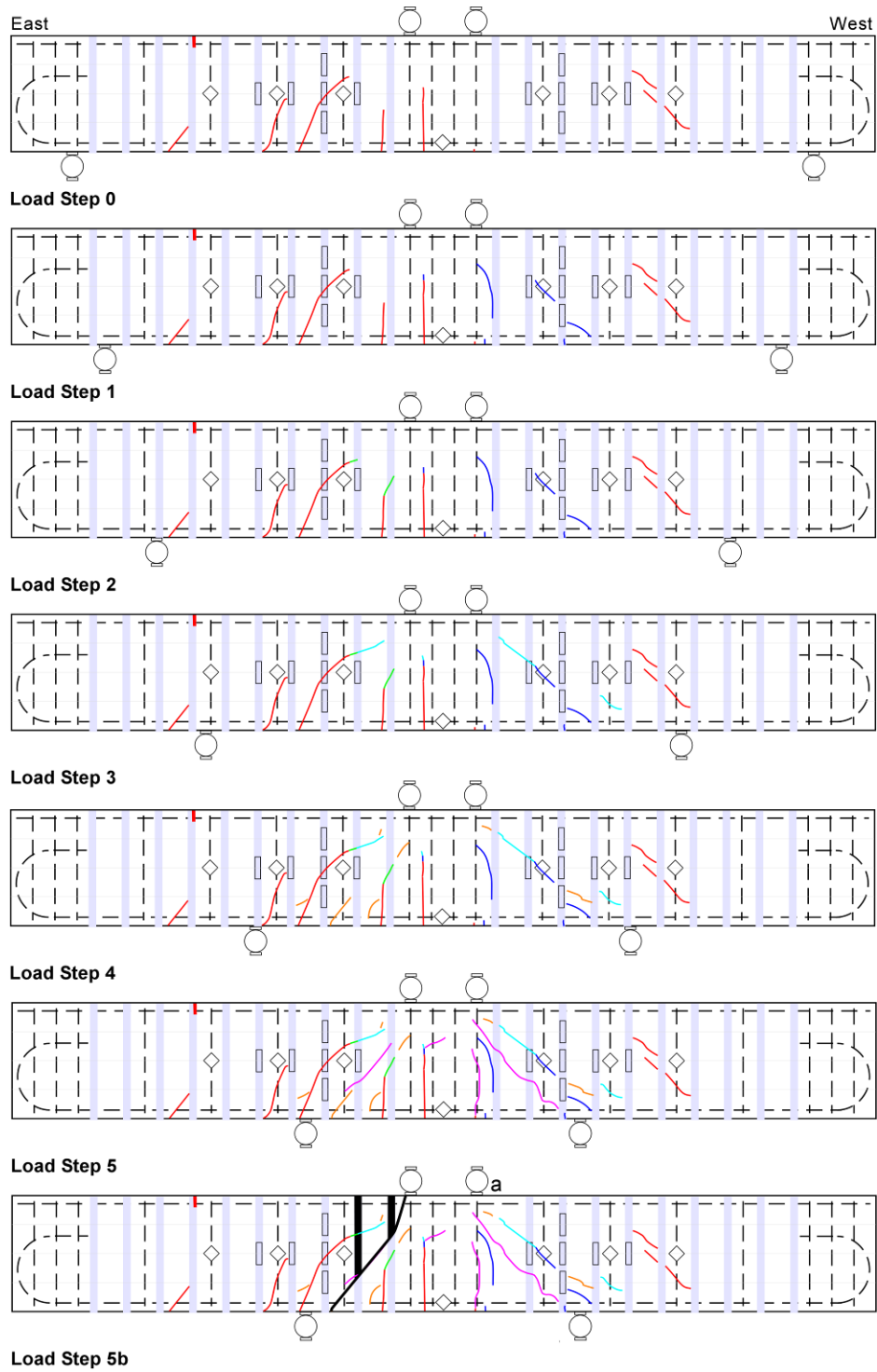
Load Step 5b

a: strip removed.

Fig. 21 – Specimen QC crack propagation maps and strain gage locations.

During load step 1 (*a/d* = 3.0), the specimen was loaded monotonically to 71 kN (16 kips).

Diagonal crack widths were not measured during this load step. During load step 2 (*a/d* =

2.5), the specimen was loaded monotonically to 89 kN (20 kips). The largest measured

diagonal crack width was 0.25 mm (0.010 in.). During load step 3 (*a/d* = 2.0), the

specimen was loaded monotonically to 111 kN (25 kips). The largest measured diagonal

crack width was 0.41 mm (0.016 in.). During load step 4 (*a/d* = 1.5), the specimen was

loaded to 156 kN (35 kips). The largest measured diagonal crack width was 0.51 mm

(0.020 in.). During load step 5 (*a/d* = 1.0), the specimen was loaded to 254 kN (57 kips).

The largest measured diagonal crack width was 0.33 mm (0.013 in.).

During load step 5 (*a/d* = 1.0), the flexural steel reinforcement yielded. In an attempt to

attain shear failure at this value of *a/d*, the strip closest to the load point on the west span

was removed for load step 5b (the west span appeared to have more extensive damage than

the east span). During Step 5b, the specimen, somewhat unexpectedly, failed on the east

span. After failure, strips in the shear span were observed to be debonded, a diagonal crack

extended through the compression zone and some stirrups fractured.

Table 14: Specimen QC loading summary.

Load Step	*a/d*	Loading Type	V_{app} (kN) [kips]	C.L. Disp. @ V_{app} (mm) [in]	Max. Measured Diagonal Crack Width (mm) [in.]
0	3.3	3 cycles	32 [7.2]	5.1 [0.20]	0.25 [0.010]
1	3.0	monotonic	36 [8.2]	4.1 [0.16]	-
2	2.5	monotonic	44 [10]	3.6 [0.14]	0.25 [0.010]
3	2.0	monotonic	58 [13]	3.0 [0.12]	0.41 [0.016]
4	1.5	monotonic	76 [17]	2.5 [0.10]	0.51 [0.020]
5	1.0	monotonic	129 [29]	3.3 [0.13]	0.33 [0.013]
5b	1.0	3 cycles	125 [28]	2.1 [0.084]	-

Specimen QT

Specimen QT underwent six load steps, as shown in Fig. 22 and 23 and Table 15, with

strip widths of 16 mm (0.625 in) in the inverted U-wrap configuration.
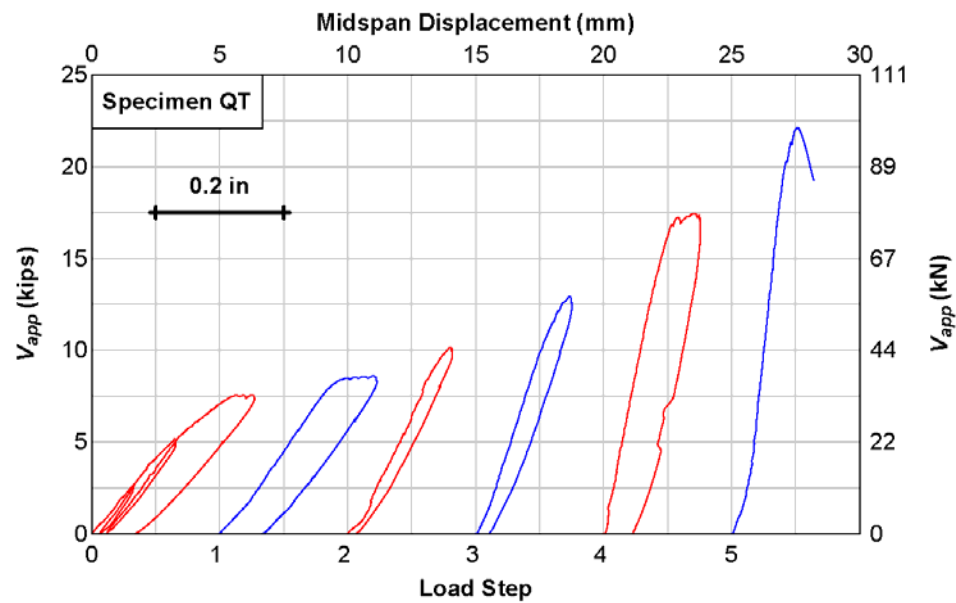
Fig. 22 – Shear versus displacement for Specimen QT.

Specimen QT displayed cracks in the concrete over its full height before any loads were

applied. These cracks were incorporated into the map shown for load step 0 and may have

been a result of handling.

Load Step 0

Load Step 1

Load Step 2

Load Step 3

Load Step 4
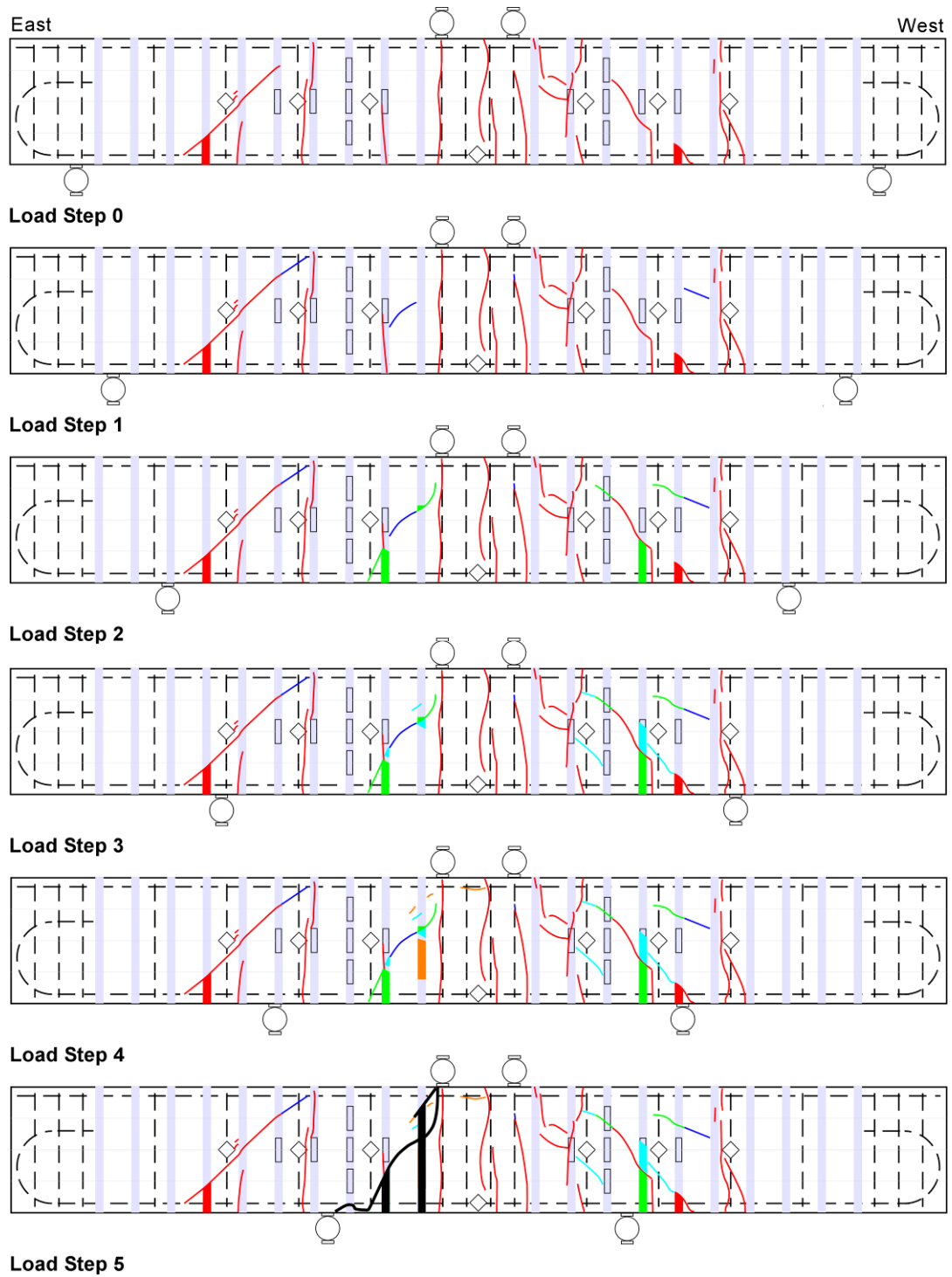
Load Step 5

Fig. 23 – Specimen QT crack propagation maps and strain gage locations.

During load step 0 (*a/d* = 3.3), the specimen was loaded cyclically to 24, 44 and 67 kN

(5.4, 10 and 15 kips). The largest measured diagonal crack width during load step 0 was

0.25 mm (0.010 in.). The maximum applied force of 67 kN (15 kips) approached the

flexural capacity of the specimen at this support configuration. Thus, the specimen was

unloaded and the supports were moved inward to allow continued testing for shear.

Instruments were zeroed for the new specimen configuration.

After each load step that did not produce a shear failure, the supports were moved inward

and instruments were zeroed.

During load step 1 (*a/d* = 3.0), the specimen was loaded monotonically to 76 kN (17 kips).

The largest measured diagonal crack width during load step 1 was 1.02 mm (0.040 in.).

During load step 2 (*a/d* = 2.5), the specimen was loaded monotonically to 90 kN (20 kips).

The largest measured diagonal crack width was 0.25 mm (0.040 in.). During load step 3

(*a/d* = 2.0), the specimen was loaded monotonically to 116 kN (26 kips). The largest

measured diagonal crack width was 0.76 mm (0.030 in.).

During load step 4 (*a/d* = 1.5), the specimen was loaded to 156 kN (35 kips). The largest

measured diagonal crack width was 1.02 mm (0.040 in). During load step 4, the specimen

developed a large crack in the west shear span and appeared to have significant damage in

the compression zone. The force-displacement curve also appeared to soften, which

seemed to indicate a flexural or interaction failure at this step. The specimen was used

again, however, and failed in shear during load step 5.

During load step 5 (*a/d* = 1.0), the specimen was loaded to 197 kN (44 kips). CFRP strips

in the west shear span were observed to be debonded, a large diagonal crack extended

through the compression zone and some stirrups were fractured.

Table 15: Specimen QT loading summary.

Load Step	*a/d*	Loading Type	V_{max} (kN) [kips]	Disp. @ V_{max} (mm) [in.]	Max. Measured Diagonal Crack Width (mm) [in.]
0	3.3	3 cycles	33 [7.5]	6.4 [0.25]	0.25 [0.010]
1	3.0	monotonic	38 [8.6]	6.1 [0.24]	1.02 [0.040]
2	2.5	monotonic	44 [10]	4.1 [0.16]	1.02 [0.040]
3	2.0	monotonic	58 [13]	3.8 [0.15]	0.76 [0.030]
4	1.5	monotonic	80 [18]	3.6 [0.14]	1.02 [0.040]
5	1.0	monotonic	98 [22]	2.5 [0.10]	-

EXPERIMENTAL RESULTS

Introduction

Experimental measurements are reported here in detail for the test specimens. These results include local and global response measurements and comparisons between different specimens, CFRP reinforcing patterns, and span length conditions. Some of the considerations for surface strain measurements in the CFRP strips are addressed compared with averaged strains from displacement sensor measurements.

Surface Strain Measurements in CFRP Strips

Strains in the CFRP were measured using a conventional uniaxial long-gage length bonded strain gage pattern for all specimens. This selected gage pattern had a fixed gage length of 51 mm (2 in.) and is commonly used to measure strains in CFRP and other composite materials that require longer gage distances to allow strain averaging. The measured strain values are generally intended to represent a localized response quantity. However, due to the different scale lengths of the specimens, the proportion of the strain gage length to overall strip height increased when the specimen scale decreased, as illustrated in Fig. 24. Thus, for the large-scale specimens the strain gage measurements still represent a relatively localized response, while for the small-scale specimens, the strain gage measurements represent a more regional response for the CFRP strips.
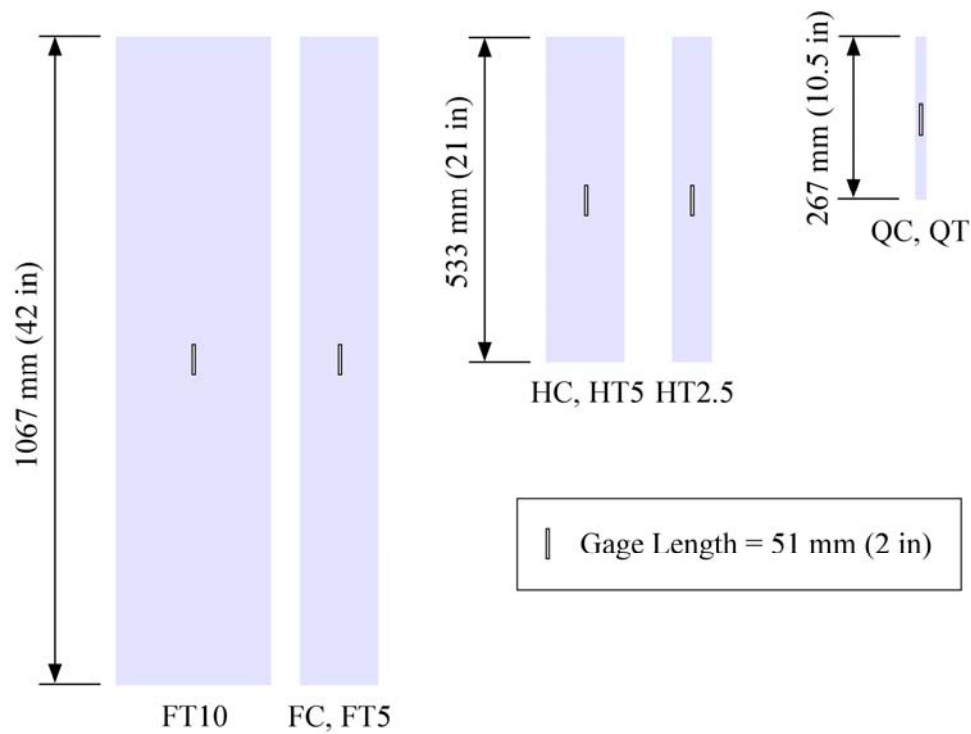
Fig. 24 – Strain gage length compared to CFRP strip heights. Gages represent 5%, 10% and 20% of the CFRP strip length at the full, half and quarter scales, respectively.

Large local strains may be expected in the CFRP, resulting from the material bridging across the cracked concrete combined with flexural-tension bending strains induced by localized debonding from the concrete surface. Due to the relatively short bond stress transfer length of the CFRP, the strains can change rapidly along the strip length and thus location of the strain gage relative to the concrete cracks and possible CFRP debonding will greatly affect the measurements. These possible sources of local strain variation will be discussed.

Strain in the section taken from diagonal displacement measurements may provide a more general perspective of the CFRP shear contribution then the local strain gage measurements as these tend to average out local variations at cracks and debonded regions.

To permit these estimates, displacement measurements were taken along 45˚ diagonals placed across the specimens in 3 panel sections within the shear span. For the failure load step, the diagonal displacement measurements were converted into average vertical strains using Mohr's circle. These average vertical strains will be compared with local strain measurements and used to estimate the CFRP contribution to shear strength.

Strain Accumulation in CFRP

All of the specimens were loaded into the inelastic range over several different load cycles that produced concrete cracking, rebar yielding and CFRP debonding. As the test specimens acquired damage, CFRP strains tended to exhibit a nonlinear loading and unloading response with plastic offset. This behavior was captured by linking measured CFRP strains from each load step to create a cumulative strain response curve. A brief description of this behavior using specimen FC as an example is provided, followed by descriptions for all the specimens.

Specimen FC was originally loaded up to 95% of the predicted flexural capacity with an $a/d = 3.3$. Diagonal and flexural cracking of the concrete as well as localized debonding of the CFRP strips were observed at this load stage without failure. Had the test continued, the specimen would have failed in flexure. To preclude this failure mode, the supports were moved inward to the loading points for an $a/d = 3.0$ and the specimen was loaded to 95% of the predicted flexural capacity for this new span length configuration. Additional diagonal and flexural cracking and CFRP debonding were observed without specimen failure. This process was repeated with the supports being moved to values of $a/d = 2.5$, 2.0 and 1.5, then back out to values of $a/d = 2.5$ and 2.0. Through this process the

specimen acquired significant areas of CFRP debonding and concrete cracking prior to the

final failure.

Measured CFRP strains were obtained from the strain gages after they were reset to zero

prior to the start of each new load cycle. Measured strain from specimen FC during the

failure load step, load step 3b ($a/d = 2.0$), is provided in Fig. 25(a).

(a)   (b)
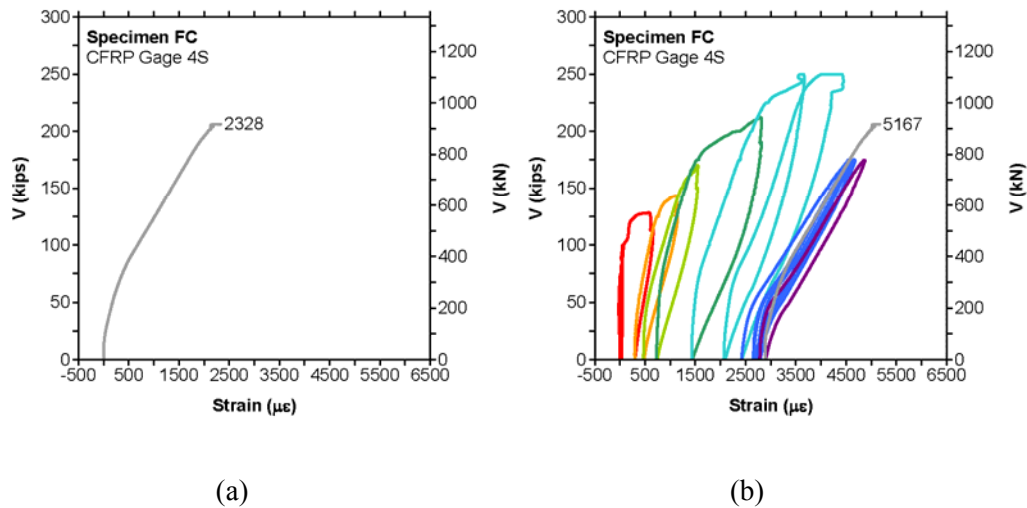
Fig. 25 – Example applied shear versus (a) strain measured at CFRP gage 4S during load
step 3b ($a/d = 2.0$) and (b) cumulative strain at CFRP gage 4S from specimen FC.

The total accumulated strain for the strain gage during the complete test is shown in Fig.

25(b). The accumulated CFRP strains were obtained by adding the measured strains,

including the final offset values, from each of the load steps. The accumulated strain in the

CFRP was much larger than that produced in the individual load steps. The accumulated

strains are useful for tracking the onset and progression of diagonal cracks in the concrete,

which will be discussed later.

Figs. 26-28 display the relationship between applied shear and CFRP strain at load step 4 (a/d = 1.5) for all specimens. CFRP strain was measured with gage 4S in the full scale specimens and gage 4E in the half and quarter scale specimens. The location of CFRP gage 4 was scaled geometrically and is thus in relatively the same location for all specimens.
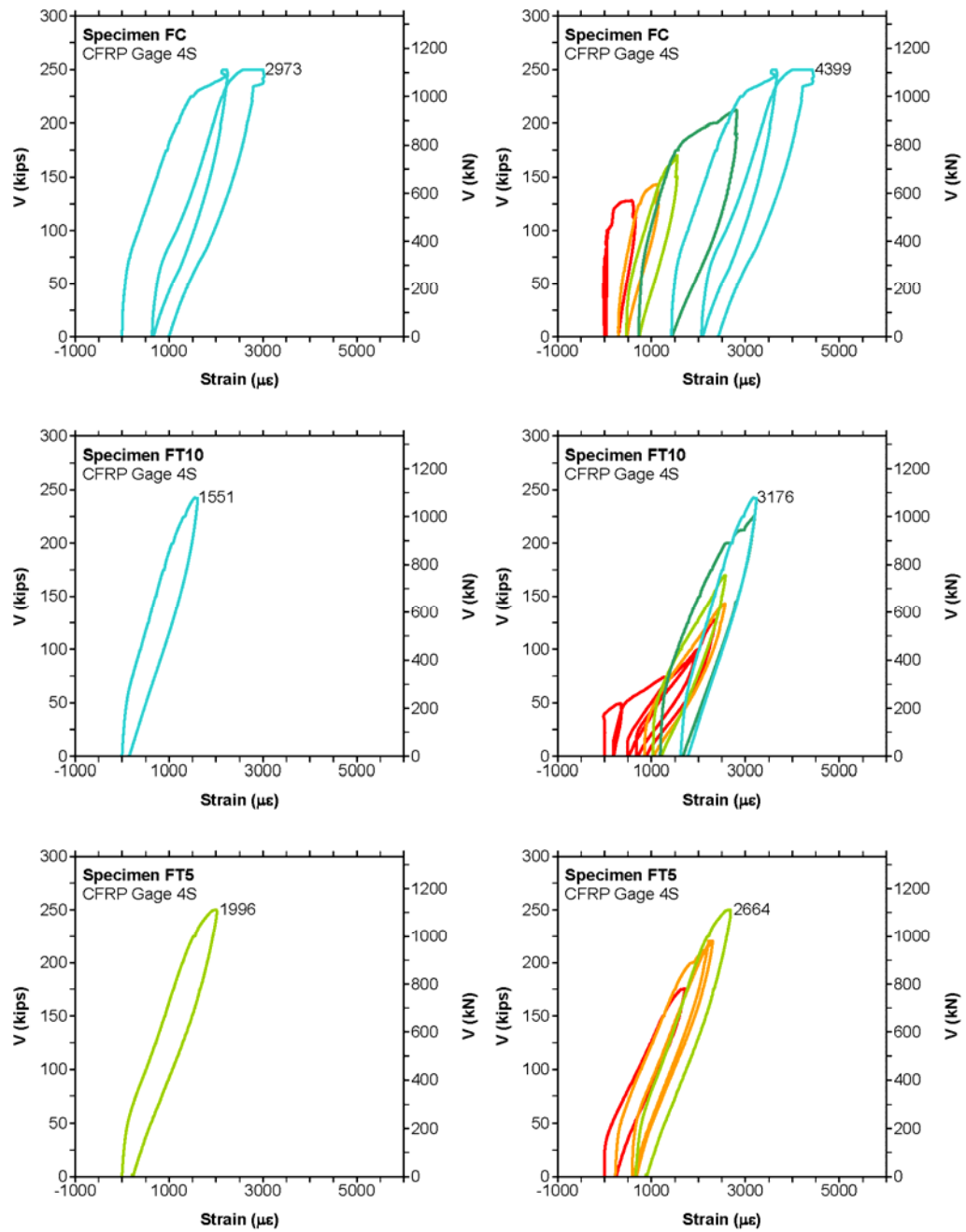
Fig. 26 – Applied shear versus measured (left column) and cumulative (right column) strain at CFRP gage 4S from full scale specimens FC, FT10 and FT5.
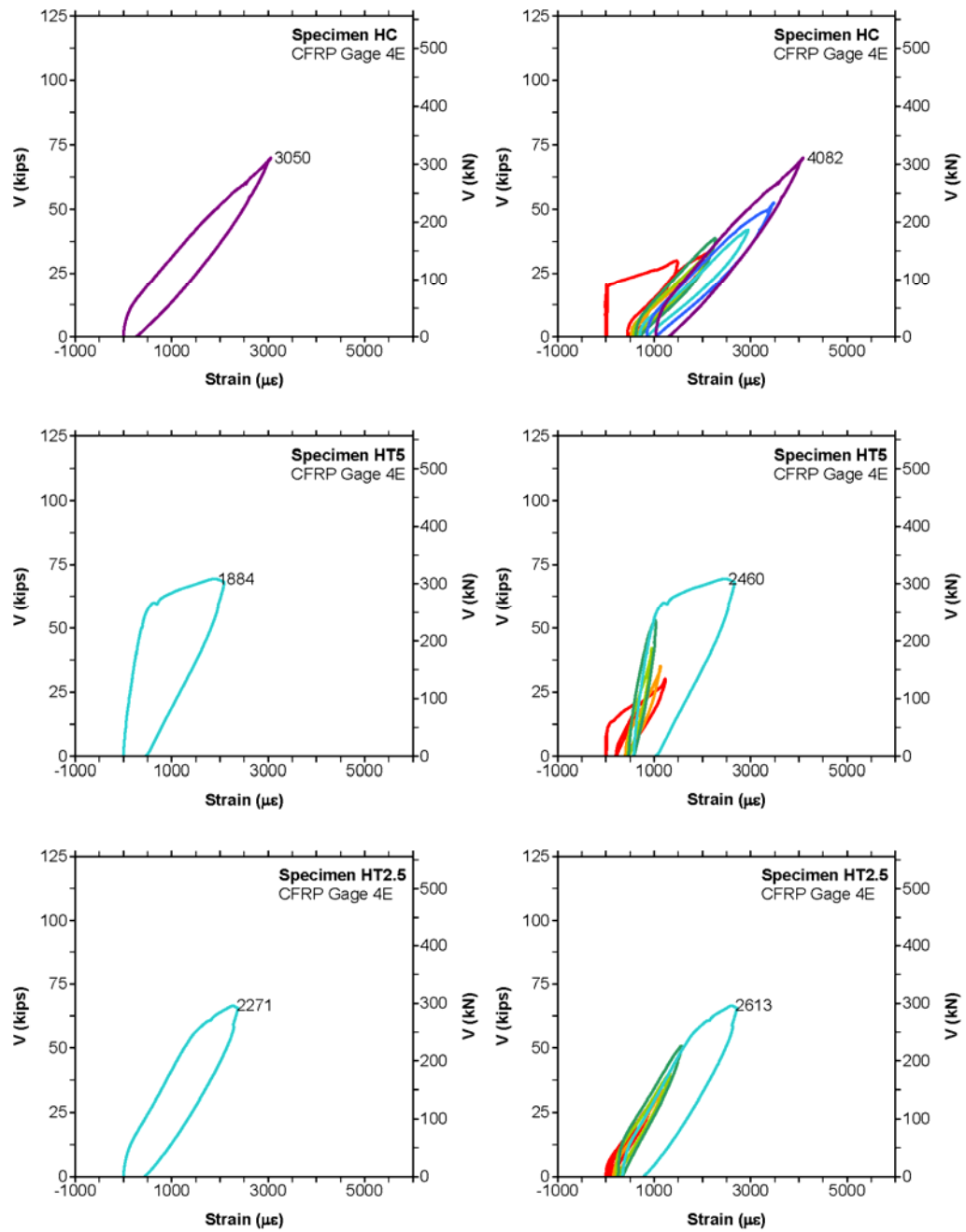
Fig. 27 - Applied shear versus measured (left column) and cumulative (right column) strain at CFRP gage 4E from half scale specimens HC, HT5 and HT2.5.
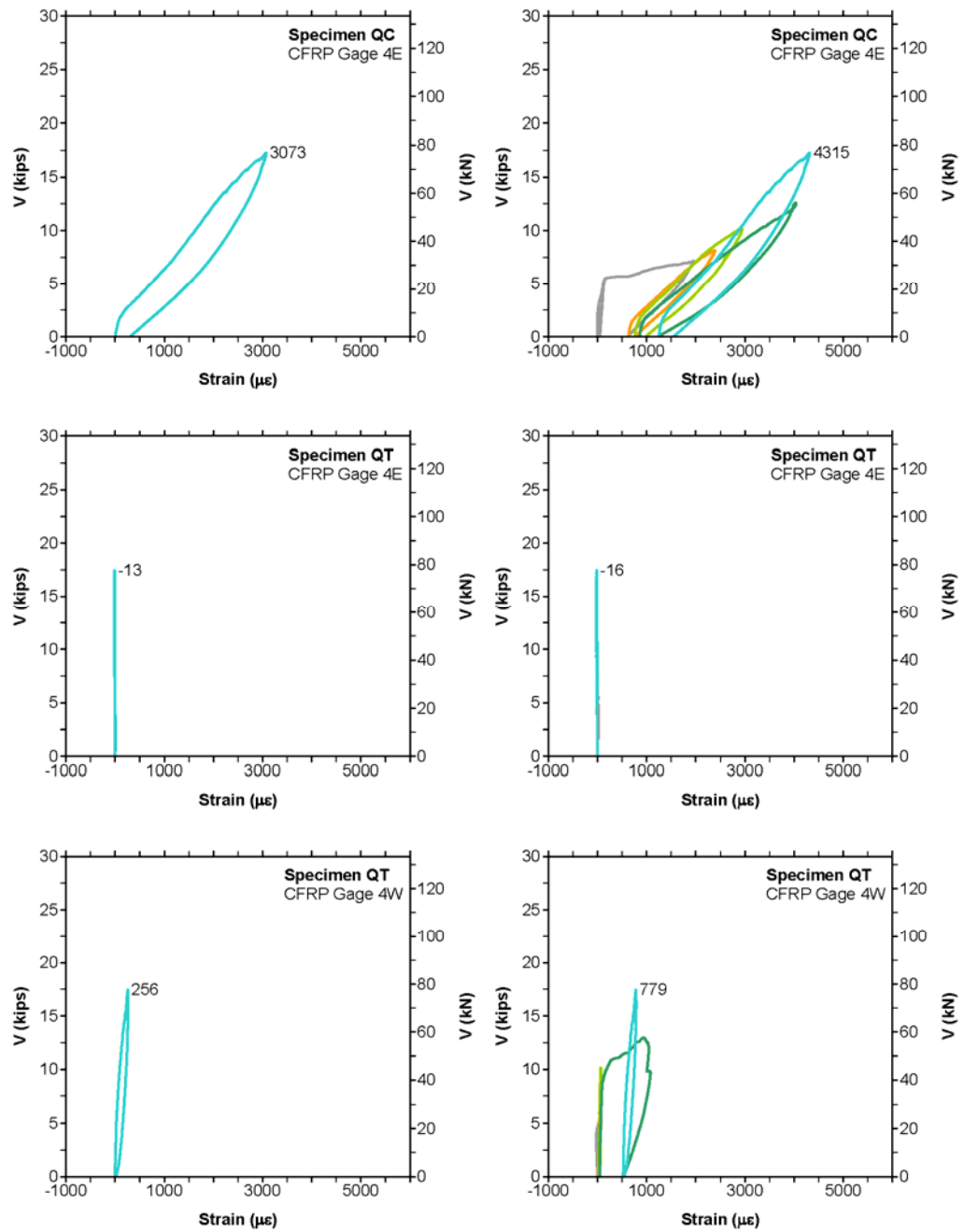
Fig. 28 - Applied shear versus measured (left column) and cumulative (right column) strain at CFRP gage 4E from quarter scale specimens QC and QT.

From Fig. 26, specimen FT5 exhibited the least amount of cumulative CFRP strain, followed by specimens FT10 and FC. Specimen FT10 possessed the largest strip width. Specimens FT10 and FT5, which were strengthened by inverted U-wraps, had lower cumulative strains than specimen FC. Specimen FT5 was first tested as specimen FT10 before portions of CFRP were manually removed.

From Fig. 27, specimen HT5 exhibited the least cumulative CFRP strain, followed by specimens HT2.5 and HC. Specimen HT2.5 had the narrowest strip width, while HC and HT5 had the same strip width. Specimens HT5 and HT2.5, which were strengthened by inverted U-wraps, had lower cumulative strains than specimen HC. Specimen HT2.5 was first tested as specimen HT5 before portions of CFRP were manually removed.

From Fig. 28, specimen QT accumulated almost no strain in CFRP gage 4E during testing. Review of the crack map shows no diagonal cracks crossing the strip on which gage 4E was affixed. Other gages on this strip (3E and 5E) also accumulated almost no strain. CFRP gage 4W, which was in the same relative location but on the west span, was used for comparison instead. Specimen QT appears to have accumulated less CFRP strain than specimen QC. Specimen QT was strengthened with an inverted U-wrap. Both specimens had the same strip width.

It appears that for all scales, cumulative CFRP strains tended to be less in the inverted U-wraps. The accumulation of almost no strain in the CFRP strip on which gage 4E from specimen QT was affixed indicates that local strain measurements are dependent on relative location of the sensor to diagonal cracks.

Local Strain Variation

Local strain variations in CFRP exist around regions of debonding, which commonly occur

where diagonal cracks cross CFRP strips. Maeda *et al.* (1997) demonstrated this through

testing and nonlinear finite element modeling of CFRP bonded to concrete across a crack.

Maeda *et al.* (1997) developed a strain distribution model and concluded that an effective

bond length resists shear stresses. The effective bond length, L_e, was calculated for all the

test specimens according to ACI 440.2R-02 Eqn. (10-7), which is provided in Eqns. 1 and

2 of the background. The resulting bond length was 48 mm (1.9 in.) for all specimens,

regardless of scale. To identify the local strain variations along the strip length, three

gages were affixed to a single strip in specimen FC and measurements were compared.

CFRP gages 3S, 4S and 5S were aligned vertically in the same CFRP strip on specimen

FC. Gage 3S was located at ¼ of the height of the specimen, gage 4S was at mid-height

and gage 5S was located at ¾ of the height of the specimen. Cumulative strains through

load step 3b ($a/d = 2.0$), the failure load step, are shown in Fig. 29. As seen in Fig. 29, the

CFRP strain was not uniformly distributed along the height of the strip.   The eventual

failure diagonal crack crossed the strip between gages 4S and 5S.
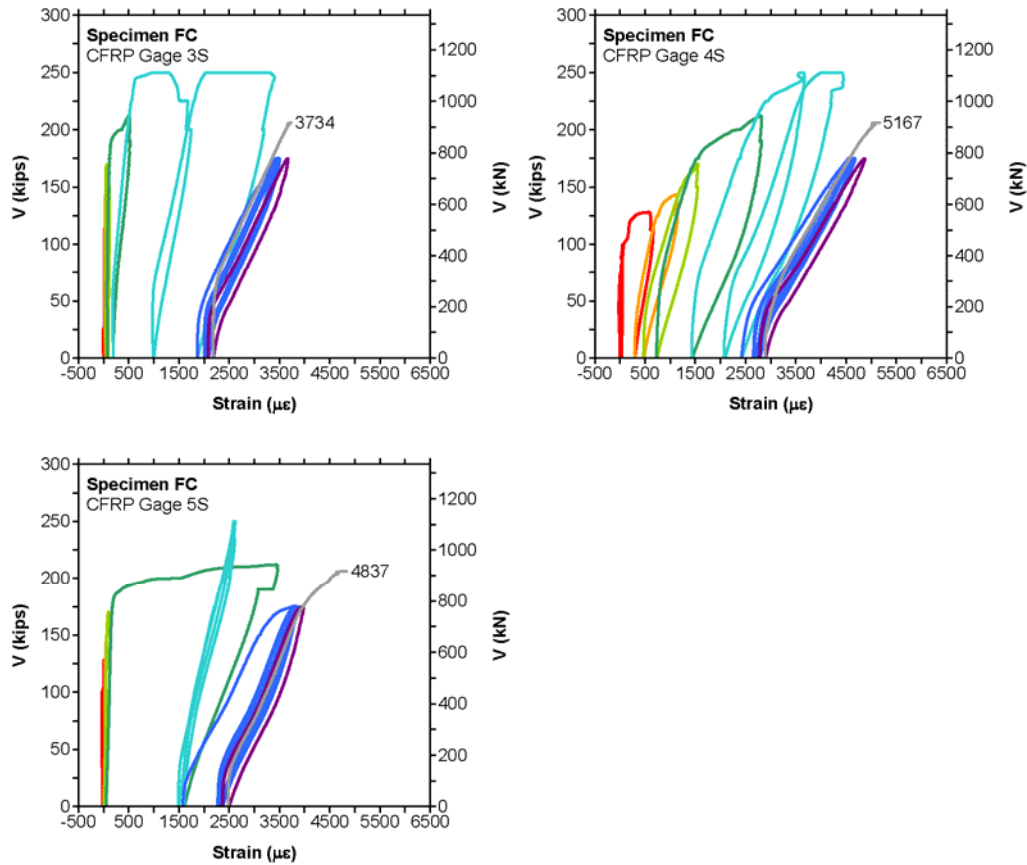
Fig. 29 – Applied shear versus cumulative strain at CFRP gages 3S, 4S and 5S from specimen FC.

According to Fig. 29, gage 3S first experienced a rapid increase in strain during load step 3 ($a/d = 2.0$) with additional significant strain proceeding in load step 4 ($a/d = 1.5$). This was due to concrete cracking followed by CFRP strip localized debonding which produced the large strains and inelastic unloading, A small debonded region above gage 3S was first observed during load step 1 ($a/d = 3.0$). During testing, the specimens were inspected to detect debonding by tapping on the CFRP surface after the applied shear had been reduced to 90% of the maximum applied shear and held constant. While this load was held, the

extent of concrete cracking and CFRP debonding were documented. Debonded CFRP was associated with a hollow sound when the surface was tapped. The debonded region above the strain gage progressed upwards away from the gage during load step 2 ($a/d = 2.5$). Growth downward toward the gage was observed during load step 4 ($a/d = 1.5$).

As seen in Fig. 29, gage 4S first experienced large strains during load step 0 ($a/d = 3.3$) with significant additional strains during load steps 1-4. CFRP gage 4S was just above a debonded region that was first recorded during load step 0. The debonded region was oriented along a diagonal crack and was approximately 50 mm (2 in.) high across the entire strip width. The debonded region expanded vertically during load steps 1 ($a/d = 3.0$) and 4 ($a/d = 1.5$).

According to Fig. 29, gage 5S first experienced large strains during load step 3 ($a/d = 2.0$). CFRP gage 5S was centered over an eventually debonded region that was first recorded during load step 3. The debonded region was approximately 250 mm (10 in.) high across the entire strip width.

It appears that larger cumulative CFRP strains were present closer to the failure diagonal crack as compared to the strains at gages located away from the crack. This indicates that even with significant observed debonding over the strip length there is still sufficient bond stress transfer between the CFRP and concrete to result in strain gradients in the strips.

Prior to the onset of diagonal cracking and CFRP debonding, the CFRP strain response was linear elastic. It appears that diagonal cracking of the base concrete followed by CFRP

debonding correlated to the observed decreased slope, large strains, nonlinear unloading and plastic offset when CFRP strain is plotted against applied shear. The very large CFRP strains, generally considered as the uniaxial strain in the material, that first occur upon concrete cracking and initial localized debonding, may be artificially inflated due to flexural-tension strains induced by debonding as will be discussed further.

Flexural Strain from Debonding

Debonding of the CFRP was observed locally around the diagonal cracks that crossed the CFRP strips. After specimen FC failed in shear, several CFRP-concrete failure surfaces were observable, as shown in Fig. 30. In some cases, the CFRP strips were able to pull away shallow concrete wedges at the diagonal crack locations, as shown schematically in Fig. 31, which were still bonded to the CFRP strip. Away from diagonal cracks, the strips lost load capacity when the adhesive bond failed along the concrete substrate just under the CFRP-concrete interface.

Fig. 30 – Photograph of a debonded CFRP strip that formerly crossed a diagonal crack (post-failure of Specimen FC).
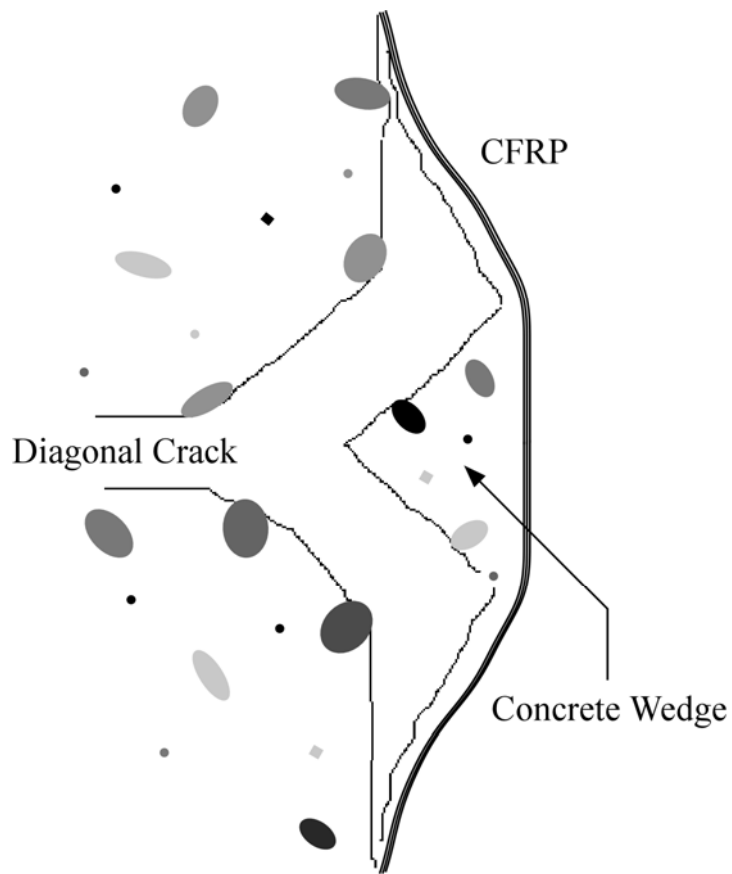
Fig. 31 – Illustrated section view of debonded CFRP at a diagonal crack.

Test observations indicated that the debonded CFRP deflected outward from the specimen and that adjacent bonded regions provided some restraint to the out-of-plane deformations. Two idealized deflected shapes of debonded CFRP are shown in Fig. 32.
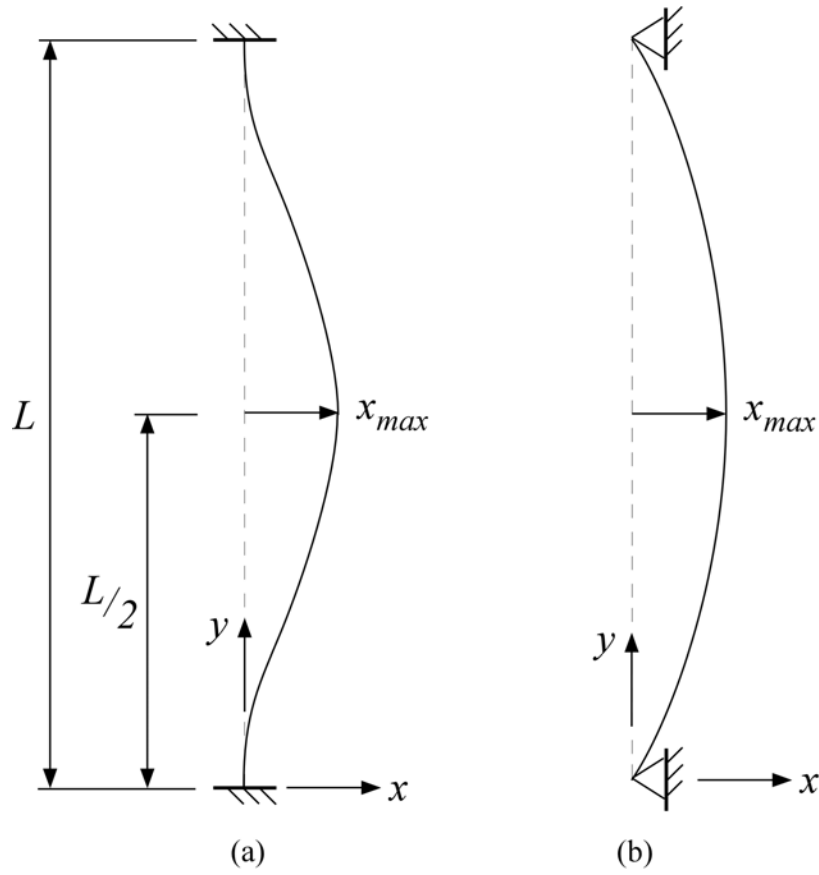
Fig. 32 – Assumed deflected shapes and boundary conditions for debonded portions of CFRP.

Assuming the boundary conditions and deflected shapes shown in Fig. 32, flexural-tension strains from debonding at the instrumented surface of the CFRP, ε_{fd}, at mid-length of the debonded region were calculated. For the fixed supports shown in Fig. 32(a), this strain may be expressed as:

$$\varepsilon_{fd} = \frac{16 x_{max} t_f}{L^2}$$

[18]

where t_f is the thickness of the CFRP, x_{max} is the maximum out-of-plane deformation, and L is the unbonded length. For the pinned supports shown in Fig. 32(b), this strain may be expressed as:

$$\varepsilon_{fd} = \frac{4x_{max}t_f}{L^2} \qquad\qquad [19]$$

These expressions for bending induced strains are presented graphically in Fig. 33 for

ranges of x_{max} and L. As seen in Fig. 33, very large flexural-tension strains may be

expected at short debonded lengths. As the debonded length increases, CFRP flexural-

tension strains decrease nonlinearly. For this test configuration, the debonded length is

limited by the height of the specimen. While flexural-tension strains appear to become

negligible when the debonded length approaches the height of the full-scale specimens,

significant bending induced surface tensile strains may still be present when the debonded

length approaches the height of the half- and quarter-scale specimens.
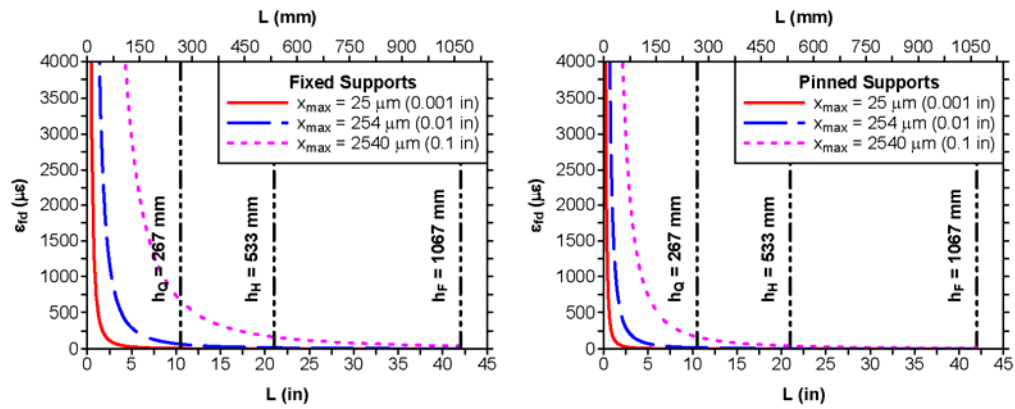
Fig. 33 – Modeled CFRP flexural-tension strains induced by debonding.

Considering actual strain gages located in the specimens, CFRP gage 5S from specimen

FC was identified as centered over a debonded strip region with $L = 250$ mm (10 in.)

during load step 3 ($a/d = 2.0$). The difference between the initial and final measured

strains at CFRP gage 5S was approximately 1540 $\mu\varepsilon$, as shown in Fig. 29. With $t_f = 1.16$ mm (0.0458 in), Eqns. 18 and 19 yield maximum displacements of 5 mm (0.21 in) and 21 mm (0.84 in), respectively. While Eqn. 18 provides a feasible maximum displacement, actual measurements would be required to verify this model.

Redistribution of Strain upon Manual Removal of CFRP

When a RC beam shear strengthened with CFRP U-wraps fails, a sudden progressive debonding of the strips is typically observed. To study the effect of bond loss along portions of adjacent CFRP strips on the remaining shear resisting components, some CFRP strips bonded to specimen FT5 were systematically removed while repeating the same load conditions during steps 2b-2h.

Support locations remained in one location ($a/d = 2.5$) and the same maximum value of shear was applied during each load step (778 kN). A detailed description of the manual removal of strips with corresponding cracking and debonding diagrams may be found in the previous experimental program. Measured strains in the internal stirrups and CFRP strips in the south span during these load steps are shown in Fig. 34.

Measured strain was studied as opposed to cumulative strain to mitigate the influence of the combined effects over the duration of the test, such as crack propagation and debonding, which were discussed previously. No strips were altered for load step 2b, which was used for the baseline to compare responses. Specimen FT5 eventually failed during load step 2h.

Internal stirrups gages 3S and 4S indicated yielding after the maximum applied shear was reached during load step 2g. CFRP gage 2S was deactivated before load step 2f since the strip it was attached to was removed up to the gage location. Likewise, CFRP gage 6S was removed before load step 2g.
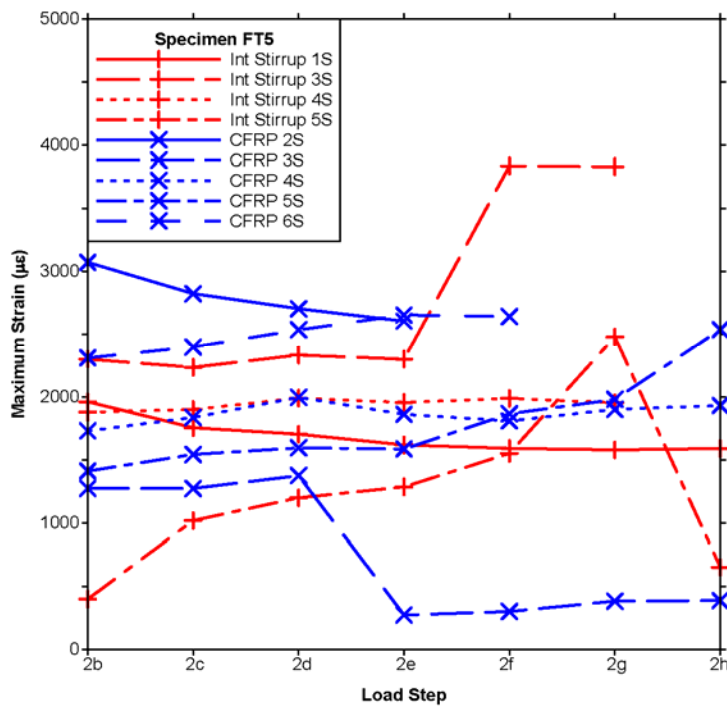
Fig. 34 – Maximum measured strain in the internal stirrups and CFRP strips during load steps 2b-2h of specimen FT5.

Internal stirrup gage 3S exhibited a significant increase in strain at load step 2f. Prior to load step 2f, the sixth seventh and eighth CFRP strips from the south end of the specimen were removed to mid-height on alternating faces. Internal stirrup gage 3S was located between the seventh and eighth strips. Fig. 34 indicates that the reduction of CFRP bonded

area in strips directly adjacent to internal stirrup gage 3S resulted in a significant strain increase in the stirrup.

Likewise, internal stirrup gage 5S exhibited a significant increase in strain at load step 2g. Prior to load step 2g, the ninth CFRP strip from the south end of the specimen was removed to mid-height. Internal stirrup gage 5S was located between the ninth and tenth strips.

Stirrup gage 1S and CFRP gage 2S showed about the same relative decrease in strain between load steps 2b and 2e. During load steps 2c, 2d and 2e, 152 mm (6 in.) was removed from the bottom of the sixth, seventh and eighth strips, respectively. Fig. 34 indicates that these removals did not significantly affect the other gages in the vicinity. Diagonal cracks and debonded CFRP were not observed to expand significantly during these load steps, which may account for the reduction in strain measurements.

Strain Compatibility

To determine whether the CFRP and internal stirrup strains were compatible, strain gage measurements were compared for adjacent components located along the same diagonal crack. Strain values from adjacent internal stirrups and CFRP strips along diagonal cracks in specimen FC are shown in Fig. 35. Load steps are presented in order (0, 1, 2, 3, 4, 2b, 2c and 3b) with an imposed manual offset of 2000 $\mu\varepsilon$ between the load steps.
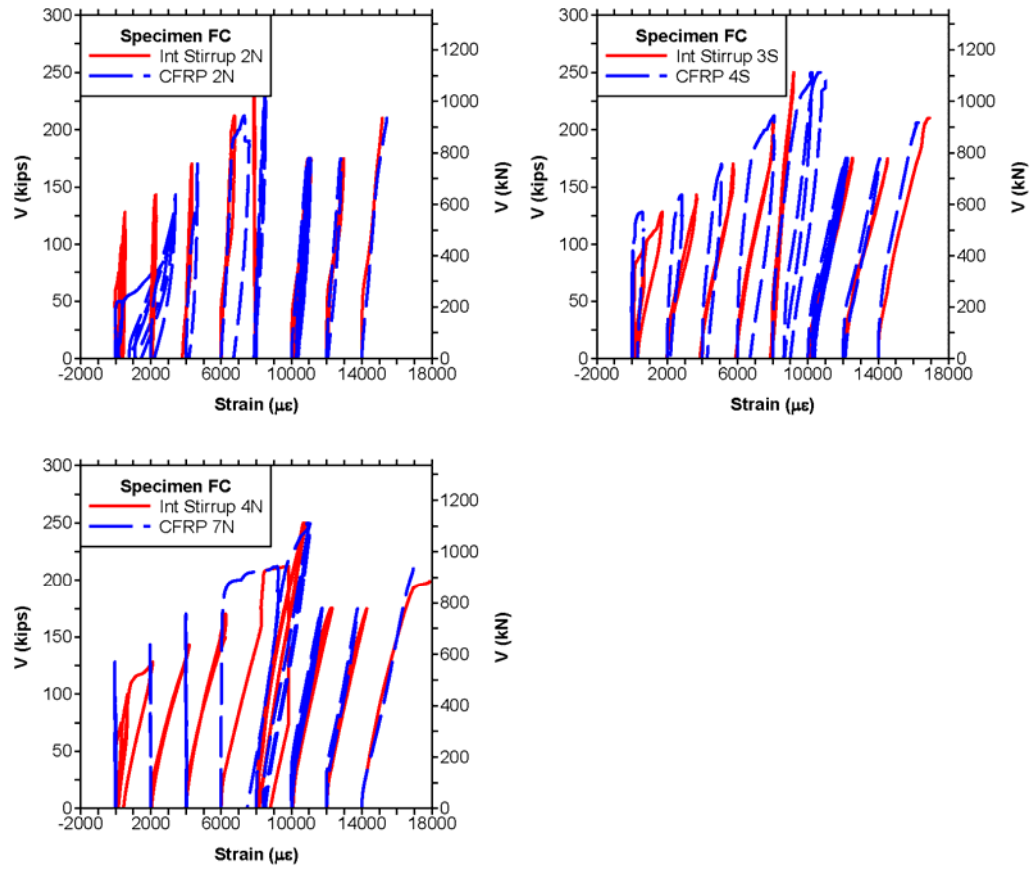
Fig. 35 – Strain in adjacent internal stirrups and CFRP strips of Specimen FC.

Strains in specimen FC were initially quite small during load step 0 ($a/d = 3.3$) prior to formation of diagonal cracking. After a diagonal crack forms, either the stirrup or strip will exhibit higher strain depending on the sensor location relative to the crack location. The strains do not appear to be compatible at these early cracking stages (through load steps 1-4). Internal stirrup strains would tend to be highest at the diagonal crack and then decrease over the development length. Development lengths, ℓ_d, for internal stirrups were calculated

according to ACI 318-05 Section 12.2.2 (Eqn. 20) and are given in Table 16. Strain gages on internal stirrups were located at mid-height of the specimens.

$$\ell_d = \left(\frac{f_y \psi_t \psi_e \lambda}{25\sqrt{f_c'}} \right) d_b \qquad [20]$$

where f_y = yield strength, ψ_t = modification for reinforcement location, ψ_e = modification for coating, λ = modification for concrete unit weight, f_c' = concrete compression strength and d_b = reinforcement diameter.

Table 16: Development lengths for internal stirrups.

Specimen	FC	FT	HC	HT	QC & QT
ℓ_d (mm) [in]	353 [13.9]	345 [13.6]	164 [6.46]	162 [6.38]	160 [6.29]
h/2 (mm) [in]	533 [21]	533 [21]	267 [10.5]	267 [10.5]	133 [5.25]

CFRP strains would likely be highest over the diagonal cracks and locally debonded areas because of the combined uniaxial and flexural-tension induced strains. CFRP strains would decrease away from debonded areas, along the effective bond length, and as debonded lengths grew. CFRP effective bond length was 48 mm (1.9 in.) for all specimens, which was much shorter than the internal steel stirrup development length.

Strains appear to be compatible during load steps 2b, 2c and 3b. Specimen FC underwent its highest applied shear and experienced widespread debonding during load step 4. After load step 4, debonded lengths may have become large enough for flexural-tension strains to become greatly reduced and for debonded regions to have reached the CFRP gages and effectively allow for average strain conditions in the components.

The strain compatibilities observed for all specimens are shown in Fig. 36. Load steps are shown in order for each specimen with an imposed manual offset of 2000 $\mu\varepsilon$ for each subsequent load step. Later load steps were not included if gage failure occurred previously or if the support location caused vastly different behavior (*i.e.* when the support was placed in between two gages, causing one gage to report zero strain while the other reported a non-zero strain). As seen in these figures, the other specimens exhibited similar stirrup and CFRP strip strain compatibility conditions to those described for specimen FC.
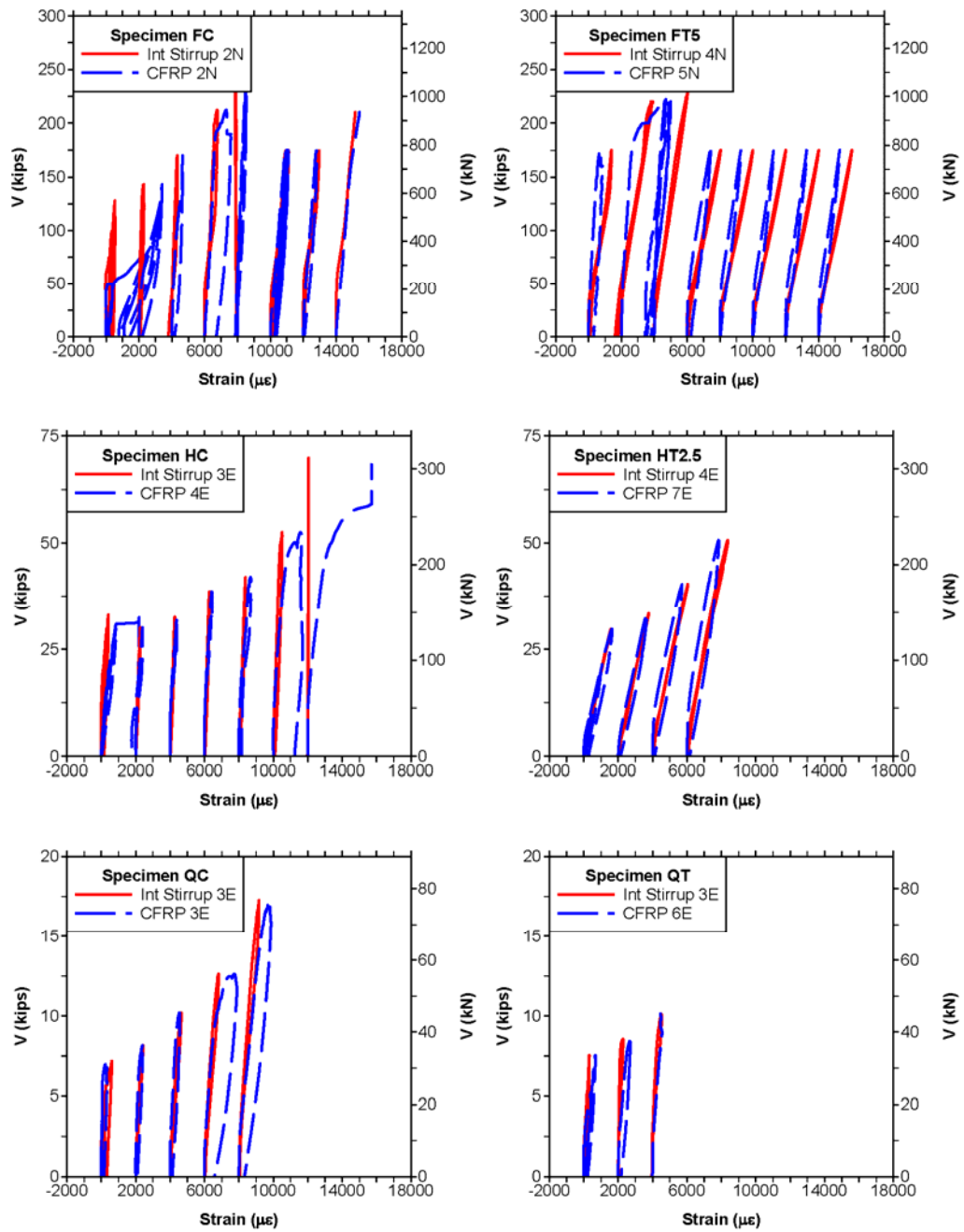
Fig. 36 – Measured internal stirrup and CFRP strains for all specimens.

Average Vertical Strain

Average vertical strains were used to estimate the CFRP shear contribution at the final

loading step when failure occurred. As discussed previously, surface bonded strain gage

measurements can contain large local variations, which may be sensitive to the scale of the

specimen relative to the instrument gage length (*e.g.* where the strain gage covers a very

small portion of CFRP strips).

The diagonal displacement measurements from the failure load step were converted into

average vertical strains using Mohr's circle, shown in Fig. 37. This conversion was based

upon five known quantities, as shown in Fig. 38: diagonal tension displacement (L_t),

diagonal compression displacement (L_c), diagonal displacement gage length (L_o), diagonal

displacement gage orientation ($\theta_{diagonal}$) and failure crack angle (θ_{crack}). Changes in the

diagonal displacement orientation were assumed to be negligible. This method was not

used for non-failure load steps since the failure crack had not evolved during the earlier

load steps.
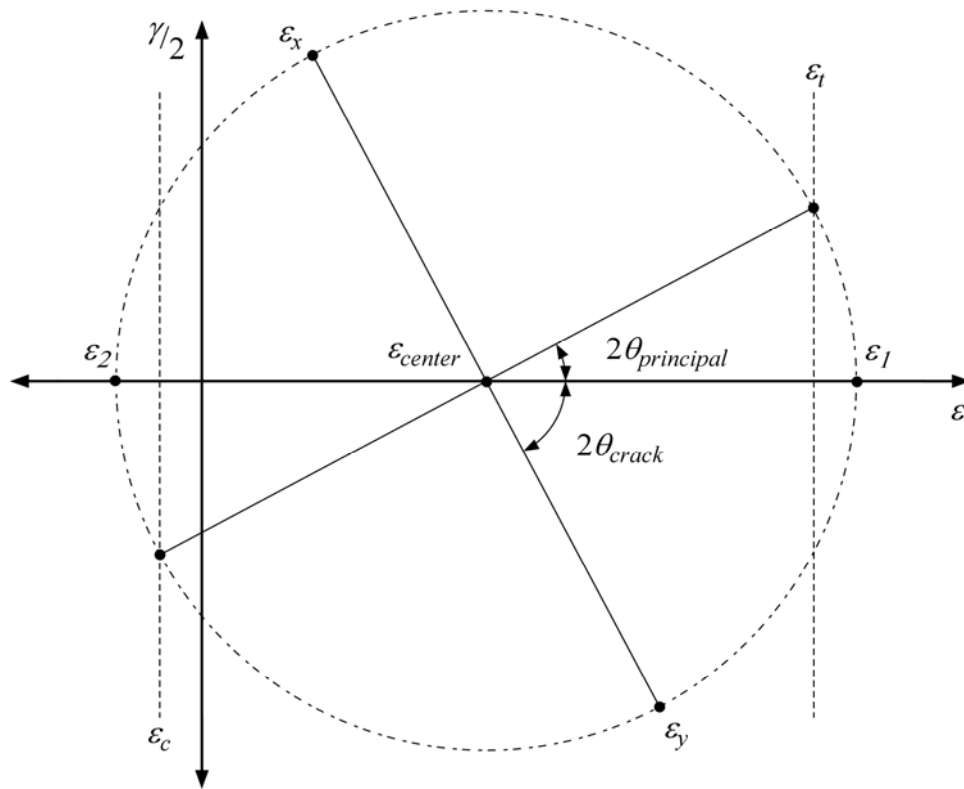
Fig. 37 – Mohr's circle for strain.
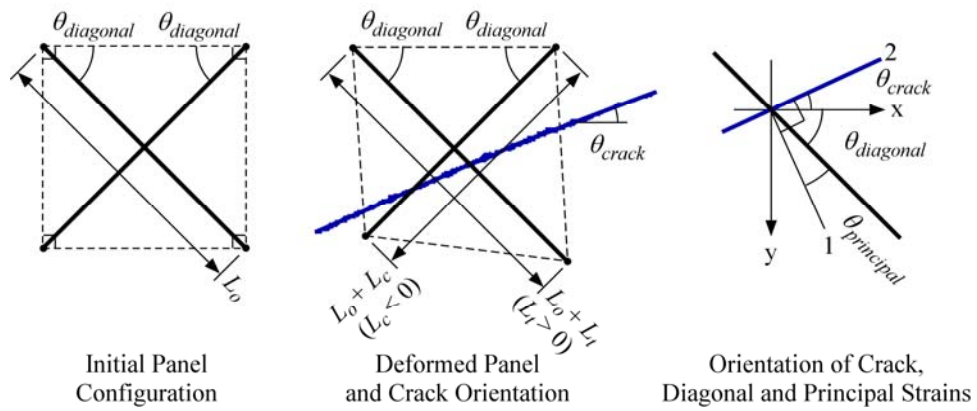
Fig. 38 – Diagonal displacement geometry.

The following describes the process of converting the diagonal displacement measurements into strains using Mohr's circle. First, the diagonal displacement measurements were converted into strains, ε_t and ε_c, using Eqns. 21 and 22. These tension and compression strains were then used to find the center of Mohr's circle, ε_{center}, using Eqn. 23. The orientation of the principal strain, $\theta_{principal}$, was assumed to be orthogonal to the failure diagonal crack orientation and was calculated using the diagonal displacement gage orientation and crack angle using Eqn. 24. The radius of Mohr's circle, R, was calculated using Eqn. 25. Principal strains, ε_1 and ε_2, as well as vertical and horizontal strains, ε_x and ε_y, could then be resolved, as shown in Eqns. 26-29.

$$\varepsilon_t = \frac{L_t}{L_o} \tag{21}$$

$$\varepsilon_c = \frac{L_c}{L_o} \tag{22}$$

$$\varepsilon_{center} = \frac{\varepsilon_t + \varepsilon_c}{2} \tag{23}$$

$$\theta_{principal} = 90° - \theta_{diagonal} - \theta_{crack} \tag{24}$$

$$R = \frac{\varepsilon_t - \varepsilon_{center}}{\cos 2\theta_{principal}} \tag{25}$$

$$\varepsilon_1 = \varepsilon_{center} + R \tag{26}$$

$$\varepsilon_2 = \varepsilon_{center} - R \tag{27}$$

$$\varepsilon_x = \varepsilon_{center} - R\cos 2\theta_{crack} \tag{28}$$

$$\varepsilon_y = \varepsilon_{center} + R\cos 2\theta_{crack} \tag{29}$$

Average vertical strains, ε_y, during the failure load step were compared with measured surface bonded strain gage strains in the CFRP and internal stirrups for specimens FC and FT5, as shown in Fig. 39. It appears that the average vertical strains correlate fairly well to the average of the bonded strain gage strains. Average strains from the diagonal deformation measurements for all specimens are shown in Fig. 40. Surface bonded strain gage strains from components crossing the failure crack are provided for comparison at the half and quarter scales.
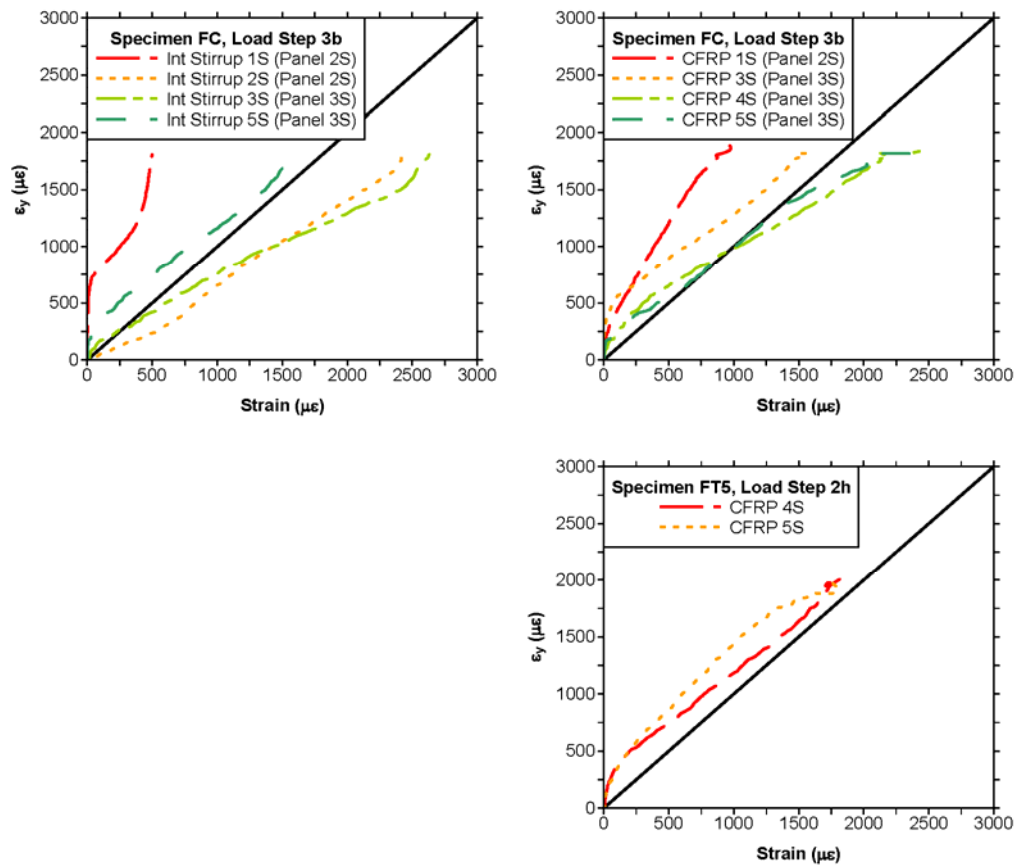
Fig. 39 – Average panel strain in the vertical direction versus surface bonded strain gage strain for specimens FC and FT5 during failure load steps (left column: internal stirrups, right column: CFRP).
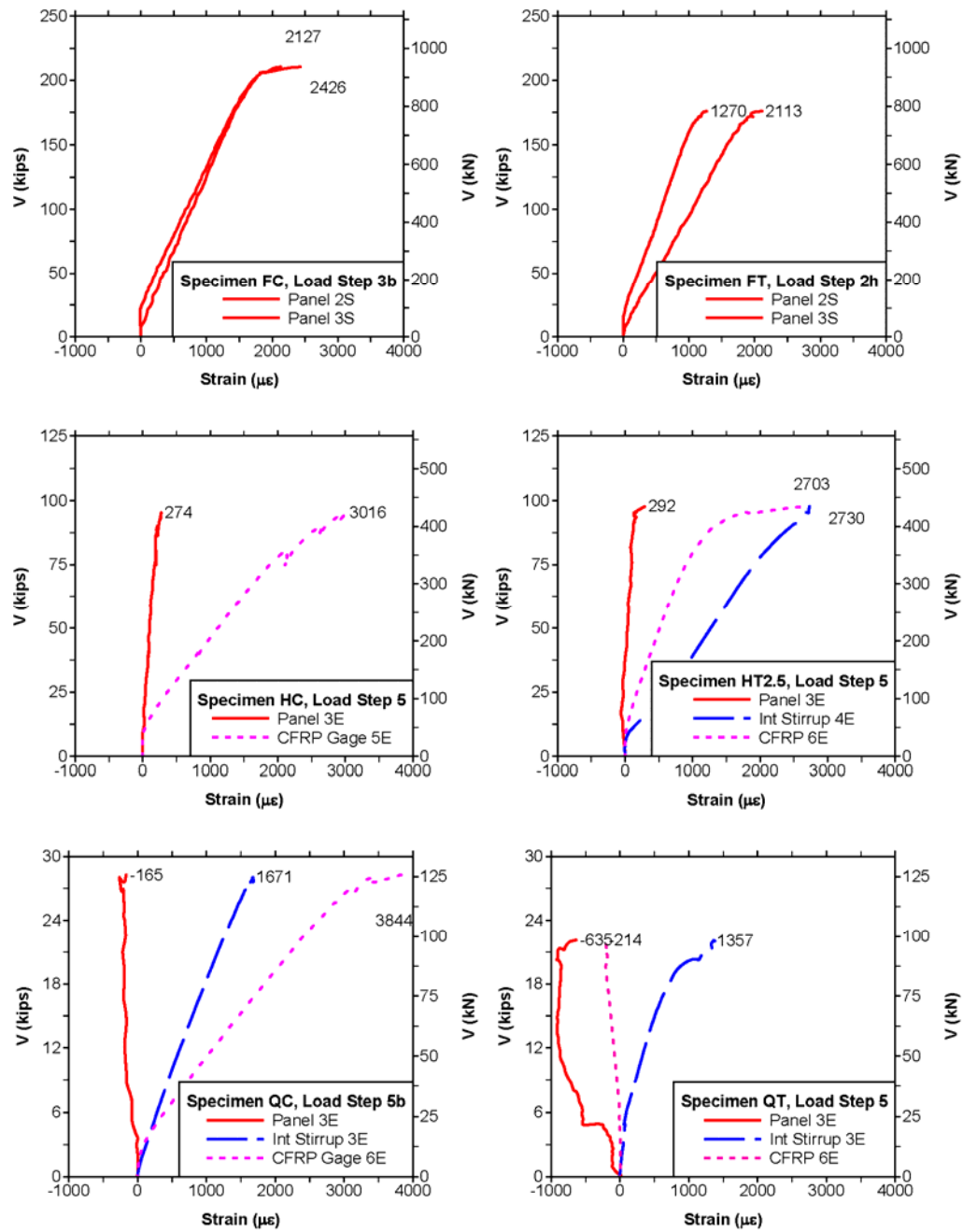
Fig. 40 – Applied shear versus average vertical strain for specimen FC during load step 3b.

Average vertical strains and surface bonded strain gage strains appear to become less correlated as the scale decreases and at the low *a/d* ratios. To estimate the CFRP contribution, average strains will be used for the full-scale specimens while internal stirrup strain measurements will be used for the half- and quarter-scale specimens. As shown by Table 16, stirrup development lengths make up a significant portion of the beam height for the half- and quarter-scale specimens and may better average strains in the section compared with the CFRP, which has an effective bond length that makes up a much smaller proportion of the beam height. In addition, the relatively large strain gage relative to the strip length and possible flexural-tension induced by local CFRP strip debonding may have larger effects on the smaller specimens.

COMPARATIVE ANALYSIS

Introduction

Since there were no control specimens, a nonlinear finite element analysis package for reinforced concrete, VecTor2©, was employed to model specimen capacity without CFRP strengthening. The CFRP shear contribution was calculated as the difference between the strengthened specimen capacity, V_{app}, and the modeled unstrengthened capacity, $(V_c + V_s)_{FEM}$.

The CFRP shear contribution calculated using finite element analysis results was compared with experimental data. For the full-scale specimens, average strains were transformed from diagonal displacements to estimate CFRP strain at capacity. For the half- and quarter-scale specimens, internal stirrup strains were used to estimate CFRP strain at capacity. CFRP strains were used to calculate the experimental CFRP contribution, $(V_f)_{exp}$.

CFRP shear contributions from finite element modeling and experimental data were compared to the ACI 440.2R-02 shear contribution, $(V_f)_{ACI}$, as described in the literature review.

All estimates of CFRP shear contribution assumed that the nominal shear capacity, V_n, was equal to the sum of the shear contributions from the concrete, V_c, steel, V_s, and CFRP, V_f, as illustrated by Fig. 41.
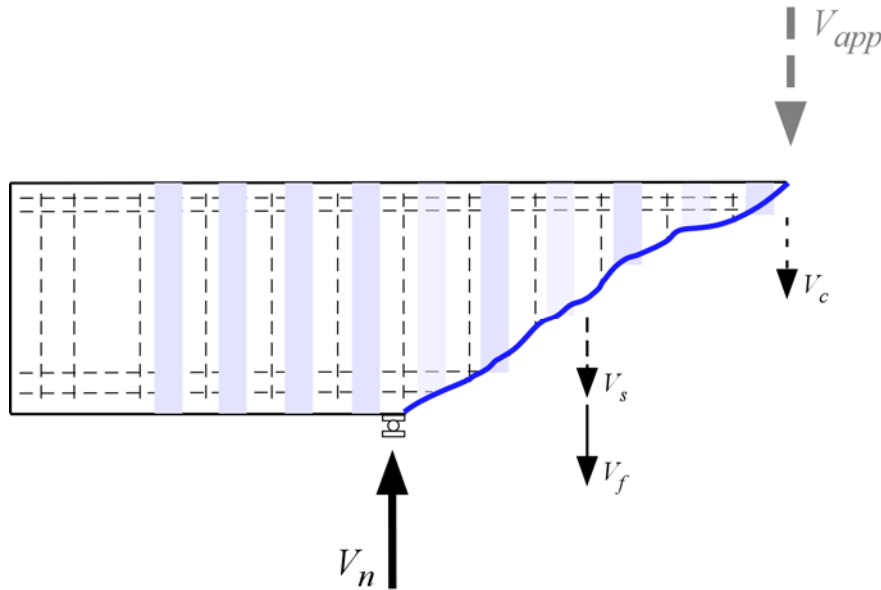
Fig. 41 – Free body diagram for specimen FC at failure.

Nonlinear Finite Element Analysis Method

VecTor2 was developed at the University of Toronto based on modified compression field

theory (MCFT) and the disturbed stress field model [Wong and Vecchio 2002]. The

package includes a graphical preprocessor, FormWorks©, and a graphical post-processor,

Augustus©.

The following constitutive models were assumed for the concrete and steel reinforcement

using the FormWorks program default settings. Referenced models may be found in the

VecTor2 user manual [Wong and Vecchio 2002].

The following models were applied to concrete. A Hognestad parabola was applied to pre-

peak compression response, with the modified Park-Kent model applied to post-peak

response, which allows enhanced strength and ductility from confinement. Compression softening was modeled by Vecchio (1992-A), which is based on the ratio of principal strains. The tension stiffening model was modified from Sato and Vecchio (2003). Post-cracking tensile stresses were assumed to descend linearly. Splitting cracks parallel to tension reinforcement were not considered. Enhanced strength from confinement was modeled by the Kupfer/Richart model. The cracking strength of concrete was calculated from the cylinder compression strength using the Mohr-Coulomb criterion and assuming an angle of internal friction of 37 degrees. The local shear stresses of elements were limited by Vecchio-Collins (1986) to avoid crack slip. Crack widths were limited to one-fifth of the maximum aggregate size. Strain from element slip was accounted for with the Vecchio-Lai (2002) stress model. A nonlinear hysteretic response with plastic offsets was selected, but not necessary since the analysis package was used as a strength capacity check for a particular load step and did not use previous damage or cyclic loading.

The following models were applied to steel reinforcement. Hysteretic response of reinforcement was governed by the Seckin model with the Bauschinger effect, which permits premature yielding upon load reversal after plastic prestraining. Dowel action was modeled as elastic-plastic according to Tassios model. The Asatsu buckling model was selected for discrete reinforcement, but not applicable since perfect bond was assumed. The Eligehausen bond stress-slip model was selected, but not applicable since perfect bond was assumed.

Specimens were modeled as plane members using the measured material properties, which were provided in the experimental program.

Concrete compression strength and maximum aggregate size were taken from cylinder

tests and mix design submittals, respectively. The full scale desired rectangular element

size was 80 mm [3.1 in.] square, which is approximately equal to the cover from the

centroid of steel. Half and quarter scale meshes were 40 and 20 mm [1.6 and 0.79 in.],

respectively. The mesh size was determined by convergence.

Reinforcing steel was modeled discretely using the measured yield and ultimate strengths

from tensile tests. The elastic modulus, E_s, was taken as 200000 MPa (29000 ksi), the

strain hardening modulus, E_{sh}, was taken as 20000 MPa (2900 ksi) and the strain hardening

strain, ε_{sh}, was taken as 10000 με.

Since statistical data were not available for the VecTor2 program, Response-2000© was

used to compare behavior for $a/d \geq 2$. Response-2000, a nonlinear sectional analysis

program based on MCFT, was developed at the University of Toronto [Bentz 2001]. This

program predicted the unrepaired member capacity to within 2% with a coefficient of

variation under 8% for a series of 44 similar full-scale RC specimens tested at Oregon

State University (Higgins *et al*. 2004).

To evaluate VecTor2, test data were used for the initial load steps of each specimen ($a/d =$

3.3). For this value of a/d, it was assumed that the behavior would be dominated by

flexure, with the CFRP having little influence. In addition, the specimens were undamaged

before this load step. As shown by Fig. 42, the VecTor2 program models the behavior of

these specimens at all scales fairly well.
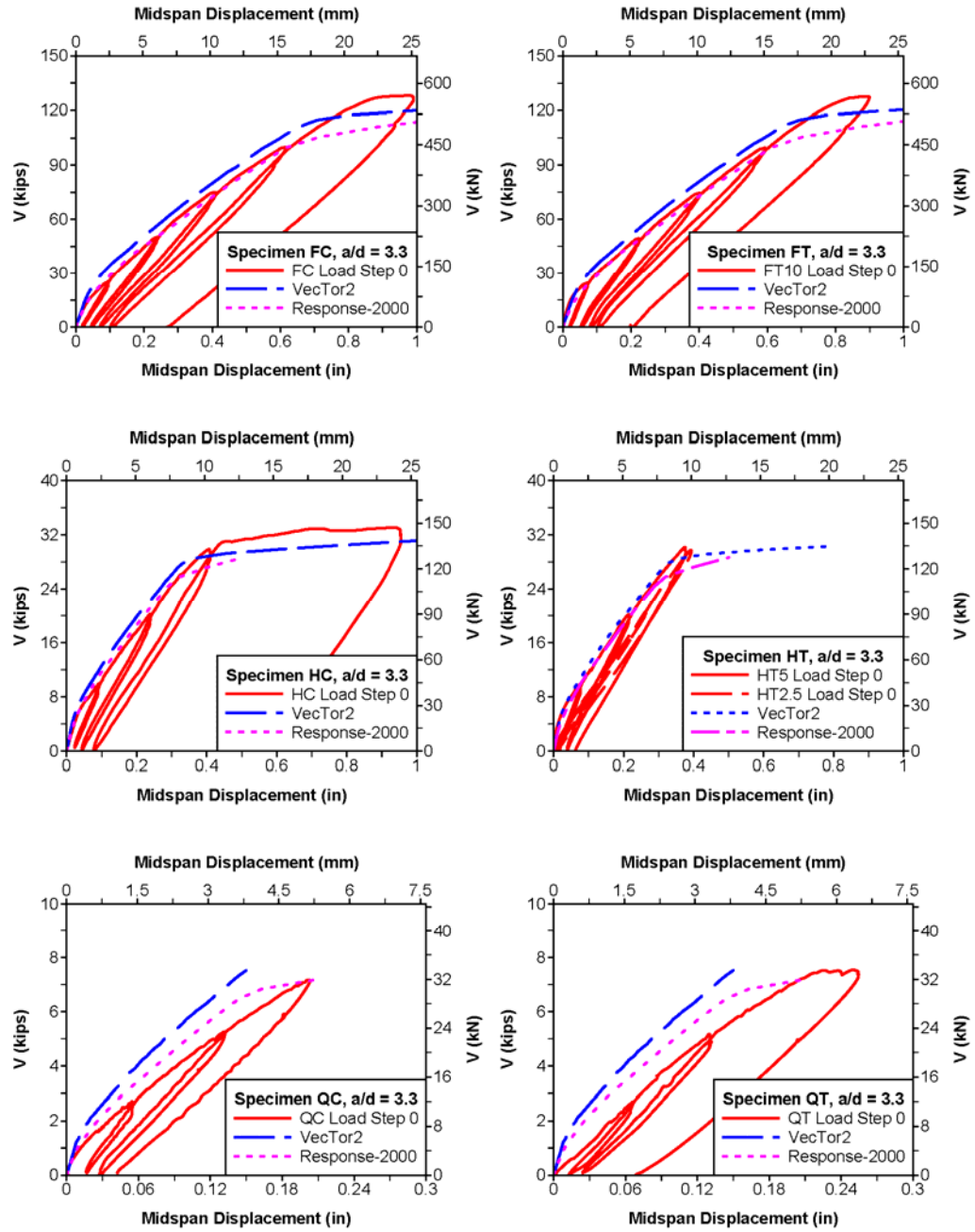
Fig. 42 – Comparison of VecTor2 and Response-2000 analysis programs at *a/d* = 3.3 for all test specimens (note: axis scales vary).

Shear Contribution of CFRP using Finite Element Analysis

Shear-displacement curves at the failure load step for each specimen are shown in Fig. 43.

VecTor2 and Response-2000 appear to provide similar models of behavior for $a/d \geq 2$ (full

scale specimens only). Test curves are generally more linear than the curves produced

from finite element analysis because of damage acquired over multiple load steps.

CFRP capacity was taken as the difference between the test capacity and the modeled

unstrengthened capacity:

$$(V_f)_{FEM} = V_{app} - (V_c + V_s)_{FEM} \qquad [30]$$

where $(V_f)_{FEM}$ = CFRP shear contribution (kN) [kips], V_{app} = tested capacity (kN) [kips],

$(V_c + V_s)_{FEM}$ = modeled unstrengthened capacity (kN) [kips]. Base capacities from FEM are

shown in Table 17, column (4). CFRP shear contributions calculated using the FEM base

capacity are shown in Table 17, column (5).
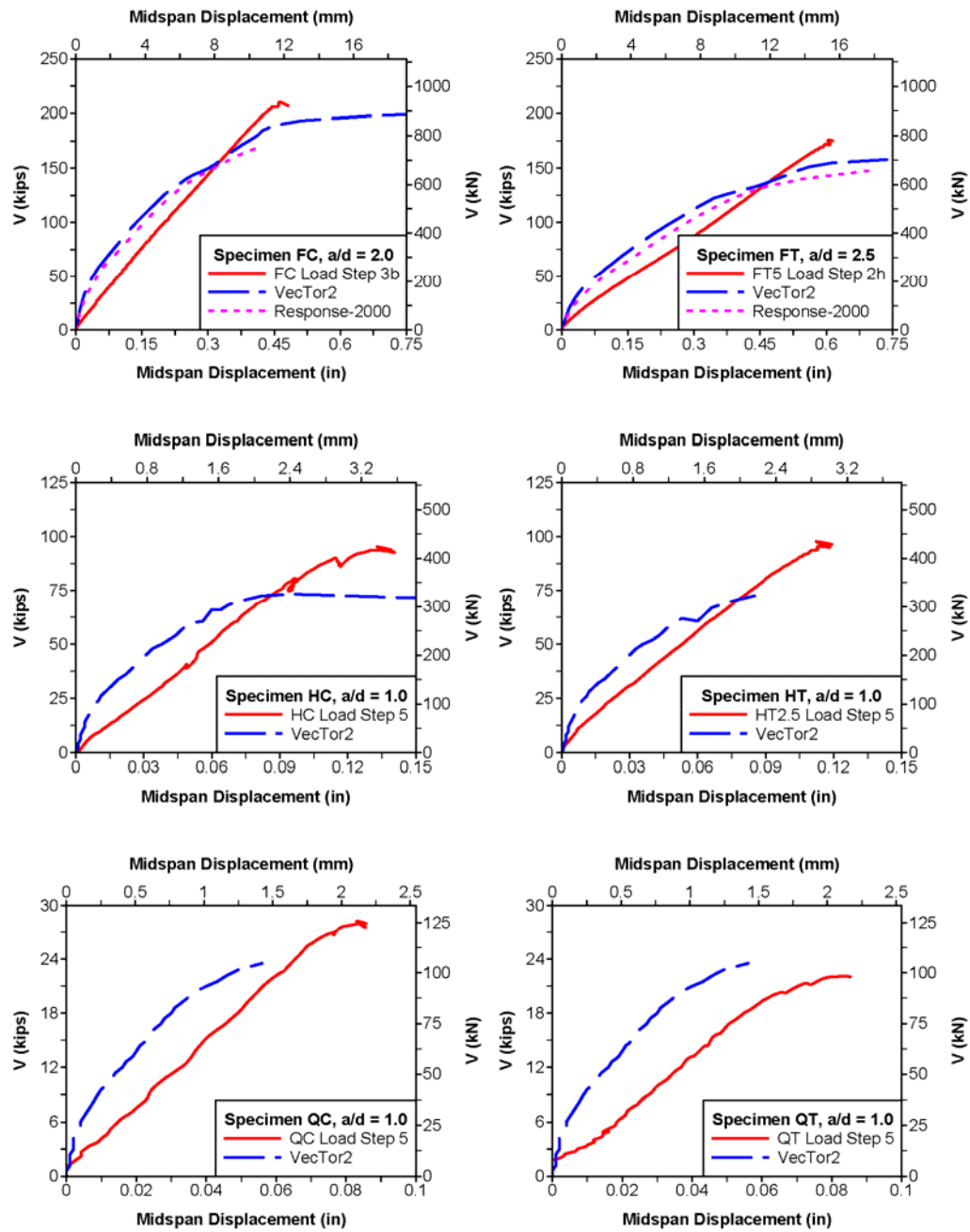
Fig. 43 – Comparison of test curves and VecTor2 modeled base capacity at failure.

CFRP Shear Contribution Using Experimental Results

The experimental CFRP shear contribution, $(V_f)_{exp}$, was calculated from maximum average

vertical strains or maximum internal stirrup strains using the following equation:

$$(V_f)_{exp} = w_f t_f E_f \sum_{i=1}^{m} n_{fi} \varepsilon_{yi} \qquad [31]$$

where w_f = CFRP strip width (mm) [in.], t_f = CFRP coupon thickness (mm) [in.], E_f =

CFRP tensile modulus (GPa) [ksi], m = number of different average strain values, n_{fi} =

number of strips corresponding to a particular value of strain (each U-wrap was counted as

two strips), ε_{yi} = a particular average value of CFRP strain. Estimated CFRP strain values

are shown in Table 17, column (6), along with the number of strips corresponding to those

values. Calculated experimental CFRP shear contributions are shown in Table 17, column

(7).

CFRP Shear Contribution Using ACI

The CFRP shear contribution was also calculated according to the provisions of ACI

440.2R-02 and ACI 318-05, as described in the literature review. ACI 440.2R-02 is

commonly used to design CFRP repairs in practice.

Given the removed strips on alternating faces of specimens FC and FT5, it was unclear

how to define the CFRP reinforcement. Since the CFRP remained bonded to the bottom or

top soffit (forming an L-shape) for specimens FC and FT5, respectively, the strips were

treated as U-wraps at twice the original spacing. All other specimens possessed intact U-

wraps.

ACI shear contributions from concrete and steel components are shown in Table 17, column (8). The CFRP shear contribution calculated according to ACI is shown in Table 17, column (9).

Table 17: CFRP shear contributions from finite element model, experimental data and ACI.

Specimen	a/d at Failure	V_{app} (kN) [kips]	$(V_c+V_s)_{FEM}$ (kN) [kips]	$(V_f)_{FEM}$ (kN) [kips]	ε_{yi} (µε) $[n_i]$	$(V_f)_{exp}$ (kN) [kips]	$(V_c+V_s)_{ACI}$ (kN) [kips]	$(V_f)_{ACI}$ (kN) [kips]	$(V_n)_{ACI}$ (kN) [kips]
(1)	(2)	(3)	(4)	(5)	(6)	(7)	(8)	(9)	(7)
FC	2.0	934 [210]	940 [211]	0[a]	2127 [3][b] 2426 [3][b]	74 [16.6]	574 [129]	66 [14.9]	641 [144]
FT5	2.5	783 [176]	778 [175]	4 [1]	1270 [2][b] 2113 [4][b]	59 [13.3]	578 [130]	66 [14.9]	645 [145]
HC	1.0	424 [95.3]	307 [69.1]	117 [26.2]	[c]	[c]	139 [31.2]	131 [29.5]	270 [60.7]
HT2.5	1.0	435 [97.7]	318 [71.5]	117 [26.2]	2730 [6][d]	89 [19.9]	140 [31.5]	66 [14.8]	206 [46.3]
QC	1.0	126 [28.3]	105 [23.5]	21 [4.8]	1671 [4][d]	36 [8.1]	36 [8.1]	16 [3.6]	52 [11.7]
QT	1.0	98 [22.1]	105 [23.5]	0[a]	1357 [4][d]	29 [6.6]	36 [8.1]	16 [3.6]	52 [11.7]

a: the addition of CFRP likely did not reduce the capacity of specimens FC and QT
b: CFRP strain estimated from average vertical strains
c: no reliable strain measurements available
d: CFRP strain estimated from internal stirrup strains

Table 18: Variation between shear contributions from finite element model and ACI.

Specimen	a/d at Failure	$\dfrac{(V_c+V_s)_{ACI}}{(V_c+V_s)_{FEM}}$	$\dfrac{(V_f)_{ACI}}{(V_f)_{FEM}}$	$\dfrac{(V_f)_{ACI}}{(V_f)_{exp}}$	$\dfrac{(V_f)_{FEM}}{(V_f)_{exp}}$	$\dfrac{(V_n)_{ACI}}{V_{app}}$
(1)	(2)	(3)	(4)	(5)	(6)	(7)
FC	2.0	0.61	-	0.90	-	0.69
FT5	2.5	0.74	-	1.12	-	0.82
HC	1.0	0.45	1.13	-	-	0.64
HT2.5	1.0	0.44	0.56	0.74	1.32	0.47
QC	1.0	0.35	0.75	0.44	0.59	0.41
QT	1.0	0.35	-	0.55	-	0.53

Comparison of Base Capacity and CFRP Contribution

Calculated values of base shear capacity and CFRP shear contribution are compared in

Table 18.

As shown in Table 18, column (3), the ACI equations for concrete and steel shear

contribution provide a base capacity lower than the finite element analysis. The ratio of

ACI-to-FEM base capacity appears to be affected by the scale of the specimen, with higher

values at the full-scale and decreasing values at the half- and quarter-scale. The ratio may

also be affected by the value of a/d at failure, which is provided in column (2). Based on

these observations, the level of conservatism for the ACI method appears to be greater for

lower values of a/d and d.

As shown in Table 18, column (4), the ACI CFRP shear contribution was generally lower

than the contribution calculated using finite element analysis, with the exception of

specimen HC. Specimen HC had twice the strip width of specimen HT2.5, though both

failed at approximately the same applied shear at an $a/d = 1$. Specimens HC and HT2.5

should therefore have had nearly the same CFRP contribution since they had

approximately the same base specimen capacity. The ACI approach may have

overestimated capacity for larger strip widths, but that could not be confirmed with this

data. The ratio of shear contributions from ACI and FEM analysis do not appear to be

affected by the scale of the specimen or by the a/d ratio.

As shown in Table 18, column (5), the ACI CFRP shear contribution was unconservative

for specimen FT5, possibly unconservative for specimen HC and conservative for the other

specimens. The ACI shear contribution appeared unconservative for specimen HC, though this could was not definitive based upon the available data. The ACI prediction became more conservative as the specimen scale decreased. As the half- and quarter-scale specimens failed at a lower value of a/d, the ACI prediction also became more conservative for lower a/d ratios. The ratio of ACI-to-experimental CFRP shear contribution appears to be affected by the scale of the specimen and possibly the a/d ratio and U-wrap orientation.

As shown in Table 18, column (6), the CFRP shear contribution calculated using finite element analysis is larger than the experimental value at the full-scale and for specimen HT2.5. The CFRP shear contribution using FEM was lower than the experimental value for the quarter-scale specimens, with no contribution provided by the CFRP for specimen QT.

Because of variability in the test data, it is difficult to draw further conclusions about scale effect on shear capacity from Tables 17 and 18. Variations in the test data include the following:

- CFRP reinforcement ratios were not the same across all scales.
- Specimens failed at different values of a/d.
- A large amount of CFRP material was removed from specimens FC and FT5 such that the specimens appeared to fail at their base capacities.
- Reliable average CFRP strain measurements were not available for specimen HC.
- Specimen QT failed below its estimated base capacity from FEM analysis.

CONCLUSIONS

Based upon the results of experimental testing:

- CFRP strains were small until crossed by a diagonal crack.

- CFRP debonding accumulated as increased loads were applied at progressively smaller *a/d* ratios.

- Debonding was observed during testing by tapping on the CFRP surface; debonded CFRP sounded hollow when compared to adequately bonded CFRP. Debonding was observed as decreased slope, large strains, nonlinear loading and unloading behavior and plastic offset when CFRP strains were plotted against applied shear.

- Debonded CFRP was observed locally around diagonal cracks that crossed the strip. After failure, some debonded CFRP strips had pulled away shallow concrete wedges at the diagonal crack. Debonded CFRP was characterized by out-of-plane deformation, which was restrained by adjacent regions of CFRP with adequate bond.

- Large local strains were measured near diagonal cracks and were attributed to flexural-tension strains induced by bending of the debonded CFRP. Two simple expressions were presented to calculate additional tensile strains from debonding. These expressions indicated that flexural-tension strains dissipated nonlinearly as the debonded length increased. Beam height provided a limit on the debonded length and, subsequently, limited the dissipation of local strains.

- Based upon the systematic removal of portions of CFRP strips, strains from removed strips appeared to redistribute to adjacent internal transverse steel reinforcement.

- Inverted U-wraps accumulated less strain than the normal U-wrap configuration with nearly identical base specimens.

- As diagonal cracks initially grew, the measured strains in steel and CFRP components were not compatible. Internal stirrup and CFRP strains became compatible along diagonal cracks once debonded CFRP regions grew such that flexural-tension strains from bending dissipated and strain gages were not farther from the debonded region than the effective bond length.

- Due to local variations from CFRP strain gage measurements, average vertical strains transformed from diagonal displacement measurements during the failure load step were used to estimate the CFRP shear contribution. This method provided reasonable average vertical strains for the full-scale specimens, but not the half- and quarter-scale specimens, which failed at smaller values of *a/d*. Internal stirrup strains were used to calculate the CFRP shear contribution at the half- and quarter-scales since the development length of transverse reinforcement took up a significant portion of the beam depth and contained the failure diagonal crack.

Based upon the comparative analysis:

- The ACI 318-05 concrete and steel shear contributions appeared to provide conservative estimates of base specimen capacity when compared to a finite element model. The ACI base capacity prediction appeared to become more conservative with decreased specimen scale and *a/d* ratio.

- The ACI 440.2R-02 CFRP shear contribution appeared to provide a conservative estimate when compared with the contribution found using the finite element

model for base capacity, except for specimen HC, which had the largest CFRP

reinforcement ratio of all the failed specimens due to relatively wide strips. This

may imply that the ACI method overestimates the capacity of wide strips, though

this could not be confirmed with the available data. Otherwise, the ACI prediction

did not appear affected by scale or a/d when compared to the prediction using

finite element analysis to model the base capacity.

- The ACI 440.2R-02 CFRP shear contribution was unconservative for some of the

  specimens when compared to the experimental shear contribution. The ACI

  method overestimated the CFRP shear contribution of specimen FT5, which was

  strengthened by an inverted U-wrap. The ACI method appeared to overestimate

  the CFRP shear contribution of specimen HC, which had the largest CFRP

  reinforcement ratio of all the failed specimens due to relatively wide strips, though

  this could not be adequately confirmed with the available test data.

RECOMMENDATIONS

Scaling Variables

Before small-scale RC specimens with discrete CFRP U-wraps are used for environmental durability studies, the effects of scaling need to be modeled carefully using a large database of tested specimens. Several variables that may affect shear capacity were identified through this research. These variables include:

- Effective depth (d)

- Shear span-to-depth ratio (a/d)

- Flexural-tension steel reinforcement ratio (ρ_s)

- Transverse steel reinforcement ratio (ρ_v)

- CFRP reinforcement ratio (ρ_f)

- U-wrap orientation (*i.e.* normal or inverted)

- CFRP strip width (w_f)

In addition, it was theorized that the number of CFRP layers, n_f, may influence shear capacity. Possible values of these variables for future testing are provided in Table 19, with justifications for each value following the table. Values in Table 19 should be viewed as an order of magnitude and not as explicit design values.

Table 19: Possible values for further scaled tests.

d (mm) [in.]	a/d	ρ_s (%)	ρ_f (%)	n_f	U-wrap orientation	w_f (mm) [in.]
900 [36]	1.0	1.0	1.0	1	normal	100 [4]
200 [9]	2.5	3.0	0.25	multiple	inverted	25 [1]

Effective Depth: Laboratory scale effective depths in the literature are commonly on the order of 200 mm (9 in). Conventional RC deck girders often possess effective depths on the order of 900 mm (36 in) as this is approximately the limit on effective depth before skin steel is required. These sizes would constitute full- and quarter-scales. While intermediate scales would benefit the understanding of scale effects, the full- and quarter-scales represent common laboratory and field scales.

Shear Span-to-Depth Ratio: The two values of *a/d* are suggested to capture the behavior of deep and slender beams.

Flexural-tension Steel Reinforcement Ratio: Laboratory scaled specimens are typically over-reinforced to avoid flexural failure. Older tests cited by the literature used lower grades of reinforcing steel and thus required higher reinforcement ratios. Actual structures commonly have lower reinforcement ratios, which this study emulated.

Transverse Steel Reinforcement Ratio: The majority of tests described in the literature used specimens without transverse steel reinforcement. To simulate field conditions, internal stirrups were included in this test series. The inclusion of internal stirrups may have made it more difficult to attain shear failures at larger values of *a/d* in the CFRP strengthened specimens. For future testing, minimum or reduced stirrups should be used.

CFRP Reinforcement Ratio: For the full- and half-scale inverted U-wrapped specimens, the CFRP reinforcement ratio had to be reduced in order to achieve shear failure.

Layers of CFRP: CFRP bond models, which include the number of layers, are commonly based on small-scale or materials tests. The effect of adding layers at the full-scale should be studied closely. Multiple layers were not considered in this study.

CFRP U-wrap Orientation: The ACI CFRP shear contribution appeared less conservative for the full-scale inverted U-wrap.

Width of CFRP: During testing, inverted and normal U-wrapped strips on the same half-scale base specimen produced about the same shear capacity at an *a/d* = 1.0 despite the U-wrap having twice the strip width of the inverted U-wrap. As *d*, *a/d* and U-wrap orientation are considered here, the CFRP strip width needs to be studied as well in order to determine what led to the similarity of shear capacities.

In order to investigate the effect of each of these properties on shear capacity as outlined, 128 specimens would be required, not including control specimens. However, not all of these specimens must be new. Though not as controlled, a review of the literature should provide some specimens having properties similar to those outlined in Table 19. For future testing, design guidelines are provided.

Future Testing

Test specimens should conform to the recommendations in ACI 440.2R-02. Before testing begins, all capacities should be predicted for shear and flexure according to the provisions of ACI 318-05 and ACI 440.2R-02. This process should be relatively straightforward and could be completed with spreadsheets. If time and resources allow for more detailed

analyses, Response-2000 should be used for beam modeling where $a/d \geq 2$ and VecTor2 (or another finite element program) should be used where $a/d \leq 2$. Specimens that conform to the properties in Table 19, but are predicted to fail in flexure should be discarded from the study.

Materials should be provided by the same manufacturers and fabricators to reduce variation in material properties. Consistent concrete mix designs and reinforcing steel grades should be verified by inspection and testing.

Minimum or low amounts of internal stirrups should be used to simulate repair of an under-reinforced girder. The same stirrup shape and reinforcement ratio should be used for all specimens, as is practical, to avoid differences in relative concrete confinement.

Specimens should be pre-cracked as that represents the most likely repair state. Pre-cracking may also enable a calibration for FEM analysis.

Only U-wraps should be considered as this represents the most common RC deck girder bridge shear strengthening application (*i.e.* where the deck prevents full wrapping). Inverted U-wraps should have their free ends terminated such that the flexural-tension steel reinforcement does not reduce the biaxial stress state that occurs when CFRP is terminated in a flexural-tension zone. In RC deck girder bridges, the flexural-tension steel is typically in the deck and thus inaccessible to the FRP strip end.

Given the significant amounts of time, materials and testing facilities required to conduct a full investigation, collaboration between research institutions is recommended. Besides providing an evaluation of FRP design methods for different scales, these specimens could be used to verify finite element analysis methods or check FRP bond models. Control specimens could also be used for deep beam research.

REFERENCES

American Concrete Institute, 2002, "440.2R-02: Design and construction of externally bonded FRP systems," *ACI Manual of Concrete Practice*, Farmington Hills, Michigan.

American Concrete Institute, 2005, "318-05: Building code requirements for structural concrete and commentary," *ACI Manual of Concrete Practice*, Farmington Hills, Michigan.

Angelakos, D., Bentz, C., and Collins, M.P., 2001, "Effect of concrete strength and minimum stirrups on shear strength of large members," *ACI Structural Journal*, May-June, pp. 290-300.

ASTM E 8-00, American Society of Testing and Materials, "Standard Test Methods for Tension Testing of Metallic Materials," ASTM, West Conshohocken, PA, 2000.

ASTM A 370-97a, American Society of Testing and Materials, "Standard Test Methods and Definitions for Mechanical Testing of Steel Products," ASTM, West Conshohocken, PA, 1997.

ASTM D 3039/D 3039M-00, American Society of Testing and Materials, "Standard Test Method for Tensile Properties of Polymer Matrix Composite   Materials," ASTM, West Conshohocken, PA, 2001.

ASTM D 4541-02, American Society of Testing and Materials, "Standard Test Method for Pull-Off Strength of Coatings Using Portable Adhesion Testers," ASTM, West Conshohocken, PA, 2002.

Bakis, C.E., Bank, L.C., Brown, V.L., Cosenza, E., Davalos, J.F., Lesko, J.J., Machida, A., Rizkalla, S.H., and Triantafillou, T.C., 2002, "Fiber-reinforced polymer composites for construction – State-of-the-art review," *Journal of Composites for Construction*, 6(2), 73-87.

Bentz, E.C., 2001, "Membrane-2000, Response-2000, Triax-2000, Shell-2000 User Manual," University of Toronto, <http://www.ecf.utoronto.ca/~bentz/manual.shtml>.

Chajes, M., Januska, T., Mertz, D., Thomson, T., and Finch, W., 1995, "Shear strengthening of reinforced concrete beams using externally applied composite fabrics," *ACI Structural Journal*, V. 92, No. 3, May-June, pp. 295-303.

Higgins, C., Miller, T.H., Rosowsky, D.V., Yim, S.C., Potisuk, T., Daniels, T.K., Nicholas, B.S., Robelo, M.J., Lee, A-Y, and R.W. Forrest, 2004, "Assessment Methodology for Diagonally Cracked Reinforced Concrete Deck Girders," Report No. FHWA-OR-RD-05-04, U.S. Department of Transportation Federal Highway Administration.

Higgins, C., Williams, G., and Elkins, L., 2006, "Capabilities of Diagonally-Cracked Girders Repaired with CFRP," *Report* No. FHWA-OR-RD-06-16, U.S. Department of Transportation Federal Highway Administration.

Horiguchi, T., and Saeki, N., 1997, "Effect of test methods and quality of concrete on bond strength of CFRP sheet," *Non-Metallic (FRP) Reinforcement for Concrete Structures, Proceedings, 3rd Symposium,* Vol. 1, Japan, pp. 265-270.

Kachlakev, D, and McCurry, D., 2000, "Testing of full-size reinforced concrete beams strengthened with FRP composites: Experimental results and design methods verification," *Report* No. FHWA-OR-00-19, U.S. Department of Transportation Federal Highway Administration.

Kani, G.N.J., 1967, "How safe are our large reinforced concrete beams," *Journal of the American Concrete Institute*, March, pp. 128-141.

Khalifa, A., Gold, W., Nanni, A., and Abel-Aziz M., 1998, "Contribution of externally bonded FRP to the shear capacity of RC flexural members," *Journal of Composites in Construction*, V. 2, No. 4, pp. 195-203.

Kuchma, D., Vegh, P., Simionopoulos, K., Stankik, B., and Collins, M.P., 1997, "The influence of concrete strength, distribution of longitudinal reinforcement and member size on the shear strength of reinforced concrete beams," *CEB Bulletin No. 237 – Concrete Tension and Size Effects*, pp. 209-229.

Maeda, T., Asano, Y., Sato, Y., Ueda, T., and Kakuta, Y., 1997, "A study on bond mechanism of carbon fiber sheets," *Non-Metallic (FRP) Reinforcement for Concrete Structures, Proceedings, 3rd Symposium,* Vol. 1, Japan, pp. 279-286.

Malvar, L., Warren, G., and Inaba, C., 1995, "Rehabilitation of navy pier beams with composite sheets," *Second FRP International Symposium on Non-Metallic (FRP) Reinforcement for Concrete Structures*, Aug., Get, Belgium, pp. 533-540.

Meier, U., Deuring, M., Meier, H., and Schwegler, G., 1993, "CFRP bonded sheets," *Fiber-Reinforced-Plastic (FRP) Reinforcement for Concrete Structures: Properties and Applications*, A. Nanni, ed., Elsevier Science Publishers, New York, pp. 423-434.

Norris, T., Saadatmanesh, H., and Ehsani, M., 1997, "Shear and flexural strengthening of R/C beams with carbon fiber sheets," *Journal of Structural Engineering*, V. 123, No. 7, pp. 903-911.

ODOT, "Oregon's Bridges 2002," Oregon Department of Transportation, Salem, Oregon.

Sato, Y., Ueda, T., Kakuta, Y,, and Tanaka, T., 1996, "Shear reinforcing effect of carbon fiber sheet attached to side of reinforced concrete beams," *Advanced Composite Materials in Bridges and Structures*, M.M. El-Badry, ed., pp. 621-627.

Tompos, E.J., and Frosch, R.J., 2002, "Influence of beam size, longitudinal reinforcement and stirrup effectiveness on concrete shear strength," *ACI Structural Journal*, September-October, pp. 559-567.

Triantafillou, T.C., 1998, "Shear strengthening of reinforced concrete beams using epoxy-bonded FRP composites," *ACI Structural Journal*, V. 95, No. 2, Mar.-Apr., pp. 107-115.

Watson Bowman Acme Corporation, "Specification: Wabo® MBrace Composite Strengthening System with Carbon Fiber Reinforcement," Amherst, NY, March 2002.

Watson Bowman Acme Corporation, "Wabo® MBrace CF130," Amherst, NY, February 2003.

Wong, P.S., and Vecchio, F.J., 2002, "VecTor2 and FormWorks User's Manual," University of Toronto.

NOTATION

a	=	length of the shear span (mm) [in.]
a/d	=	shear span-to-depth ratio
A_{fv}	=	area of FRP shear reinforcement with spacing s_f, (mm^2) $[in.^2]$
A_s	=	area of flexural-tension steel reinforcement (mm^2) $[in.^2]$
A_v	=	area of transverse steel reinforcement within spacing, s (mm^2) $[in.^2]$
b_w	=	beam web width (mm) [in.]
d	=	effective depth, distance from extreme compression fiber to centroid of flexural-tension steel reinforcement (mm) [in.]
d_f	=	effective depth of FRP shear reinforcement (mm) [in.]
E_f	=	tensile modulus of elasticity of FRP (GPa) [ksi]
E_{fu}	=	ultimate tensile modulus of elasticity of FRP (GPa) [ksi]
$E_{fu}*$	=	tensile modulus of elasticity of FRP based on nominal fabric thickness (GPa)[ksi]
f_{bond}	=	direct tension pull-off strength of FRP bonded to concrete (MPa) [psi]
f_c'	=	specified compressive strength of concrete (MPa) [psi]
f_{fe}	=	effective FRP tensile strength (MPa) [ksi]
f_{fu}	=	design ultimate FRP tensile strength (MPa) [ksi]
$f_{fu}*$	=	design ultimate FRP tensile strength based on nominal fabric thickness (MPa) [ksi]
f_t	=	concrete split cylinder tensile strength (MPa) [ksi]
f_{ult}	=	ultimate tensile strength of reinforcing steel (MPa) [ksi]
f_y	=	yield strength of steel reinforcement (MPa) [ksi]
f_{yt}	=	yield strength of transverse steel reinforcement (MPa) [ksi]

h	=	overall height of reinforced concrete beam (mm) [in.]
k_1	=	modification factor applied to κ_v for concrete strength
k_2	=	modification factor applied to κ_v for FRP wrapping scheme
L	=	overall length (mm) [in.]
L_e	=	effective bond length of FRP laminate (mm) [in.]
M_{max}	=	actual maximum moment capacity (kN-mm) [in.-kips]
M_n	=	ACI nominal moment capacity (kN-mm) [in.-kips]
P	=	actuator force (kN) [kips]
P_{max}	=	force corresponding to actual maximum moment capacity (kN) [kips]
n	=	number of plies of FRP reinforcement
s	=	spacing of transverse steel reinforcement
s_f	=	spacing of FRP shear reinforcement (mm) [in.]
St. Dev.	=	standard deviation
t_f	=	nominal thickness of one ply of FRP reinforcement (mm) [in.]
t_f*	=	nominal FRP fabric thickness (mm) [in.]
V	=	shear force (kN) [kips]
V_{app}	=	applied shear force (kN) [kips]
V_c	=	nominal shear strength provided by concrete with steel flexural reinforcement (N) [lb]
V_f	=	nominal shear strength provided by FRP shear reinforcement (N) [lb]
V_n	=	nominal shear strength (N) [lb]
V_s	=	nominal shear strength provided by transverse steel reinforcement (N) [lb]
w_f	=	width of FRP reinforcing plies (mm) [in.]
α	=	inclination angle of stirrups (degrees)

ε_{fd} =   FRP strain induced by debonding (mm/mm) [in./in.]

ε_{fe} =   effective strain level in FRP reinforcement; strain level at section failure

           (mm/mm) [in./in.]

ε_{fu} =   design rupture strain of FRP reinforcement (mm/mm) [in./in.]

ρ_f =   FRP reinforcement ratio [Khalifa *et al.* 1998]

     = $\dfrac{nt_f}{b_w}\dfrac{w_f}{s_f}$

ρ_s =   longitudinal flexural-tension steel reinforcement ratio

     = $\dfrac{A_s}{b_w d}$

ρ_v =   transverse steel reinforcement ratio

     = $\dfrac{A_v}{b_w s}$

ϕ =   strength reduction factor

κ_v =   bond-dependent coefficient for shear

ψ_f =   additional FRP strength reduction factor

APPENDIX A

Discussion of Scaling for Experimental Specimens

To produce different sized specimens with CFRP shear strengthening, a number of scaling decisions were required that attempted to balance the intended structural behaviors and permit consistent development of specimens focused on future environmental exposure testing.

The overarching consideration was to provide reasonably consistent geometric scaling between three different specimen sizes. The prototype full-scale specimens were intended to reflect reasonable geometric proportions for cross-section as well as both flexural and transverse steel reinforcing ratios. The overall dimensions of the full-scale specimens in the test program were based on dimensions commonly seen at field-scale for conventionally reinforced concrete bridge girders from the mid-twentieth century. The half- and quarter-scale specimens were then developed to reflect the full-scale specimen geometry. The overall specimen cross-section and span lengths were ideally scaled based on the full-scale prototype. The applied structural forces, including moment and shear (and their interaction), were geometrically scaled very closely due to the approximately similar specimen depths, span lengths and geometrically scaled support and loading systems.

To minimize concrete material scaling considerations, a single batch of concrete, with a 13 mm (0.5 in.) maximum aggregate size was used across all scales to reduce concrete material variability. Scaling aggregate sizes would have required three separate mixes, which could have led to wider variations in concrete strengths. The 13 mm (0.5 in.)

aggregate size was selected for all scales to allow adequate flow of the fresh concrete for the cover requirements of the quarter-scale specimens.

Consistent heats of longitudinal reinforcing steel were used across the scales to reduce variability in steel mechanical properties. Using consistent heats, 16 #19 [#6] bars were required for flexural-tension steel at the full-scale, 4 were required at the half-scale and 1 was required at the quarter-scale to maintain the same reinforcement ratio. The 16 bars at the full-scale were bundled to produce an equivalent area of four bars each. Due to selection of the same material and bar size, the development lengths were not geometrically scaled. To overcome this, flexural-tension bars at the half- and quarter-scale were hooked to reduce the development length. The key consideration was to have the flexural steel developed at the region *d* away from the loading points in the high shear region for all scales. Closely-spaced stirrups were provided outside the shear spans to provide additional development from confinement. Different sizes of longitudinal reinforcing steel could have been used, but it would have been difficult to maintain the same reinforcement ratios and there would have been wider variations in material properties.

The effective depth of the flexural steel, *d*, was nearly geometrically scaled, with the ratio of d/d_{full} equal to 0.49 at the half-scale and 0.25 at the quarter-scale.

The same transverse steel reinforcement ratio was maintained across all scales. Closed #13 [#4] stirrups had been used for full-size test specimens in previous research and were adopted for the full-scale specimens in this research. To geometrically scale the stirrup

spacing, the bar size was reduced to #6 [#2] at the half-scale. Decreasing the bar size at the quarter-scale would have been difficult to achieve with commercially available products. Wire reinforcement could have been used to make custom stirrups at the quarter-scale, but it would have been difficult to match the material properties of the full- and half-scales (A615 Gr. 280 [40 ksi] and A36, respectively). Thus, single leg stirrups were used at the quarter-scale instead of a closed stirrup. Further, single bars were provided for compression and tension reinforcement and the specimen width was too narrow to accommodate a double-leg stirrup. Single legs also required a shorter spacing than a closed stirrup and could not provide additional confinement to the compression zone compared with the double-leg stirrups used at half- and full-scales. The use of different stirrup sizes at the different scales produced different scales of development lengths relative to the beam depths.

Initially, the CFRP reinforcement was geometrically scaled by strip width and spacing, with only a single layer of CFRP, providing unequal reinforcement ratios. Multiple layers of CFRP would have been required at the full- and half-scales to maintain the same reinforcement ratio as the quarter-scale specimens. As testing progressed and the level of CFRP reinforcement had to be reduced to produce shear-dominant failures, an attempt was made to match reinforcement ratios. Ultimately, the failed specimens did not have matching reinforcement ratios.

Because the CFRP reinforcement was scaled to produce similar reinforcing ratios by adjusting the strip widths and spacing, the CFRP-concrete bond stresses could not be scaled consistently. Geometrically scaled beam height, CFRP strip width and CFRP strip

spacing would have led to equal bond shear stresses had multiple plies been used and

maximum applied shears scaled similarly at matching values of *a/d*.   Scaling the bonded

surface area of the CFRP and using multiple plies to maintain a single reinforcement ratio

would help to clearly demonstrate a scale effect in future research.

Based on the scaling considerations, the following ACI 318-05 and 440.2R-02 properties

were calculated for the three scales, as shown in Tables A1 and A2: nominal moment

capacity, M_n; concrete shear contribution, V_c; steel shear contribution, V_s; FRP shear

contribution, V_f; nominal shear capacity, V_n; development length, ℓ_d; development length

with standard hook, ℓ_{dh}; and effective FRP bond length, L_e. Properties that did not scale

well are indicated in **bold**.

The FRP bond stress, τ, which is not an ACI property, was calculated using the following

equation:

$$\tau = \frac{A_f f_{fe}}{2 L_e w_f} \qquad \text{[A1]}$$

where A_f = area of FRP shear reinforcement within spacing s_f, f_{fe} = effective FRP stress, w_f

= FRP strip width and s_f = FRP strip spacing. The pressure applied to a concrete section

(with area $b_w s_f$) by a single CFRP strip was calculated to compare stress concentrations at

the different scales:

$$\frac{A_f f_{fe}}{b_w s_f} \qquad \text{[A2]}$$

where b_w = beam web width.

Table A1: Specimen design properties using nominal material properties.

Scale	Full	Half	Quarter
M_n (kN-m) [ft-kips]	1567 [1156]	207 [153]	25 [18.5]
V_c (kN) [kips]	252 [56.6]	62 [14.0]	16 [3.6]
V_s (kN) [kips]	205 [46.2]	49 [11.0]	12 [2.8]
V_f (kN) [kips]	197 [44.4]	92 [20.7]	42 [9.4]
V_n (kN) [kips]	667 [150]	203 [45.6]	70 [15.8]
FRP Bond Stress, τ (kPa) [psi]	2491 [361]	2346 [340]	2074 [301]
$(A_f f_{fe})/(b_w s_f)$ (kPa) [psi]	593 [86]	1117 [162]	1972 [286]
Flexural ℓ_d or ℓ_{dh} (mm) [in.]	2087 [82.2]	417 [16.4]	334 [13.1]
Stirrup ℓ_d (mm) [in.]	371 [14.6]	167 [6.57]	167 [6.57]
L_e (mm) [in.]	51 [2.0]	51 [2.0]	51 [2.0]

Table A2: Specimen properties at failure using actual material properties.

Specimen	FC	FT5	HC	HT2.5	QC	QT
M_n (kN-m) [ft-kips]	1554 [1146]	1556 [1148]	193 [142]	193 [142]	25 [18.4]	25 [18.4]
V_c (kN) [kips]	314 [70.5]	320 [71.9]	78 [17.6]	80 [17.9]	21 [4.7]	21 [4.7]
V_s (kN) [kips]	258 [58.1]	258 [58.1]	60 [13.6]	60 [13.6]	16 [3.5]	16 [3.5]
V_f (kN) [kips]	66 [14.9]	66 [14.9]	131 [29.5]	66 [14.8]	16 [3.5]	16 [3.5]
V_n (kN) [kips]	641 [144]	645 [145]	270 [60.7]	205 [46.2]	52 [11.7]	52 [11.7]
FRP Bond Stress, τ (kPa) [psi]	3519 [510]	3519 [510]	3519 [510]	3531 [512]	3251 [472]	3251 [472]
$(A_f f_{fe})/(b_w s_f)$ (kPa) [psi]	200 [29]	200 [29]	1593 [231]	800 [116]	745 [108]	745 [108]
Flexural ℓ_d or ℓ_{dh} (mm) [in.]	1619 [63.7]	1587 [62.5]	320 [12.6]	316 [12.4]	250 [9.8]	250 [9.8]
Stirrup ℓ_d (mm) [in.]	352 [13.9]	345 [13.6]	164 [6.5]	162 [6.4]	160 [6.3]	160 [6.3]
L_e (mm) [in.]	48 [1.9]	48 [1.9]	48 [1.9]	48 [1.9]	48 [1.9]	48 [1.9]